

**CHARACTERIZING THE ENVIRONMENTS OF
CORE-COLLAPSE SUPERNOVAE WITH MUSE**

SUBMITTED BY

THALLIS DE LOURENÇO PESSI

TO THE

**FACULTAD DE INGENIERÍA Y CIENCIAS
INSTITUTO DE ESTUDIOS ASTROFÍSICOS**

**In partial fulfillment of the requirements for the degree of Doctor of
Philosophy in Astrophysics**

Supervisor: Prof. José L. Prieto Katuranic

Co-supervisor: Dr. Joseph P. Anderson

UNIVERSIDAD DIEGO PORTALES

Santiago, Chile

2024

© 2024, Thallis de Lourenço Pessi

Se autoriza la reproducción total o parcial, con fines académicos, por cualquier medio o procedimiento, incluyendo siempre la cita bibliográfica del presente documento y su autor.


Acta de Deliberación
Defensa de Tesis Doctoral

En Santiago, el 10 de junio de 2024 el Tribunal de Defensa de Tesis Doctoral compuesto por el profesor Dr. José Luis Prieto (UDP), Dr. Joseph Anderson (ESO, Chile), Dra. Evelyn Johnston (UDP), Dr. Giuliano Pignata (Universidad Andrés Bello, Chile), y Dra. Jan Eldridge (University of Auckland, Nueva Zelanda), sobre la base del texto del proyecto, la exposición del doctorando y sus respuestas a las intervenciones de los miembros del tribunal, ha resuelto aprobar la tesis doctoral *CHARACTERIZING THE ENVIRONMENTS OF CORE-COLLAPSE SUPERNOVAE WITH MUSE* del doctorando THALLIS DE LOURENCO PESSI.

Los miembros del Tribunal firman para constancia.



José Prieto
Supervisor, UDP

 6/17/2024

Joseph Anderson
Co-supervisor, ESO Chile



Evelyn Johnston
UDP



Giuliano Pignata
Universidad de Tarapacá, Chile



Jan Eldridge
University of Auckland, Nueva
Zelanda



Chiara Mazzucchelli
Ministro de fe

Facultad de Ingeniería y Ciencias – Av. Ejército Libertador 441, Santiago

À minha família.

To my family.

Não sou nada.
Nunca serei nada.
Não posso querer ser nada.
À parte isso, tenho em mim todos os sonhos do mundo. [...]
Escravos cardíacos das estrelas,
Conquistamos todo o mundo antes de nos levantar da cama;
Mas acordamos e ele é opaco,
Levantamo-nos e ele é alheio,
Saímos de casa e ele é a terra inteira,
Mais o sistema solar e a Via Láctea e o Indefinido. [...]
Álvaro de Campos, 1928.

*Faz anos navego o incerto.
Não há roteiros nem portos.
Os mares são de enganos
e o prévio medo dos rochedos
nos prende em falsas calmarias.
As ilhas no horizonte, miragens verdes.
Eu não queria nada além
de olhar estrelas [...]
Caio Fernando Abreu.*

Abstract

Core-collapse supernovae (CCSNe) mark the explosive end in the life of massive stars. The study of the environment where they occur can help to explain their explosion mechanisms and constrain their progenitor stars. In this thesis, I present the results of a local environment analysis of a large sample of 112 CCSNe detected by the ASAS-SN survey and observed by the modern integral field spectrograph MUSE, at the Very Large Telescope (VLT). The untargeted nature of ASAS-SN allows for a minimally biased study of CCSN populations, while MUSE allows for a spatially detailed spectroscopic analysis of their environments.

I show comparative results of metallicity, $H\alpha$ equivalent width (EW), star formation rate (SFR), and extinction at the local SN sites between the different CCSN subtypes. Stripped envelope (SE) SNe occur in environments with higher values of metallicity than SNe II, and SNe II and IIn have very similar metallicities, ages, and SFRs, indicating that these events explode in similar environments. I also show that the luminosity of SESNe shows a weak correlation with metallicity in their environments, suggesting an intrinsic relation between metallicity and the amount of ^{56}Ni produced in these events. I further discuss a metallicity dependence on the occurrence of CCSNe relative to star formation (SF) in their host galaxies. I show that the CCSN metallicity distribution is significantly lower than the overall distribution of SF within the host galaxies. I estimate the occurrence of CCSN per unit SF as a function of metallicity and show that there is a strong decrease as metallicity increases. Finally, I discuss different possible explanations for these results and the implication of these results for different fields of astrophysics.

Ultimately, this thesis presents a detailed and homogeneous characterization of CCSN host galaxies selected from ASAS-SN, an untargeted survey, and the largest study to date of CCSN host galaxies with the MUSE instrument.

Resumen

Las supernovas (SNs) de colapso gravitacional (CG) marcan el final explosivo en la evolución de estrellas masivas. El estudio del ambiente en las galaxias anfitrionas donde ocurren puede ayudar a explicar sus mecanismos de explosión y estrellas progenitoras. En esta tesis, presento los resultados del análisis del ambiente de una gran muestra de 112 SNCGs detectados por el *ASAS-SN survey* y observados por el moderno espectrógrafo de campo integral MUSE, en el *Very Large Telescope*. La naturaleza no sesgada del ASAS-SN permite un estudio homogéneo de las poblaciones de SNCGs, mientras que MUSE permite un análisis espectroscópico espacialmente detallado de sus ambientes.

En este trabajo, muestro resultados comparativos de metalicidad, ancho equivalente de $H\alpha$, tasa de formación estelar, y extinción en los sitios de las SNs entre los diferentes subtipos de SNCGs. La SNs sin envoltorio (SE) ocurren en ambientes con valores de metalicidad más altos que SNs II, y SNs II y IIn tienen metalicidades, edades y SFRs muy similares entre ellas, lo que indica que estos eventos explotan en ambientes similares. También, muestro que la luminosidad de SNSEs muestran una débil correlación con la metalicidad en sus ambientes, sugiriendo una relación intrínseca entre la metalicidad y el ^{56}Ni producido en estos eventos. Además, analizo la dependencia de la metalicidad en la aparición de SNCGs en relación con la formación estelar (FE) en sus galaxias anfitrionas. Muestro que la distribución de metalicidad de las SNCGs es significativamente menor que la distribución general de FE dentro de las galaxias anfitrionas. Estimo la ocurrencia de SNCGs por unidad de FE en función de la metalicidad y muestro que hay una fuerte disminución a medida que aumenta la metalicidad. Finalmente, analizo diferentes explicaciones posibles para estos resultados y las implicaciones de estos resultados para diferentes campos de la Astrofísica.

En última instancia, esta tesis presenta una caracterización detallada y homogénea de las galaxias anfitrionas de SNCG seleccionadas de ASAS-SN, un estudio no sesgado y el estudio

más grande hasta la fecha de las galaxias anfitrionas de SNCGs con el instrumento MUSE.

Acknowledgements

My academic journey was marked by dedication, hard work, but also by a lot of luck in meeting and working with the most amazing people I could ever know. Therefore, many are the people that contributed for the completion of this work and that I would like to thank here.

First, I am very thankful for the unconditional love and support of my family during this whole journey. I am grateful for having my Mother, Father, Brother and Grandmother by my side during this period. I am thankful for the friends I have made in Chile, and accompanied me in this journey: Aish, Isha, Jenny, Manuel, Karen, Keila, Ksenia, Tatevik, Trisha, and Ranajit. I am thankful for Gabriela for being a great friend during the last years. I am particularly thankful for the amazing community of Brazilian astronomers in Santiago: Ana Posses, Ana Lourenço, Camila, Danielle, Douglas, Florence, Larissa, Pedro, Priscilla, and Tuila. You have made me feel like home during this period.

I am thankful for the IEA at UDP for providing an excellent environment for the students, especially during the rough pandemic times. I would like to thank the professors: Chiara, Claudio, Evelyn, Lucas, Manuel, Paula, and Roberto, for the best advices. I am thankful for Catalina and Valentina to have always helped solving the most diverse issues. I am especially thankful for my office mates at Pehuen for creating a wonderful place to work: Dejene, Elena, Grace, Hamideh, Prachi, Trystan, and Yaherlin.

Finally, this thesis would not be complete without the hard work of my two advisors, Jose and Joe. I am very thankful for their support, energy, and enthusiasm put in in guiding me through the projects presented here. I feel extremely lucky to have had the opportunity to work with such inspiring astronomers and amazing human beings. The time we worked together has marked deeply my academic journey and has inspired me to continue in this career.

Contents

Abstract	ix
Resumen	xii
Acknowledgements	xiii
List of Figures	xix
List of Tables	xxi
1 Introduction	1
1.1 Supernovae	1
1.2 The progenitors of supernovae	3
1.3 The environments of supernovae	6
1.4 The scope of this thesis	9
2 A characterization of ASAS-SN CCSN environments with VLT+MUSE	13
2.1 Context	13
2.2 Abstract	14
2.3 Introduction	15
2.4 Sample selection and data reduction	19
2.5 Analysis	24
2.5.1 HII region segmentation	24
2.5.2 Analysis of physical parameters	29
2.6 Results	33
2.6.1 Oxygen abundance	34

2.6.2	H α equivalent width	37
2.6.3	Star formation rate	37
2.6.4	Extinction	38
2.7	Discussion	40
2.7.1	Constraints on progenitor properties	40
2.7.2	Environment versus light curve properties	43
2.8	Conclusions	46
2.9	Acknowledgements	49
2.10	Appendix	50
2.10.1	BPT analysis	50
2.10.2	Parameter tests	51
2.10.3	Metallicity gradients	53
2.10.4	Measured fluxes and physical parameters	54
2.10.5	Statistics results, KS, and AD tests.	54
2.10.6	The SLSN 2015bn	57
2.10.7	Photometry and light curve parameters	65
2.10.8	Entire tables	69
3	A metallicity dependence on the occurrence of core-collapse supernovae	83
3.1	Context	83
3.2	Abstract	83
3.3	Introduction	84
3.4	Data and Methods	86
3.5	Results	88
3.6	Discussion	92
3.7	Conclusions	96
3.8	Appendix	97
3.8.1	O3N2 and N2 Indicators	97
4	Legacy of this thesis	99
4.1	Publications	99
4.2	Conferences and presentations	100

4.3	Schools, training, and other research experience	101
4.4	Observational experience	102
5	Summary and conclusions	105
6	Perspectives and future work	109

List of Figures

1.1	Supernova 2023ixf in the galaxy M101	2
1.2	The Crab Nebula	3
1.3	Classification scheme of supernovae based on their spectroscopic properties .	4
1.4	The explosion site of SN 2008bk	5
1.5	Pixel statistics from the proximity to H α emission between different SN types	7
1.6	HII regions identified in four SN host galaxies from the CALIFA survey	8
1.7	The galaxies NGC 3568, NGC 3157, and NGC 7371	10
1.8	ESO's Picture of the week: Uncovering supernova secrets	11
2.1	The different SN types in our sample	24
2.2	Properties of the SNe II and their hosts in our sample	27
2.3	MUSE RGB image composition of the galaxy NGC 3456	31
2.4	Cumulative distributions for the oxygen abundance	35
2.5	Cumulative distributions for the oxygen abundance	36
2.6	Cumulative distributions of the H α EW	38
2.7	Cumulative distributions of Σ SFR	39
2.8	Cumulative distributions of the line of sight extinction	40
2.9	SNe II LC parameters as a function of the environment	46
2.10	SESNe LC parameters as a function of the environment	47
2.11	SNe IIn LC parameters as a function of the environment	47
2.12	BPT diagram of the HII regions in our sample	51
2.13	Cumulative distributions for different tests	53
2.14	Oxygen abundances fit for ASASSN-16ba	54
2.15	Spectrum fitting for the SLSN 2015bn	66

2.16	Example of a second order polynomial fitting	69
3.1	The cumulative distribution of SFR sorted by O/H	88
3.2	Cumulative distributions of the fraction of SF as a function of O/H	90
3.3	The oxygen abundance NCR for the CCSNe	91
3.4	The occurrence of CCSNe per unit of SF as a function of O/H	92
3.5	The occurrence rate of CCSNe, given by the O3N2 and N2 indicators	98

List of Tables

2.1	General properties of the SNe and their host galaxies.	25
2.2	Distance properties of the HII regions related to each SN.	26
2.3	Phase of the observations relative to the SN peak luminosity, for the events that presented broad spectral features at their position.	30
2.4	IFUanal parameters used in the tests.	52
2.5	Measured fluxes of different emission lines at the nearest HII region to each SN.	55
2.6	Physical properties of the HII region related to each SN.	56
2.7	Oxygen abundance statistics.	58
2.8	Oxygen abundance KS values.	59
2.9	Oxygen abundance AD values.	60
2.10	H α EW statistics.	61
2.11	H α EW KS values.	61
2.12	H α EW AD values.	62
2.13	Σ SFR statistics.	62
2.14	Σ SFR KS values.	63
2.15	Σ SFR AD values.	63
2.16	Extinction statistics.	64
2.17	Extinction KS values.	64
2.18	Extinction AD values.	65
2.19	LC parameters of the SNe II.	67
2.20	LC parameters of the SESNe.	68
2.21	LC parameters of the SNe IIn.	69

2.22 Entire version of Table 2.1. 69

2.23 Entire version of Table 2.2. 72

2.24 Entire version of Table 2.5. 75

2.25 Entire version of Table 2.6. 78

2.26 Entire version of Table 2.19. 80

3.1 The occurrence rate of CCSN per unit of SF, as a function of abundance. . . 93

Chapter 1

Introduction

*Ora (direis) ouvir estrelas! Certo,
Perdeste o senso!” E eu vos direi, no entanto,
Que, para ouvi-las, muita vez desperto
E abro as janelas, pálido de espanto...*

1.1 Supernovae

A supernova (SN, Figure 1.1) is a luminous explosion associated with the end of the life of certain types of stars. These events can eject matter to extremely high velocities, with a typical kinetic energy of $\sim 10^{51}$ ergs. The study of these luminous events has a deep impact in many fields of astronomy: SN explosions can be responsible for dramatic changes in the evolution of a galaxy, being capable of triggering or quenching the formation of new stars (Matteucci and Greggio, 1986; Martig and Bournaud, 2010); they are thought to be the main formation channel of dust (Kozasa et al., 2009) and heavy elements, thus being the main drivers of chemical enrichment in galaxies (Kobayashi and Nakasato, 2011; Karlsson, Bromm, and Bland-Hawthorn, 2013); due to their relatively high luminosity and homogeneity, Type Ia SNe are famously used as an accurate distance indicator (e.g., Phillips, 1993; Hamuy et al., 1996; Phillips, 2005). This type of SN has been used as a tool for many breakthroughs in cosmology, such as the estimate of the Hubble constant, and the discovery of dark energy (Riess et al., 1998; Perlmutter et al., 1999).

Supernovae in the Milky Way have been observed by the naked eye and have been regis-

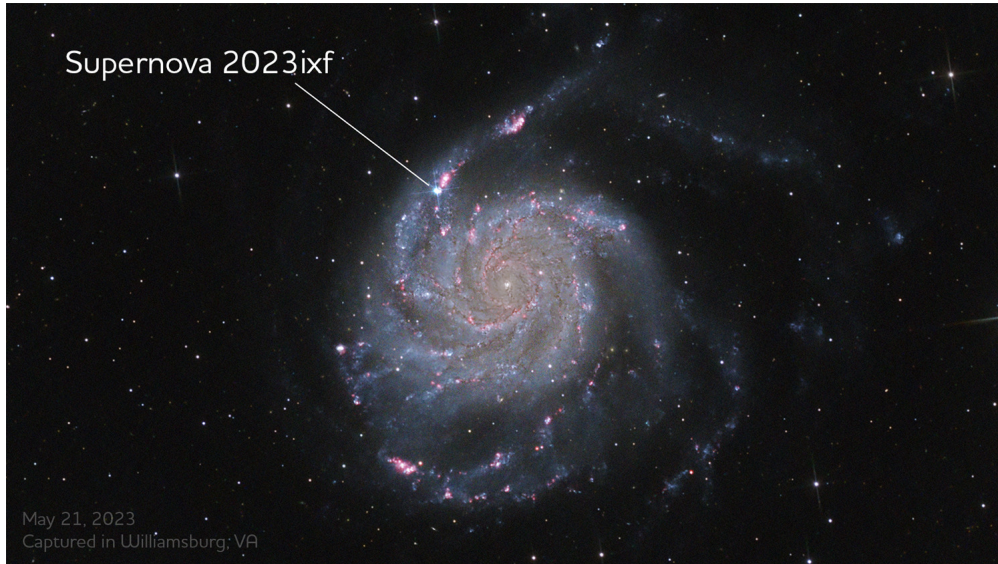


Figure 1.1: The Type II Supernova 2023ixf in the galaxy M101. Image credits: Georgii Konkov [<https://www.astrobin.com/v59gi8/>].

tered by ancient astronomers. Some of these remarkable events include the SN 1054, which gave origin to the Crab Nebula (Figure 1.2), and the SN 1604, famously observed by Johannes Kepler. The modern search for extragalactic SN explosions started with Fritz Zwicky, who created the term *supernova*, and began the systematic photographing of these events in the 1930s. The first SNe discovered by Zwicky shared many observational similarities, including very regular light curves and a conspicuous absorption feature near 6100 \AA in their spectra. Later observations discovered events with more heterogeneous light curves and very characteristic Balmer lines of hydrogen in emission. These two classes of SN were called, respectively, Type I and Type II SNe by Minkowski (1941).

Figure 1.3 shows a classification scheme based on features present in the spectra of SNe. SNe in the first category discovered by Zwicky, now called Type Ia SNe, show strong absorption features of Si and no signal of H. Two other types lacking the distinctive Balmer lines of Type II SNe are now known: Type Ib SNe, which shows strong absorption features of He, and Type Ic SNe, which are devoid of H and He, but present weak absorption lines of Si. Some Type Ic SNe show broad absorption features of Si and have been labeled Ic-BL. Some events were discovered to show a transition between a hydrogen-rich to a helium-rich event; these are called Type IIb SNe. Type IIb, Ib, and Ic SNe are usually referred to together as stripped-envelope supernovae (SESNe), due to the lack of an H envelope when their progenitor star exploded (see Filippenko, 1997, for a review on SN classification).



Figure 1.2: The Crab nebula, remnant of SN 1054, observed by the James Webb Space Telescope. Image credits: NASA, ESA, CSA, STScI, T. Temim.

SN explosions can also happen inside a very dense circumstellar medium (CSM), which gives rise to narrow emission lines in their spectra, due to the interaction of the ejecta with the dense CSM. Type IIn SNe are generated by an H-rich CSM, while Type Ibn SNe arise in He-rich CSM (Pastorello et al., 2008). Recently, Type Icn SNe have been identified, which lack both H and He, but have C and O-rich CSM (e.g., Fraser et al., 2021; Davis et al., 2023; Nagao et al., 2023). These events are referred to together as interacting SNe. Finally, events that have high luminosities, with typical absolute optical-wavelength magnitudes $\lesssim -21$, have been labeled superluminous (SL) SNe. They can be classified as H-rich, or SLSNe-II (e.g., Ofek et al., 2007), and H-poor, or SLSNe-I (Quimby et al., 2011).

1.2 The progenitors of supernovae

The different observed features in SNe indicate that the different SN types are generated by distinct progenitor stars and explosion mechanisms. Type Ia SNe are thought to be the

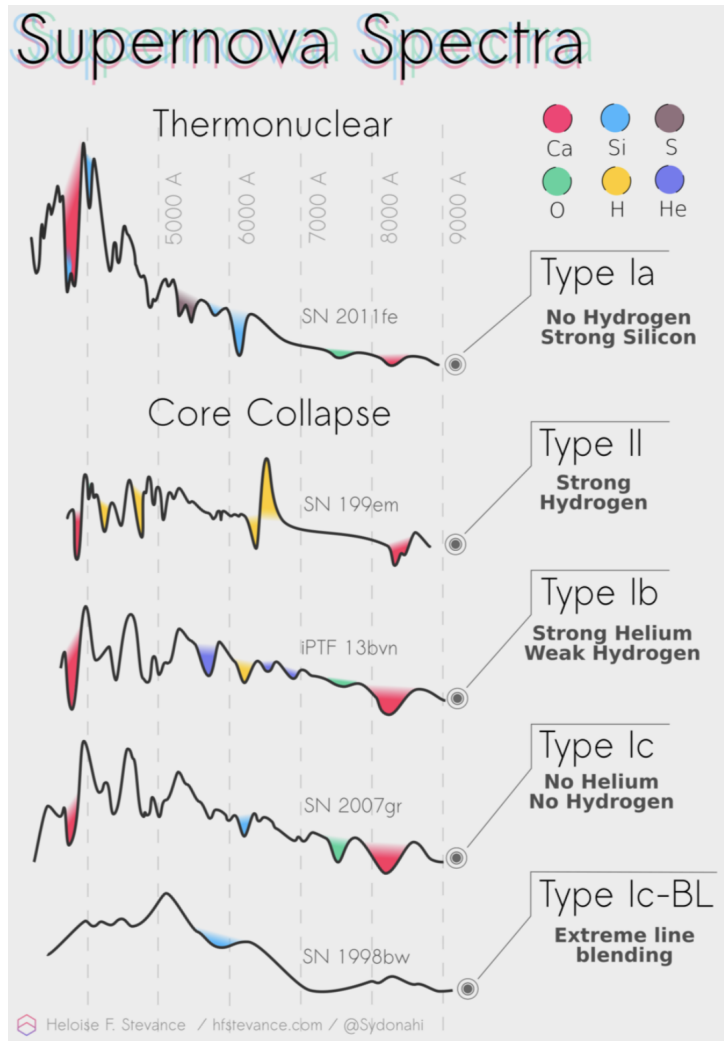


Figure 1.3: Classification scheme of supernovae based on their spectroscopic properties. Image credits: Heloise Stevance [<https://www.hfstevance.com/ccsne>].

thermonuclear explosion of white dwarf (WD) stars, the end product in the evolution of stars with zero-age main sequence (ZAMS) mass lower than $8 M_{\odot}$ (Hoyle and Fowler, 1960). WDs that give origin to Type Ia SNe are composed of C and O in a highly electron degenerated state. When these stars reach a mass limit of $1.4 M_{\odot}$ through accretion from a companion, carbon burning is initiated, and their structure can no longer support the dramatic changes in pressure leading to thermonuclear runaway. There are, however, debates on the nature of the companion to the CO WDs (for a recent review see, e.g., Ruiter, 2020), with scenarios pointing to accretion from a non-WD companion star, called single-degenerate (Whelan and Iben, 1973; Nomoto, 1982), or the merger between two WDs, referred to as the double-degenerate scenario (Webbink, 1976; Iben and Tutukov, 1984).

A CCSN occurs either by the collapse of a ONeMg core, for stars with ZAMS masses

$\approx 8 - 10 M_{\odot}$ (electron-capture SNe, Miyaji et al., 1980; Nomoto et al., 1982), or the collapse of an Fe core for ZAMS masses $\gtrsim 10 M_{\odot}$ ¹ (Bethe et al., 1979; Bethe, 1990). The ZAMS mass limit for CCSN progenitors varies for the different subtypes (e.g., Meynet et al., 1994), and the mass ranges of stars that produce a CCSN explosion might not be continuous, with many regions of “explodability” (e.g., Pejcha and Thompson, 2015; Sukhbold et al., 2016; Ebinger et al., 2020; Zapartas et al., 2021). Red supergiant (RSG) stars are thought to be the progenitors of Type II SNe, with observational evidence pointing to RSG progenitors with a mass range between $\sim 8 - 20 M_{\odot}$. (Smartt, 2015; Smartt et al., 2009). However, the RSG populations in the Milky Way and the Magellanic Clouds present ZAMS masses up to $\approx 25 - 30 M_{\odot}$, and the lack of SNe II arising from such massive RSGs is known as the “RSG problem” (Smartt, 2009; Kochanek, 2020). Some examples of direct observations of Type II SN progenitor stars include SN 2008cn (an RSG with a mass of $< 16 M_{\odot}$, Maund, Reilly, and Mattila, 2014), SN 2008bk (Van Dyk et al., 2012, an RSG with $\sim 8 M_{\odot}$, Figure 1.4), and SN 2012aw (an RSG with $\sim 12.5 M_{\odot}$, Fraser, 2016).



Figure 1.4: The explosion site of SN 2008bk. The pre-explosion image (left-most panel) shows a RSG star that disappeared (right-most panel) after the explosion (center panel). Image credits: Mattila et al. (2010).

The mechanism behind the H-stripping in the progenitor stars of SESNe is still uncertain: the main scenarios propose the stripping from binary interactions or strong winds in single massive stars (e.g., Yoon, Woosley, and Langer, 2010; Eldridge et al., 2013; Kim, Yoon, and Koo, 2015). This class of SN lacks a significant number of direct progenitor detection, with only a few being observed so far. Some examples include the SN IIb 1993J (with a progenitor consistent with a RSG in a binary system, Maund and Smartt, 2009) and the SN Ib 2019yvr

¹Very massive stars with ZAMS masses $\approx 140 - 260 M_{\odot}$ are expected to produce pair-instability SNe, via the thermonuclear runaway explosion during the oxygen burning phase (e.g., Schulze et al., 2024).

(with a progenitor consistent with a single luminous star, Kilpatrick et al., 2021a; Sun et al., 2022; Fox et al., 2022).

Type IIn SNe are expected to be generated by stars with relatively larger masses than Type II SNe, as the large amount of CSM observed in these events require energetic episodes of mass-loss in the pre-SN stage (e.g., Smith, 2014). Although the sample of direct progenitor detections of SNe IIn is small, LBV-like variability observed in pre-SN stages might indicate a connection with more massive progenitors (Ryder et al., 1993; Gal-Yam and Leonard, 2009; Mauerhan et al., 2013; Pastorello et al., 2013; Elias-Rosa et al., 2016). On the other hand, environment studies (e.g., Anderson et al., 2012; Taddia et al., 2013; Kangas et al., 2017) and the progenitor of SN 1998S (an RSG, Mauerhan and Smith, 2012) might favor the scenario of relatively less massive stars as SN IIn progenitors. Type Ibn SNe are proposed to be generated by massive H-poor WR stars (Pastorello et al., 2007). Although no direct detection of Type Ibn progenitor has yet been made, environment studies suggest a connection to older stellar populations or a diversity of progenitor masses (Hosseinzadeh et al., 2019; Ben-Ami et al., 2023). Finally, the progenitor systems behind the extreme energies observed in SLSNe are still uncertain, with the main scenarios proposing the interaction with CSM (e.g., Sorokina et al., 2016), pair instability (e.g., Yan et al., 2015), and energy injection from a compact object, like a magnetar (e.g., Woosley, 2010).

1.3 The environments of supernovae

In the lack of a substantial number of direct progenitor imaging, except for Type II SNe (e.g., Smartt, 2015), the analysis of the properties of SN locations can provide essential information on the physical processes behind SNe and their subtypes. Early studies found a correlation of Type II SNe and SESNe to spiral galaxies and, more specifically, to their spiral arms (Maza and van den Bergh, 1976; van Dyk, 1992; McMillan and Ciardullo, 1996; Bartunov, Tsvetkov, and Filimonova, 1994). These are places of constant star formation, and where most young stars are located, therefore showing a connection between these SN types to massive progenitors. Type Ia SNe, on the other hand, do not show any preference for location and galaxy type, being found in spiral and elliptical galaxies (Maza and van den Bergh, 1976; van Dyk, 1992; McMillan and Ciardullo, 1996; Bartunov, Tsvetkov, and

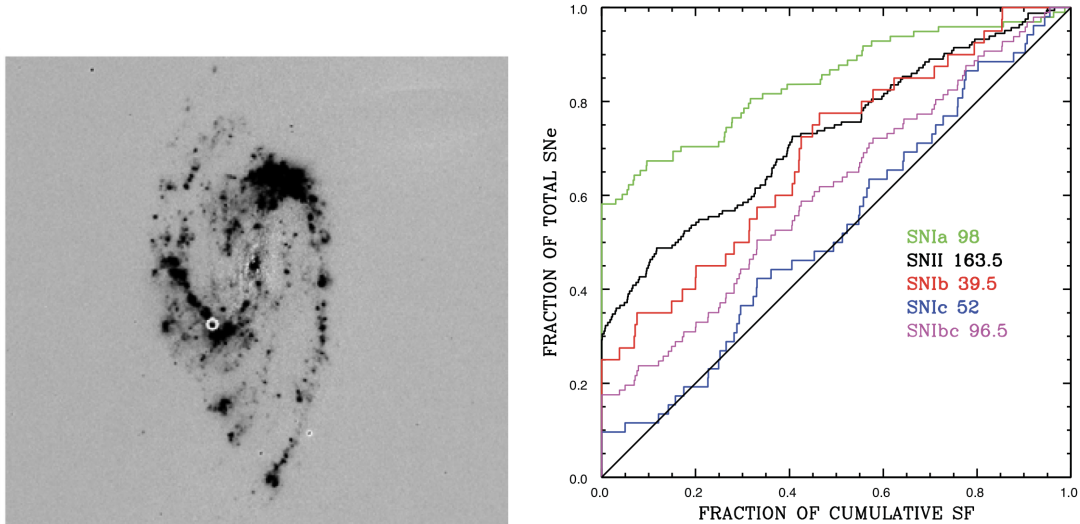


Figure 1.5: *Left*: Negative continuum-subtracted $H\alpha$ image of the galaxy NGC 3627, that hosted the Type II SN 2009hd, adapted from Anderson et al. (2012). *Right*: Cumulative distribution of pixel statistics from the proximity to $H\alpha$ emission between different SN types, from Anderson et al. (2012)

Filimonova, 1994). Elliptical galaxies are formed by old stellar populations, having stopped star formation for a long time. This observation suggests a connection between Type Ia SNe and older stellar populations.

The advancement of astronomical instruments and techniques (using both photometry and spectroscopy), allowed for a more detailed analysis of the local environments of SNe and the measurement of physical parameters of their associated star-forming regions, such as the stellar population age and metallicity (for a historical review of SN environment studies, see Anderson et al., 2015). Early analysis of the radial distribution of SNe showed that Types Ib and Ic are more concentrated near the core of their host galaxies than Type II events (van den Bergh, 1997; Wang, Höflich, and Wheeler, 1997; Tsvetkov, Pavlyuk, and Bartunov, 2004), implying the existence of a metallicity dependence of the former types. This would support the scenario of a single progenitor for Type Ib and Ic SNe, as higher metallicity single stars would produce stronger winds, capable of shedding the outer layers of the star away (e.g., Mokiem et al., 2007). These results, however, were contested by Anderson et al. (2015), who showed that these types of SNe are more centrally concentrated than Type II SNe in disturbed galaxies, systems that do not present a well-behaved metallicity gradient (Kewley et al., 2010; Sánchez et al., 2014).

Pixel statistics (James and Anderson, 2006; Fruchter et al., 2006) on $H\alpha$ imaging of SN

host galaxies showed that Type Ic SNe followed $H\alpha$ emission, a tracer of high-mass star-formation, while Types II and Ib did not show a strong correlation with this parameter, as it is shown in Figure 1.5 (Anderson et al., 2012). Instead, Anderson et al. (2012) showed that Type II SNe followed the near-UV emission in their host galaxies, which is connected to relatively older star-formation (e.g., Gogarten et al., 2009). This result is consistent with Type Ic SNe being formed by relatively younger and more massive stars than Type II SNe (for other analyses of pixel statistics, see e.g., Kelly, Kirshner, and Pahre, 2008; Raskin et al., 2008; Kangas et al., 2013). In the case of Type IIn SNe, Habergham et al. (2014) showed that these events have a very similar degree of association to host galaxy $H\alpha$ emission to Type IIP SNe. Other analyses of their environments also found no association to younger or more metal-rich stellar populations, showing very similar properties to normal SNe II (Taddia et al., 2013; Anderson et al., 2012; Kangas et al., 2017; Kuncarayakti et al., 2018). This result contrasts the scenario of very massive stars as their progenitors, although a bimodal distribution of progenitors has also been suggested (e.g., Ransome et al., 2022).

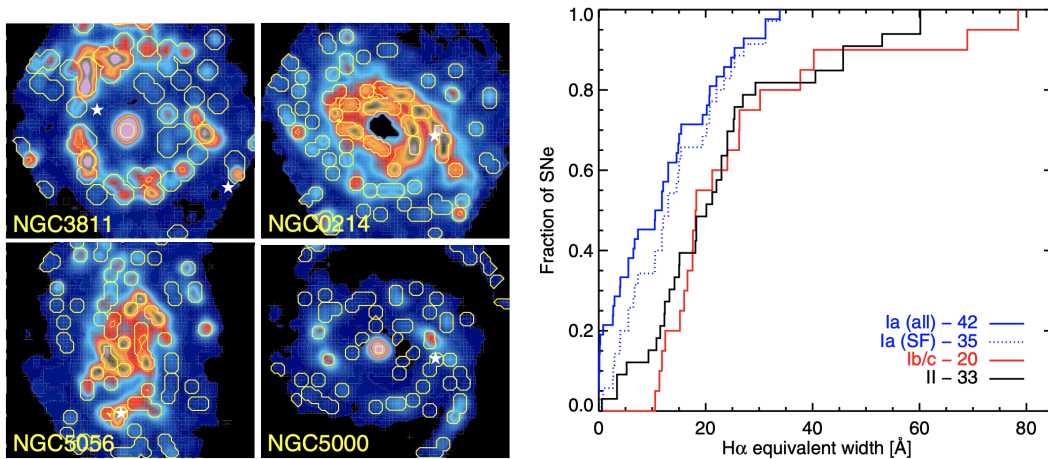


Figure 1.6: *Left*: HII regions identified in four SN host galaxies from the CALIFA survey, from Galbany et al. (2014). *Right*: Cumulative distribution of $H\alpha$ equivalent width between Type Ia, II and Ib/c SNe, from Galbany et al. (2014)

The advent of Integral Field Units (IFUs) affords a more precise analyses of SN environments, as the ability of spatially resolved spectroscopy in a large field-of-view (FoV) enables a study of individual HII regions within host galaxies. Using IFU spectroscopy of HII regions from the CALIFA survey, Galbany et al. (2014) showed that there are no significant differences in metallicity, star formation rate (SFR), and the equivalent width (EW) between the environments of Types II, Ib, and Ic SNe. This suggests progenitors with similar ages and

masses for the three types and supports the scenario of binary interaction being the main mechanism of at least a fraction of CCSNe (Figure 1.6). Similar results were found in the analysis of the PISCO SN host compilation (Galbany et al., 2018), where larger values of $H\alpha$ EW were found at the local environment of Type Ic SNe, but no significant differences were found in the values of SFR and metallicity between Type II, Ib and Ic SN (for other IFU analyses see, e.g., Kuncarayakti et al., 2018; Lyman et al., 2018). The significance of the difference between metallicity values for the distinct CCSN subtypes is still uncertain. Some authors find, for example, no preference of Type Ic SNe to higher metallicities, having very similar values to Type II and Type Ib SNe (Kuncarayakti et al., 2013a; Kuncarayakti et al., 2013b; Anderson et al., 2015; Schulze et al., 2021), while other studies do find significant differences in the environment metallicity of SNe II and SESNe (see, e.g., Prantzos and Boissier, 2003; Boissier and Prantzos, 2009; Prieto, Stanek, and Beacom, 2008; Arcavi et al., 2010; Modjaz et al., 2011).

The commissioning of the Multi-Unit Spectroscopic Explorer (MUSE, Bacon et al., 2014) instrument at the Very Large Telescope (VLT) represented a revolution in the use of integral field spectroscopy for many fields of astronomy. With a spatial sampling of 0.2×0.2 arcsec, a FoV of 1 arcmin^2 (in Wide Field Mode), and reaching a medium spectroscopic resolution of $R \sim 3000$ with wide wavelength coverage (480 – 930 nm), the instrument is still the most advanced IFU unit in operation. The remarkable capabilities of MUSE in the study of SN environments were demonstrated by Galbany et al., 2016a, who analyzed 6 nearby galaxies that hosted 11 SNe and presented a new method for comparing HII region properties within SN host galaxies, which was made possible due to the high angular resolution of the instrument.

1.4 The scope of this thesis

The analysis of the environments of SN explosions has been proved to be an excellent tool in the understanding of the physical processes and progenitors of the different types of SNe. In recent years, studies using IFU data have been capable of deriving physical properties of HII regions near the SN explosion site with great spatial and spectral resolution, allowing for good statistical estimates of their environments. The MUSE instrument at the VLT represents an

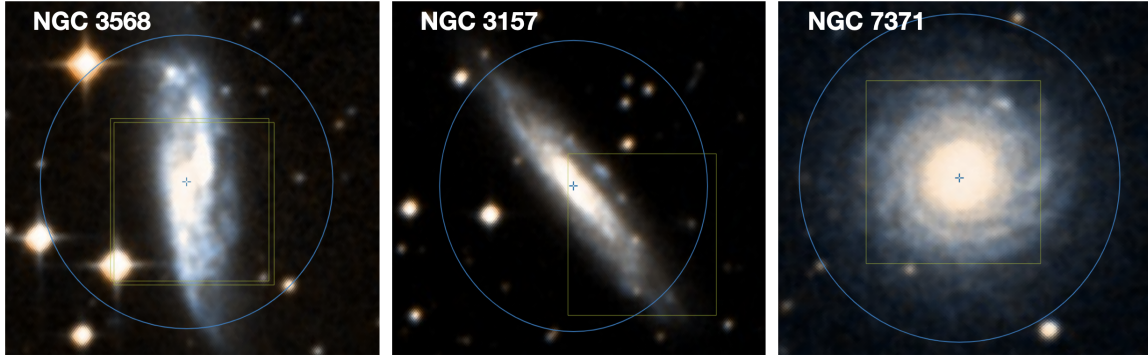


Figure 1.7: The galaxies NGC 3568, NGC 3157, and NGC 7371 hosted CCSNe detected by the ASAS-SN survey and are part of the AMUSING dataset. The yellow boxes highlight the regions observed by the MUSE instrument. The images were taken from the ESO Archive Science Portal.

exciting advance in the study of SN environments, as its remarkable angular resolution and large FoV allow for very precise characterization of their host galaxies.

This thesis presents the largest study to date of CCSN host galaxies observed by the MUSE instrument. Most of the data were acquired by the All-weather MUSE Supernova Integral field Nearby Galaxies (AMUSING) survey, and are composed of 111 nearby galaxies that hosted CCSNe discovered between 2013 and 2018 (Figures 1.7 and 1.8). One important drawback of the existing studies of CCSNe environments using IFU data is the heterogeneity of the SN samples: most come from different surveys, including pointed and panoramic surveys, as well as amateur discoveries, with little or no control for biases and systematics. One of the main goals of this work is to avoid biases towards environment parameters and to use a very *homogeneous* sample of CCSNe as a function of their host galaxy properties. To produce such a homogeneous and untargeted analysis, all of the CCSNe in the sample were selected to have been detected and/or discovered by the All-Sky Automated Survey for Supernovae (ASAS-SN, Shappee et al., 2014), an all-sky survey of bright transients with minimal detection biases and high spectroscopic completeness for SN studies.

ASAS-SN is currently composed of 24 telescopes around the world and has the goal of monitoring the entire sky to discover nearby and bright events (Shappee et al., 2014; Kochanek et al., 2017; Holoien et al., 2017; Holoien et al., 2017a; Holoien et al., 2017b; Holoien et al., 2019; Neumann et al., 2023a). The survey is almost spectroscopically complete, with almost all the discovered transients having an associated spectrum and classification (Holoien et al., 2019). An important feature of ASAS-SN is that, as an all-sky survey,

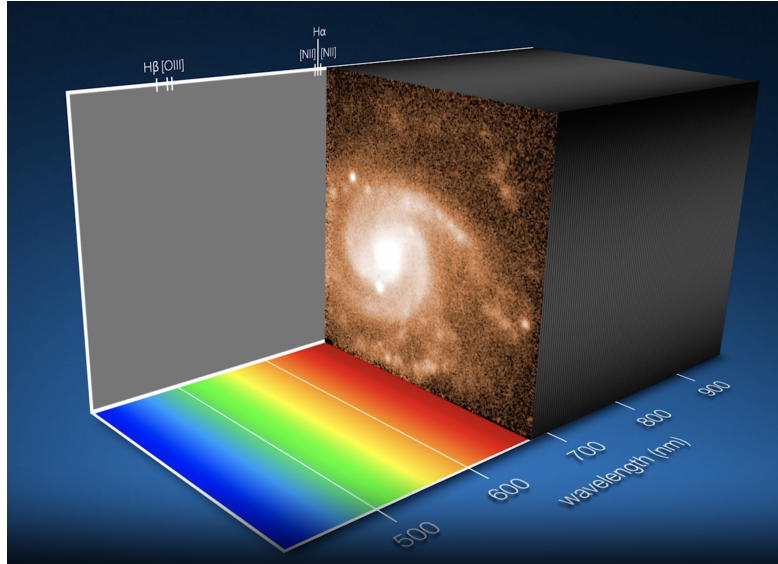


Figure 1.8: NGC 3456 is part of our dataset and featured ESO’s Picture of the week: Uncovering supernova secrets. Image credits: ESO / T. Pessi et al. [<https://www.eso.org/public/videos/potw2345a/>].

it does not target particular galaxies. In addition, ASAS-SN discovered more transients in the central parts of galaxies than any previous professional and amateur surveys (Holoien et al., 2017; Holoien et al., 2017a; Holoien et al., 2017b; Holoien et al., 2019; Neumann et al., 2023b). These features allow the ASAS-SN survey to serve as an ideal tool for the study of nearby SN populations, as it is not biased toward brighter and more extended galaxies.

The outstanding capabilities of MUSE and the untargeted nature of the sample obtained from ASAS-SN served as the main motivations for producing the analysis presented in this thesis. In Chapter 2, I present the first article resulting from this analysis. In this chapter, I describe the sample properties, our methodology to study the HII regions within the galaxies, and the comparative analysis for the different CCSN subtypes for the main analyzed parameters: metallicity (as given by the oxygen abundance), $H\alpha$ EW, SFR, and extinction. I also present an analysis of how the environmental properties are related to the intrinsic CCSN explosion properties derived from their light curves. Finally, I discuss the implications of these results for our understanding of CCSN progenitors. Chapter 3 is composed of the second article from this analysis, where I describe an intriguing result found when comparing the CCSN location metallicities to the overall metallicities of all the star-forming regions in their host-galaxies: the occurrence of CCSNe per unit star-formation seem to be higher at low

metallicity environments, by a very significant factor. I discuss possible explanations for this observed effect and the implications for our knowledge of CCSN formation. In Chapter 4, I describe additional activities performed during the Ph.D. and their impact on my formation, and in Chapter 5, I present a summary and conclusions of the results reported in the thesis. Finally, in Chapter 6, I present my perspective and plans for the future.

Chapter 2

A characterization of ASAS-SN core-collapse supernova environments with VLT+MUSe

*E conversamos toda a noite, enquanto
A via-láctea, como um pátio aberto,
Cintila. E, ao vir do sol, saudoso e em pranto,
Inda as procuro pelo céu deserto.*

2.1 Context

This chapter is composed by the article Pessi et al. (2023a), which was accepted for publication at the Astronomy & Astrophysics journal on 15 June 2023 and published online on 29 August 2023 (doi: 10.1051/0004-6361/202346512). The authors of this work are Thallis Pessi, Jose L. Prieto, Joseph P. Anderson, Lluís Galbany, Joseph D. Lyman, Christopher Kochanek, Subo Dong, Francisco Förster, Raul González-Díaz, Santiago Gonzalez-Gaitan, Claudia P. Gutiérrez, Thomas W.-S. Holoién, Phillip A. James, Cristina Jiménez-Palau, Evelyn J. Johnston, Hanindyo Kuncarayakti, Fabián Rosales-Ortega, Sebastian F. Sánchez, Steve Schulze, and Benjamin Shappee.

2.2 Abstract

The analysis of core-collapse supernova (CCSN) environments can provide important information on the life cycle of massive stars and constrain the progenitor properties of these powerful explosions. The MUSE instrument at the Very Large Telescope (VLT) enables detailed local environment constraints of the progenitors of large samples of CCSNe. Using a homogeneous SN sample from the All-Sky Automated Survey for Supernovae (ASAS-SN) survey, an untargeted and spectroscopically complete transient survey, has enabled us to perform a minimally biased statistical analysis of CCSN environments. We analyze 111 galaxies observed by MUSE that hosted 112 CCSNe – 78 II, nine IIn, seven IIb, four Ic, seven Ib, three Ibn, two Ic-BL, one ambiguous Ibc, and one superluminous SN – detected or discovered by the ASAS-SN survey between 2014 and 2018. The majority of the galaxies were observed by the the All-weather MUSE Supernova Integral field Nearby Galaxies (AMUSING) survey. Here we analyze the immediate environment around the SN locations and compare the properties between the different CCSN types and their light curves. We used stellar population synthesis and spectral fitting techniques to derive physical parameters for all HII regions detected within each galaxy, including the star formation rate (SFR), $H\alpha$ equivalent width (EW), oxygen abundance, and extinction. We found that stripped-envelope supernovae (SESNe) occur in environments with a higher median SFR, $H\alpha$ EW, and oxygen abundances than SNe II and SNe IIn/Ibn. Most of the distributions have no statistically significant differences, except between oxygen abundance distributions of SNe Ic and SNe II, and between $H\alpha$ EW distributions of SESNe and SNe II. The distributions of SNe II and IIn are very similar, indicating that these events explode in similar environments. For the SESNe, SNe Ic have higher median SFRs, $H\alpha$ EWs, and oxygen abundances than SNe Ib. SNe IIb have environments with similar SFRs and $H\alpha$ EWs to SNe Ib, and similar oxygen abundances to SNe Ic. We also show that the postmaximum decline rate, s , of SNe II correlates with the $H\alpha$ EW, and that the luminosity and the Δm_{15} parameter of SESNe correlate with the oxygen abundance, $H\alpha$ EW, and SFR at their environments. This suggests a connection between the explosion mechanisms of these events to their environment properties.

2.3 Introduction

Core-collapse supernovae (CCSNe) are luminous explosions associated with the deaths of massive ($\geq 8 M_{\odot}$) stars (Bethe et al., 1979; Woosley and Weaver, 1986; Arnett et al., 1989). The study of these events has a deep impact in many fields of astronomy, as these explosions are responsible for dramatic changes in the evolution of a galaxy, triggering or ending the formation of new stars (Matteucci and Greggio, 1986; Martig and Bournaud, 2010). CCSNe display a variety of properties in their light curves (LCs) and spectra that are directly connected to the evolution of their progenitor stars and to explosion properties (for example, explosion energy and ^{56}Ni mass). Type II SNe (hereafter SNe II) are characterized by broad hydrogen features in their spectra, while SNe Ib and SNe Ic are devoid of hydrogen, with the latter showing little or no helium. Some SNe Ic show broad lines in their spectra, being labeled SNe Ic-BL (Mazzali et al., 2002), and they are well-known for being associated with gamma-ray bursts (GRBs, Patat et al., 2001; Woosley and Bloom, 2006). SNe I Ib are transitional events that are similar to SNe II at very early times but the hydrogen lines vanish during their later evolution (Filippenko, Matheson, and Barth, 1994). The lack of hydrogen in SNe I Ib, Ib, and Ic reflects the loss of the progenitor star's envelope during the last stages before death, and hereafter are called together stripped-envelope SNe (SESNe). For a review of spectroscopic classification of SNe, readers can refer to Filippenko (1997) and Gal-Yam (2017). Some SNe occur inside a dense circumstellar medium (CSM), giving rise to narrow emission lines in their spectra due to the interaction of the ejecta with the dense CSM. If the medium is H-rich, these are called SNe IIn (Schlegel, 1990), while when the medium is He-rich, they are labeled SNe Ibn (Pastorello et al., 2008). Recently, SNe Icn have been discovered, and lack both H and He, but with a C- and O-rich CSM (Gal-Yam et al., 2021; Perley et al., 2022).

SNe II are thought to arise from single red supergiants (RSGs) with a mass range between $\sim 8 - 20 M_{\odot}$ (Smartt, 2015). Stars with zero-age main sequence (ZAMS) masses larger than $8 - 9 M_{\odot}$ develop an Fe core at the end of their evolution, which collapses when it reaches the Chandrasekhar mass¹ (See reviews by Bethe, 1990; Mezzacappa, 2005; Burrows

¹This sentence has been changed from the original publication, which reads: "Since Fe nuclei have strong binding energies, the process of nuclear fusion can no longer occur in the core of these stars, leading to gravitational collapse".

and Vartanyan, 2021). This scenario is supported by several direct observations of progenitor stars. Maund and Smartt (2009) found a RSG to be the progenitor of SN 2003gd and Maund et al. (2015) showed that the progenitor of SN 2008cn was consistent with a RSG with a mass of $< 16 M_{\odot}$. Maund, Reilly, and Mattila (2014) analyzed five SN II progenitors and found them to be consistent with RSGs with masses between $8.4 - 12.0 M_{\odot}$. Van Dyk et al. (2012) found the progenitor of SN 2008bk to be a RSG with $\sim 8 M_{\odot}$, and Fraser (2016) showed that the disappeared progenitor of SN 2012aw was a RSG with $\sim 12.5 M_{\odot}$ (also see the review by Smartt, 2015).

SESNe have only a few progenitors detected through direct imaging. For SNe IIb, some of their observed progenitors are consistent with yellow supergiant (YSG) or blue supergiant (BSG) stars with masses between ~ 13 to $19 M_{\odot}$ (e.g., Maund et al., 2011; Van Dyk et al., 2014; Folatelli et al., 2015). Maund and Smartt (2009) found a RSG to be the progenitor of SN 1993J and interacting binary systems have also been proposed for some of the observed progenitors of these events (e.g., Fox et al., 2014). The type of stars that become SNe Ib and Ic is also not clear. The mechanism needed to explain the shedding of the envelopes of hydrogen and/or helium before the core-collapse can be due to two distinct pathways: they might be lost through strong winds within a Wolf-Rayet (WR) or similar star, or they might lose mass through binary interactions (Yoon, Woosley, and Langer, 2010). While the former scenario requires more massive progenitors – a 20 to $40 M_{\odot}$ star for SNe Ib, and a $\gtrsim 40 M_{\odot}$ star for SNe Ic, at solar metallicity, following the rotating single-star model from Georgy et al. (2009) – the latter could arise from relatively lower mass progenitors, similar to normal SNe II. Only a few candidate companion stars have been detected in preexplosion images of SESNe. Kilpatrick et al. (2021a) found the progenitor of the SN Ib 2019yvr to be consistent with a single luminous star, although the nature of the preexplosion counterpart of SN 2019yvr is still under debate (see e.g., Sun et al., 2022), and recently Fox et al. (2022) have shown the candidate companion of the SN Ibc 2013ge to be a main-sequence B supergiant star.

Given the lack of a significant sample of direct detections of progenitor stars and binary companions of SESNe, indirect methods such as the analysis of the environment around these events can aid in constraining their properties (for a historical review of SN environment studies, see Anderson et al., 2015). Pixel statistics of $H\alpha$ emission in SN host galaxies

showed that SNe Ic traced $H\alpha$ emission, while SNe II and Ib do not show a strong correlation with these regions (Anderson et al., 2012), implying that SNe Ic arise from more massive stars. By analyzing the host galaxies of SESNe, Arcavi et al. (2010) and Modjaz et al. (2011) found that SNe Ic happen in environments with higher metallicities than SNe Ib and IIb. Anderson et al. (2010), Leloudas et al. (2011), and Sanders et al. (2012), however, did not find any significant difference in the environment metallicity between SNe Ic, Ib, and IIb (also see Cronin et al., 2021; Mayker Chen et al., 2023, for recent analyses).

SNe IIn are expected to arise from progenitor stars with a considerably larger mass than the progenitors of normal SNe II, as the observed amount of CSM observed in these events require extreme episodes of mass-loss in the pre-SN stages (e.g., Smith, 2014). A possible class of progenitor stars for SNe IIn are luminous blue variables (LBVs); massive stars that are characterized by very strong and episodic mass-loss. This scenario is consistent with the progenitor detections of SNe IIn and the LBV-like variability observed in some preexplosion observations (Ryder et al., 1993; Gal-Yam and Leonard, 2009; Mauerhan et al., 2013; Pastorello et al., 2013; Elias-Rosa et al., 2016). However, Anderson et al. (2012), Habergham et al. (2014), and Ransome et al. (2022) showed that SNe IIn have very similar degree of association to host galaxy $H\alpha$ emission to SNe II, and Taddia et al. (2013) demonstrated that they also happen in environments with very similar metallicity to SNe II. By analyzing the locations of LBV stars in the Large Magellanic Cloud (LMC) and M33 galaxies, Kangas et al. (2017) found no correlation between the spatial distribution of these massive stars and SNe IIn, favoring less massive progenitors. In fact, a RSG star is thought to be the progenitor of the SN IIn 1998S, indicating that these stars could generate at least a fraction of these transients (Mauerhan and Smith, 2012; Taddia et al., 2015b). However, Smith (2019) also argue that LBV stars are usually isolated and are not found in the most star-forming regions of galaxies, clouding the interpretation of SNe IIn environment studies. A similar scenario of distinct progenitor stars is also possible for SNe Ibn. Although massive H-poor WR stars were the first proposed progenitor for this class of transients (Pastorello et al., 2007), recent environment studies found a connection to older stellar populations and to a diversity of potential progenitors (Hosseinzadeh et al., 2019; Ben-Ami et al., 2023).

Recently, many SN environment analyses have used the capabilities of Integral Field Units (IFUs) to perform spatially resolved spectroscopy over a large field-of-view, allowing for the

study of individual HII regions within host galaxies and for a more precise study of the host galaxy as a whole. Using the CALIFA survey, Galbany et al. (2014) showed that there is no significant difference in the metallicities of the environments of SNe II, Ib, and Ic. In addition, the star formation rate (SFR) and the H α equivalent width (EW) also showed no significant difference between the CCSN types. The remarkable capabilities of the Multi-unit Spectroscopic Explorer (MUSE, Bacon et al., 2014) instrument at the Very Large Telescope (VLT) in the study of SN environments were demonstrated by Galbany et al. (2016a). They analyzed six nearby galaxies that hosted 11 SNe, and presented a new method for comparing HII region properties within SN host galaxies, which was made possible by the high angular resolution of the instrument. A larger analysis combining MUSE and VIMOS data (Le Fèvre et al., 2003) was made by Kuncarayakti et al. (2018), who analyzed 83 nearby SN explosion sites. They found no significant difference between the metallicity of the different CCSN environments, but showed that SNe Ic are associated with the youngest stellar populations, followed by SNe Ib, IIb, and II.

Most of the SN environment studies used SNe compiled from various surveys, many of which were of a galaxy-targeted nature, including pointed and panoramic surveys, as well as amateur discoveries, with little or no control for biases and systematics. Such surveys are biased toward SNe discovered in bigger and therefore more metal rich galaxies, a factor that might affect the final result. Heterogeneous samples might also have classification and publication biases (see e.g., Perley et al., 2016, for a discussion on the selection biases on their analysis). Sample selection has a large effect in the analysis of SN environments, as demonstrated by, for example, Sanders et al. (2012), Galbany et al. (2016b), and Galbany et al. (2018). Sanders et al. (2012) showed that, when combining different spectroscopic measurements from the literature, SNe Ib, Ic, and IIb appear to have very similar values of metallicity, but significant differences are seen if SNe from untargeted samples are used. Galbany et al. (2018) used the PISCO SN host compilation of 232 galaxies and found similar results to Galbany et al. (2014), but also demonstrated that significant differences in the environments of the different CCSN types were found when applying an untargeted selection of host galaxies (also see Taggart and Perley 2021 and Schulze et al. 2021 for discussions on integrated properties of SN host galaxies drawn from homogeneous samples).

In our new sample, we use a homogeneous SN sample from the All-Sky Automated

Survey for Supernovae (ASAS-SN) survey, an untargeted and spectroscopically complete survey of transients, which allows us to perform a minimally biased statistical analysis of their environments. The importance of untargeted surveys can already be seen in the ASAS-SN study of SNe Ia rates as a function of host galaxy properties (Brown et al., 2019), which found no dependence of SN Ia occurrence to star formation activity in the galaxies.

In the current work (Paper I), we analyze the local environment of 112 ASAS-SN CCSNe, exploring the physical properties of HII regions centered at the SN positions. We also look for correlations between their environments and LC properties, when photometry is available. In Paper II we will fully exploit the IFU nature of our data, and compare the local environment of each SN to all the HII regions in their host galaxies. We present the sample selection and data reduction in Section 2.4. In Section 2.5, we discuss the different analysis methods used to study the physical parameters of our sample, and in Section 3.5 we present our results. A comparison of our results to previous studies and the implications for our understanding of CCSN progenitors is given in Section 2.7. Our conclusions and final remarks are presented in Section 3.7.

2.4 Sample selection and data reduction

The All-weather MUSE Supernova Integral field Nearby Galaxies (AMUSING) survey is a long-term “filler” programme that uses MUSE in suboptimal atmospheric conditions to obtain integral field observations of galaxies that hosted SNe (Galbany et al., 2016a, Galbany et al. in prep.). With a spatial sampling of 0.2×0.2 arcsec, a field of view of 1 arcmin^2 (in Wide Field Mode), and a mean spectroscopic resolution of $R \sim 3000$ with wide wavelength coverage (480 – 930 nm), MUSE is one of the most advanced Integral Field Units (IFUs) in operation.

Each semester AMUSING has focused on a different specific science case. In semesters P96 (2015 October 1 to 2016 March 31) and P103 (2019 April 1 to 2019 September 30), AMUSING observed galaxies that hosted SNe discovered or recovered by the ASAS-SN survey, with the aim of constraining differences in SN progenitor properties through studying their parent stellar populations, together with investigating the rates of SNe with respect to environmental properties. ASAS-SN started operation in 2011 (with transient

alerts beginning in 2013), with the goal of monitoring the entire sky with rapid cadence in search of nearby and bright transients (see e.g., Shappee et al., 2014; Kochanek et al., 2017, for technical details on the survey). Given the relatively shallow depth of the survey, the SNe are all relatively bright, and spectral classifications are possible in nearly all cases. This makes the survey almost spectroscopically complete, in the sense that almost all the discovered transients have an associated spectrum and classification: as of 2019, 97 per cent of ASAS-SN discoveries were spectroscopic classified (Holoien et al., 2019). ASAS-SN is also an all-sky survey that does not target particular galaxies. As shown in Holoien et al. (2019), one quarter of the SN host galaxies had no previous spectroscopic redshift estimates, and some SN hosts were not described in any existing galaxy catalog. This allows the ASAS-SN survey to serve as an ideal tool for the study of nearby SN populations, as it is not biased toward brighter and more extended galaxies. In addition, ASAS-SN discovered more SNe in the central parts of galaxies compared with previous professional and amateur surveys, again lowering observational biases (Holoien et al., 2017; Holoien et al., 2017a; Holoien et al., 2017b; Holoien et al., 2019; Neumann et al., 2023b).

Between 2013 and 2018, ASAS-SN detected a total of 449 transients that were spectroscopically confirmed as CCSNe (Holoien et al., 2017; Holoien et al., 2017a; Holoien et al., 2017b; Holoien et al., 2019; Neumann et al., 2023b). The events selected to be observed by AMUSING had a heliocentric redshift of ≤ 0.02 and an observability constraint from the Paranal observatory ($\text{DEC} \leq 25^\circ$). For the 2014 to 2017 events, only SNe with an apparent magnitude at peak luminosity of $V \leq 17.0$ mag were selected (following Holoien et al., 2017; Holoien et al., 2017a; Holoien et al., 2017b; Holoien et al., 2019), while for the 2018 events a cut on $V \leq 18.0$ mag was applied (following Neumann et al., 2023b). For the period P96, AMUSING proposed observations of 13 SNe II, four SNe IIn, and one SN Ibn. From those, eight SNe were observed (six II, one Ibn, and one IIn). For the period P103, AMUSING proposed observations of 52 SNe II, 18 SESNe, and nine interacting SNe. From those, 71 SNe were observed (47 II, seven IIb, seven IIn, five Ib, four Ic, and one Ibn). AMUSING obtains observations with different observing conditions, with variable sky transparency and seeing. The data presented here were obtained with a median seeing of ~ 0.9 . An additional 39 galaxies that hosted ASAS-SN SNe (29 II, five Ic, two IIb, one IIn, one Ibn, and one

SLSN) between 2014 and 2018 were obtained from the ESO Archive Science Portal². While using archival data could lead to biases in the final sample selection, we recalculated our results with a reduced sample only containing those SN hosts observed through AMUSING. No difference in the results were seen and thus we choose to keep the archival data in our sample.

The MUSE datacubes were reduced using the ESO reduction pipeline³ (version 1.2.1, Weilbacher et al., 2014). The pipeline applies corrections for the bias, flat-field, geometric distortions and illumination, and performs wavelength calibration and sky subtraction. All of the data obtained in P96 were reduced by the AMUSING collaboration, while data from P103 were directly obtained from the ESO Archive Science Portal (for P103, observations were processed by ESO and uploaded in semi-real time at the Science Portal). Further astrometric corrections were applied in the reduced data: the cubes were registered to the Gaia DR2 (Gaia Collaboration et al., 2018) source catalog via VizieR Queries⁴ (Ginsburg et al., 2019) and compressed in the wavelength direction to create an image and Gaussians are fit at a 10-pixel box centered at the position of all cataloged sources within the datacube field of view (FoV). Finally, the average astrometric shift is calculated and the WCS is updated. Additional flux calibration correction was achieved by producing synthetic *r*- and *i*- band images from the MUSE datacube, and comparing aperture photometry performed on the synthetic images to photometry using the same aperture from PanSTARRS (Kaiser et al., 2002; Chambers et al., 2016; Flewelling et al., 2020), SDSS (York et al., 2000), or DES (Flaugher, 2005; The Dark Energy Survey Collaboration, 2005) *r* and *i* images. The MUSE datacubes were then scaled to the fluxes to the survey values (Galbany et al. in prep.).

From our initial sample of 117 CCSN hosted by 116 galaxies (with the galaxy NGC 5962 hosting two SNe: SN 2016afa and SN 2017ivu), in three SN host galaxies (NGC 1566, NGC 6907, and ESO 560-G013) the region where the SN was located is affected by contamination due to an ionizing source other than star formation, and is therefore not useful for our analysis (see section 2.5.1 for details of our emission-line extraction and analysis techniques). This is determined by a Baldwin, Phillips, and Terlevich (BPT)-diagram (Baldwin, Phillips, and Terlevich, 1981) test (see Figure 2.12 and a description of the BPT analysis of our SN

²<http://archive.eso.org/scienceportal/home>

³<http://www.eso.org/sci/software/pipelines/>

⁴<https://astroquery.readthedocs.io/en/latest/vizier/vizier.html>

host galaxy HII regions is given in Appendix 2.10.1), where these regions fall above the Kauffmann et al. (2003) line. The galaxy NGC 3256 was also excluded from the final sample, as it contains galactic-scale outflows that could affect the interpretation of the physical properties of the environment close to the SN position (López-Cobá et al., 2020). Finally, the host galaxy of ASASSN-15lv (GALEXASC J015900.57-322225.2) was excluded, as the signal-to-noise ratio (SNR) was low for any meaningful analysis (see Section 2.5.1 for a discussion on the SNR threshold on our analysis). After these cuts we are left with 112 SNe in 111 galaxies. We did not exclude any galaxy based on its inclination and thus the sample might include highly inclined galaxies, which could include extra uncertainties to the SN environment analyses due to extinction and line of sight confusion.

Table 2.1 shows the general properties of the 112 CCSNe and their host galaxies. The SN names, types, coordinates and host galaxy names were obtained from Holoien et al. (2017), Holoien et al. (2017a), Holoien et al. (2017b), and Holoien et al. (2019), and Neumann et al. (2023b). The galaxy coordinates and Galactic extinctions were taken from the NASA-IPAC Extragalactic Database (NED)⁵, while the host *B* band absolute magnitudes were taken from HyperLeda⁶ (Makarov et al., 2014). The host redshifts were estimated using a spectrum from a 1 diameter aperture centered at the galaxy core, extracted from each datacube, using the peaks of the main emission lines (Balmer H α and H β , and [OIII] λ 5007) or the minimum of the H α and H β absorption features, and are reported in Table 2.1. The initial redshifts were converted to heliocentric redshifts by using Astropy SkyCoord⁷ and to CMB frame redshifts using the dipole coordinates from Lineweaver (1997). Table 2.2 reports the redshift estimated in the cosmic microwave background frame (z_{cmb}) and the derived luminosity distance (D_L). Since our sample comprises nearby galaxies, the D_L values were estimated using a cosmic flow model for the Local Universe (Carrick et al., 2015)⁸, assuming a flat curvature, $H_0 = 70 \text{ km s}^{-1} \text{ Mpc}^{-1}$ and $\Omega_M = 0.3$.

Figure 2.1 shows the distribution of the different CCSN types in our sample. There are 78 II, nine IIn, seven IIb, seven Ib, four Ic, three Ibn, two Ic-BL, one ambiguous Ibc (SN 2017gax has an ambiguous classification, as reported in Jha, 2017), and one SLSN. SNe II

⁵<https://ned.ipac.caltech.edu>

⁶<http://leda.univ-lyon1.fr/>

⁷<https://docs.astropy.org/en/stable/api/astropy.coordinates.SkyCoord.html>

⁸<https://cosmicflows.iap.fr/>

dominate the sample, comprising 69% of all the SNe. In the magnitude-limited sample of Li et al. (2011a), the ratio between SNe II and SESNe (including SNe IIb) was estimated to be ~ 2.0 . The same ratio in our sample is of 3.4 ± 1.9 , including the seven SNe IIb, seven Ib, four Ic, one ambiguous Ibc, and two Ic-BL. This ratio is estimated using the median of a binomial distribution, with the uncertainty given by the 90% confidence range. The ratio of 0.4 ± 0.2 between SNe Ic and Ib is lower than the estimated by Li et al. (2011a) (~ 1.6). On the other hand, the ratios of SNe II to SNe IIn (8.8 ± 1.7) and IIb (8.7 ± 1.4) are higher than Li et al. (2011a) (~ 1.9 and ~ 3.2 , respectively), indicating an underrepresentation of the latter types. We also note that low number statistics may dominate the relative numbers of all SNe other than SNe II.

In Figure 2.2 we show a comparison of 77 SNe II and their host galaxy properties in our sample to 116 SNe II from Anderson et al. (A14, 2014) and Gutiérrez et al. (G17, 2017). The latter samples are heterogeneous and comprise SNe detected and followed by a number of different surveys between 1986 and 2009. We also show a comparison with 19 SNe II to be within low-luminosity galaxies from Gutiérrez et al. (G18, 2018). The top and middle panel of Figure 2.2 show, respectively, the distribution of peak apparent and V -band absolute magnitudes of the SNe. One can see that the ASAS-SN CCSN sample is shifted to brighter magnitudes, with a median V -band apparent magnitude of 16.2 mag, as compared to the 17.3 mag for A14/G17 and 16.5 mag for G18. This could be due to ASAS-SN being a magnitude-limited survey, with a limit of detection of $V \sim 17.5$, thus discovering transients with brighter apparent magnitudes (Desai et al. in prep). Another possibility is the intrinsic differences in the SNe due to the observation selection effect. The middle panel shows that the ASAS-SN events are shifted to intrinsically brighter values, with the median absolute magnitude of the ASAS-SN being ~ -17.6 mag, while the A14/G17 and G18 samples show a median ~ -16.7 mag. Because ASAS-SN detects brighter events, making a redshift cut on the sample decreases the bias toward brightness and makes it almost complete in a given volume. The bottom panel of Figure 2.2 shows the distribution of 60 SNe II host absolute magnitudes in B band (M_B) and CMB redshifts (z_{cmb}) in our sample. The redshifts span between ~ 0.002 and ~ 0.025 , with a median at ~ 0.012 . The ASAS-SN sample is concentrated at relatively nearby host galaxies, with a median redshift slightly smaller than the A14/G17 galaxies (median ~ 0.015), but slightly larger than the G18 galaxies (median

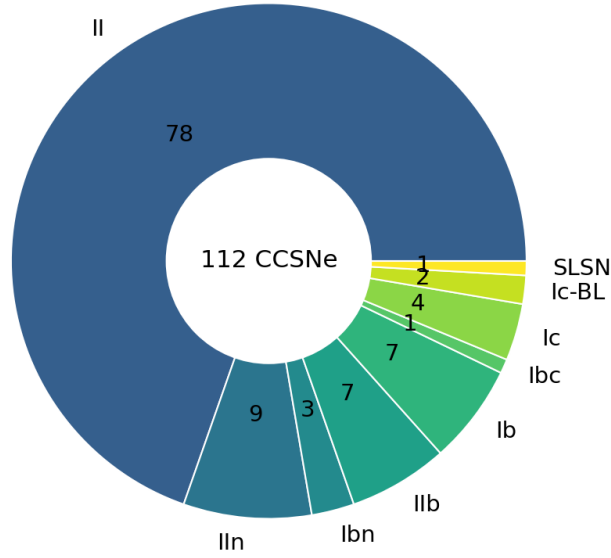


Figure 2.1: Distribution of the different SN types for the 112 events in our sample.

~ 0.011). The most important difference of the ASAS-SN CCSNe to heterogeneous and targeted samples is evident also in the bottom panel of Figure 2.2: as a heterogeneous sample, the A14/G17 SNe are biased toward brighter galaxies and do not cover the lower end of the host M_B values (with a median absolute magnitude at ~ -20.6 mag). As a targeted sample, on the other hand, the G18 sample is biased toward fainter galaxies (with a median absolute magnitude at ~ -17.7 mag). The ASAS-SN host galaxies show a more spread distribution of M_B , with values between ~ -16.5 and ~ -22.0 mag, and a median at ~ -19.6 mag. This shows the completeness of our sample in terms of galaxy brightness and size, which highlights the unbiased nature of our analysis of the CCSN environments.

2.5 Analysis

2.5.1 HII region segmentation

CCSNe are known to be generated by relatively young and massive stars, making the delay time between the progenitor formation and its explosion short enough for the star to be close to its birth site (e.g., Zapartas et al., 2017). This assumption makes the closest HII region a useful probe of the physical properties of their progenitors. We therefore analyze the HII

Table 2.1: General properties of the SNe and their host galaxies.

Name	Type ^a	RA ^b	DEC	Host Galaxy Name	z_{host}	$A_{v,MW}$ ^c	$M_{B,host}$ ^d
SN2018eog	II	20 28 11.970	-03 08 13.47	2MASS J20281135-0308096	0.01886	-	-
SN2018ant	II	08 36 31.450	-11 49 40.73	MCG-2-22-22	0.019784	0.192	-20.67
ASASSN-18oa	II	01 30 27.120	-26 47 05.98	ESO476-G16	0.019744	0.055	-20.94
SN2018bl	II	08 24 11.590	-77 47 16.55	ESO18-G9	0.017773	0.357	-20.94
SN2018evy	IIIn	18 22 38.170	+15 41 47.66	NGC6627	0.017647	0.611	-20.94
SN2018cho	IIIn	00 13 26.515	+17 29 19.57	IC4	0.016558	0.173	-20.72
SN2018ie	II	10 54 01.060	-16 01 21.40	NGC3456	0.013954	0.211	-20.76
...							

^a The entire table is available in the online version of the article and in Appendix 2.10.8. ^b All the supernova types, coordinates, and host galaxy names are taken from Holoien et al. (2017), Holoien et al. (2017a), Holoien et al. (2017b), and Holoien et al. (2019), and Neumann et al. (2023b); ^c RA and DEC are given in the J2000 epoch; ^d The Galactic extinction, $A_{v,MW}$, was taken from the NASA-IPAC Extragalactic Database (NED); ^e The host galaxy absolute magnitudes in B band, M_B , were taken from HyperLeda.

Table 2.2: Distance properties of the HII regions related to each SN.

Name	z_{cmb}	D_L (Mpc) ^a	d_{proj} (pc) ^b	r_{HII} (pc) ^c	$Area_{HII}$ (kpc ²)
SN2018eog	0.0180	79.1	0.0	460.2	5.99
SN2018ant	0.0207	91.9	0.0	534.6	3.29
ASASSN-18oa	0.0190	86.8	0.0	504.8	2.94
SN2018bl	0.0181	80.2	0.0	466.3	0.68
SN2018evy	0.0173	77.1	0.0	448.6	1.90
SN2018cho	0.0155	68.1	0.0	396.3	0.49
SN2018ie	0.0151	67.7	0.0	393.6	0.49
...					

The entire table is available in the online version of the article and in Appendix 2.10.8. ^a The luminosity distance, D_L was estimated using the CMB redshift, z_{cmb} , and a cosmic flow model for the Local Universe. ^b d_{proj} is the projected distance between the SN position and their related HII region. $d_{proj} = 0$ means that the HII region is centered at the SN position. ^c The HII region radius, r_{HII} , and area, $Area_{HII}$, are estimated from the projected size in pixels of the identified regions.

region at the SN location and use it as a proxy for the study of the direct environment around the explosion. In order to identify the distinct HII regions in each galaxy and to improve their SNR, we use the segmentation method of these regions (as used in, e.g., Galbany et al., 2016a; Lyman et al., 2018), which consists in combining the observed signal of adjacent spaxels into one region. We use IFUanal¹⁰ (Lyman et al., 2018) through the “nearest bin” method to perform HII region segmentation in the datacubes and to obtain emission line and stellar continuum fittings for the spectra in each region. IFUanal is optimized to perform HII region segmentation on MUSE datacubes. We run the code on the cubes corrected by the host redshift and Galactic extinction. The Galactic reddening correction was made using the values from Schlafly and Finkbeiner (2011) for the Milky Way toward the host galaxy.

Figure 2.3 shows the MUSE RGB image composition of the galaxy NGC 3456, located at ~ 62.9 Mpc. The galaxy hosted SN Ic 2018ie, whose position is marked by the yellow star. The top panel in the right column of Figure 2.3 shows the section of the galaxy covered by the MUSE observation. The middle panel in the right column of Figure 2.3 shows the H α map of the galaxy, and the bottom panel shows the resulting oxygen abundance in the D16 index for the segmented HII regions in the galaxy.

IFUanal segments the HII regions in the following steps: First, an H α map is produced by simulating a 30Å filter centered on the H α emission line, subtracting the continuum level and applying a Gaussian filter to avoid peaks in the noise. The code uses three main parameters

¹⁰<https://ifuanal.readthedocs.io/en/latest/index.html>

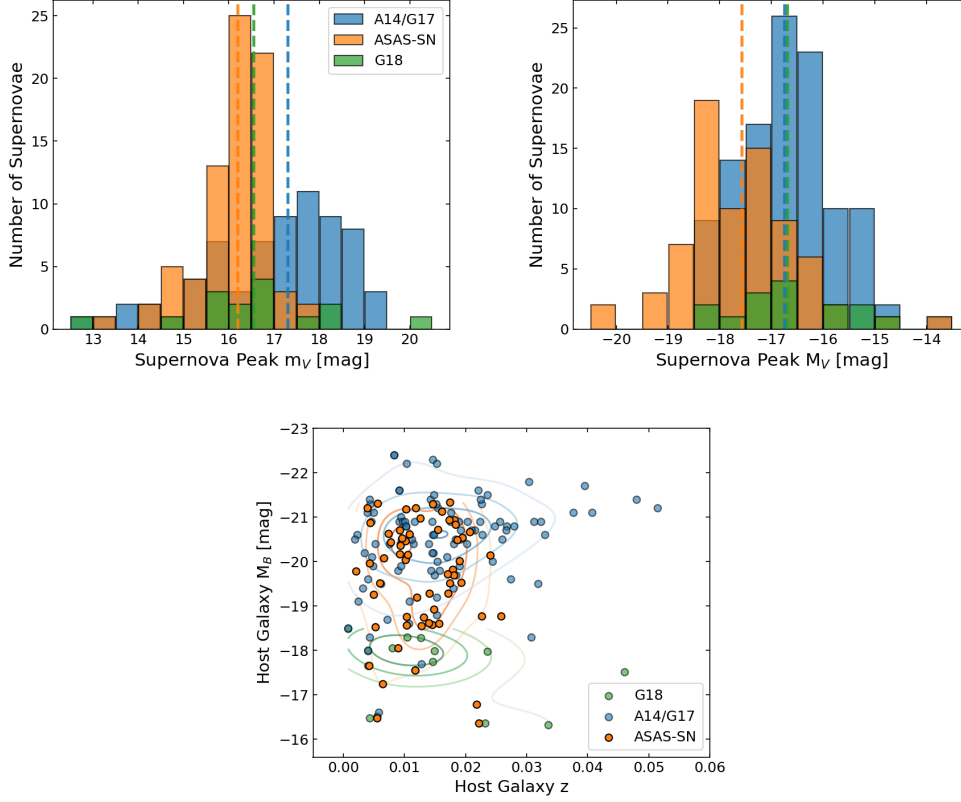


Figure 2.2: Comparison of the properties of the SNe II and their hosts in our sample to the SNe II presented in A14/G17 and G18. The top left and right panels show, respectively, the distribution of the apparent (m_V) and absolute (M_V) magnitudes in V band at peak brightness for the transients. Apparent magnitudes for the A14/G17 sample are estimated using values of M_V , distance modulus, host and Milky Way extinction provided by the authors, while for the G18 sample apparent magnitudes are estimated using the M_V and Milky Way extinction values provided in the paper. The bottom panel shows the distribution of the SN host galaxy redshift as a function of the host absolute magnitude in B band, M_B . For A14/G17 and G18, the host redshift is estimated using the recession velocity, while for the ASAS-SN sample we use the host z_{CMB} reported in Table 2.2.

to define the HII regions based on the $H\alpha$ emission map: a minimum flux threshold to define seed peaks from which the region is allowed to expand from; a maximum radius in pixels for the region size; and a maximum flux threshold. All the pixels around the brightest peak will therefore be included in the HII region up to the maximum flux or the maximum predefined distance radius. We use a minimum threshold of three times the standard deviation of the $H\alpha$ flux in a background region of the datacube, and a maximum flux of 10 times the standard deviation of the $H\alpha$ flux. We find that these parameters generate the best region segmentation and, after a series of tests with different parameters, varying the parameters around these values do not result in any significant difference in the final results (see Appendix

2.10.2).

Since the galaxies in our sample have a large range of distances ($\sim 10 - 167$ Mpc), we separate them into two groups to define the maximum radius of the segmented bins: for galaxies closer to 30 Mpc we use a maximum bin radius of 10 px, and for more distant galaxies we use a maximum bin radius of 6 px. This leads to a median bin radius size ~ 336 pc, which is similar in size to observed HII regions (see e.g., Crowther, 2013). One caveat is that the regions are circular of very similar sizes, while real HII regions have different shapes and sizes.

The spectra are averaged using an arithmetic mean, producing one spectrum for each region. STARLIGHT is used to perform stellar continuum fitting (Cid Fernandes et al., 2005; Mateus et al., 2006), with simple stellar population synthesis models from Bruzual and Charlot (2003) for the MILES spectral library (Sánchez-Blázquez et al., 2006) and using an initial mass function (IMF) from Chabrier (2003) with a mass range $0.1 - 100 M_{\odot}$. The components of the base models have ages from 1 Myr to 13 Gyr for four metallicities, $Z = 0.0004, 0.008, 0.02, 0.05$ (Lyman et al., 2018). The emission lines of the continuum-subtracted spectra were fit using multiple Gaussians. Only the emission lines with a SNR¹¹ of > 3 are fit, so their fluxes, EWs and uncertainties can be properly estimated. The uncertainty in each parameter is estimated through the propagation of uncertainties in the fittings of the individual emission lines.

For the analysis presented in this work, we selected HII regions centered at the SN positions, with most of the regions selected (90 regions) being exactly at the SN coordinates. Although an HII region is spatially coincident with a SN, there is a possibility of chance alignment due to the lack of three-dimensional information on the line of sight (see, e.g., Sun et al., 2021; Sun, Maund, and Crowther, 2023). However, it is important to note that our analysis (and in general these types of environment analyses) are statistical in nature. While the environment properties of any given SN may not be directly related to the event's progenitor properties, for a large sample of events the overall distribution of environment properties can be used to constrain the progenitors of that SN type.

For 27 of the SN locations, the signal was still dominated by the transient, with broad

¹¹The SNR is given by the ratio of the line flux estimated from a Gaussian fit and the total flux uncertainty, which is given by a combination in quadrature of the statistical and photon noise uncertainty.

lines distinct from the narrow emission features expected for the underlying HII region. Table 2.3 reports the SN names and their phase at the observation date relative to peak luminosity, given in days. We masked the region around the SN for these cases, until only narrow emission lines of the underlying HII region can be detected. The spectra for these cases are extracted from the annulus resulting from this masking.

If the fit of the extracted spectrum at the SN position has a SNR of > 3 , we extract the $H\alpha$ flux and EW, oxygen abundances, and extinction (see Section 2.5.2 for a description of the physical parameters used in this work). If the SNR is < 3 , we fit the $H\alpha$ emission profile at the SN position and use the spectrum of the nearest HII region up to a distance of 1 kpc (this was necessary for 11 regions) to derive the oxygen abundance. A total of 13 SNe have an HII region at a distance larger than 1 kpc. In these cases, we extract the spectrum at the SN position and fit the $H\alpha$ emission profile. If the SN is hosted by a dwarf galaxy, we use the oxygen abundance of the nearest HII region, as dwarf galaxies usually have homogeneous metallicity distributions (Taibi et al., 2022). If the SN is hosted by a spiral galaxy, we use the observed oxygen abundance gradient to extract the value at the SN position, as described in Appendix 2.10.3. One exception is ASASSN-14jb. Although it has a projected distance of 1.4 kpc from the nearest HII region, its explosion site was analyzed in detail by Meza et al. (2019b), who showed that the SN was consistent with a low metallicity environment similar to the outer edges of its host galaxy. Based on the arguments from Meza et al. (2019b), we use the physical properties derived from the nearest HII region for ASASSN-14jb.

2.5.2 Analysis of physical parameters

Oxygen abundance indicators

The nebular emission lines of HII regions are tracers of ionization produced by young stellar populations. Since oxygen has very strong nebular emission lines that dominate the spectra of HII regions together with H lines, its abundance can be used as a proxy to indicate the amount of metals present in the interstellar medium. One of the most commonly used methods to estimate HII region oxygen abundances is the O3N2 index, introduced by Alloin et al. (1979), which uses the $H\alpha$, $H\beta$, $[OIII]\lambda 5007$, and $[NII]\lambda 6584$ emission lines. The index was also used by Pettini and Pagel (2004), who used a calibration based on photoionization

Table 2.3: Phase of the observations relative to the SN peak luminosity, for the events that presented broad spectral features at their position.

SN	Phase (d)
ASASSN-14dp	+540
ASASSN-14jb	+391
ASASSN-14kp	+399
ASASSN-15fz	+1576
ASASSN-15lh	+424
SN2015bf	+1277
ASASSN-16at	+1208
ASASSN-16bw	+778
ASASSN-16in	+1076
ASASSN-16jt	+1064
ASASSN-16oy	+1031
ASASSN-16po	+341
SN2017ivu	+527
SN2016bmi	+538
SN2016gkg	+436
ASASSN-17is	+402
ASASSN-17je	+269
ASASSN-17jp	+394
ASASSN-17kx	+320
ASASSN-17ny	+722
ASASSN-17oj	+554
ASASSN-17qp	+667
SN2017ahn	+472
SN2017bif	+447
SN2017bzb	+780
ATLAS17hpc	+673
SN2017gmr	+338

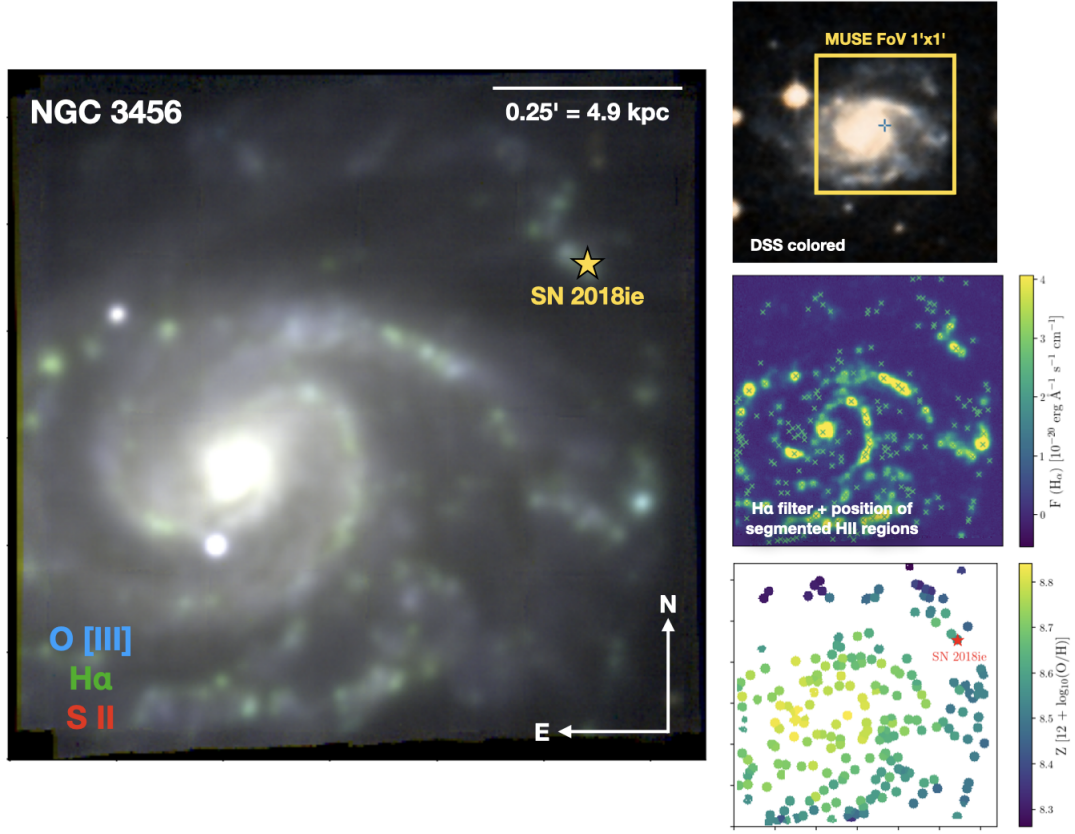


Figure 2.3: MUSE RGB image composition of the galaxy NGC 3456 where the O [III] emission is blue, $H\alpha$ is green, and SII is red. The top panel in the right column shows the MUSE pointing from where the observation of the galaxy was taken, obtained from the ESO Archive Science Portal and based on a Digitized Sky Survey (DSS) colored image of the galaxy. The galaxy is located at $z \approx 0.0142$ and hosted the SN Ic 2018ie, where its position is marked by the yellow star. The middle panel in the right column shows the $H\alpha$ luminosity, with the markers indicating all HII regions identified by IFUanal and used to obtain the other parameters from the datacube. The bottom panel reports the physical parameter map for the oxygen abundance of the segmented HII regions obtained from IFUanal.

models. Here, we use the O3N2 index calibration given by Marino et al. (2013, p. M13), who used the observations of multiple HII regions to estimate the electron temperature. The O3N2 index has the advantage of being insensitive to extinction and flux calibration, because of the similar wavelengths of the $H\alpha$ /[NII] and $H\beta$ /[OIII] line pairs.

We also use the N2 index calibration given by M13, which has been extensively studied by many authors (e.g., Storch-Bergmann, Calzetti, and Kinney, 1994; van Zee, Salzer, and Haynes, 1998; Raimann et al., 2000). The oxygen abundance given by the N2 index is defined by the line ratio between [NII] λ 6584 and $H\alpha$, again minimizing the sensitivity to reddening corrections and flux calibration. Finally, we use the oxygen abundance indicator described

in Dopita et al. (2016, p. D16). The D16 index is calibrated using photoionization models and is also insensitive to reddening. It uses the ratio between $[\text{NII}]\lambda 6584$ to $[\text{SII}]\lambda\lambda 6717, 31$ and $[\text{NII}]\lambda 6584$ to $\text{H}\alpha$ as an estimate of chemical abundance. This method provides the highest values of oxygen abundance in our analysis (see discussion in Section 2.6.1) and, as described in Dopita et al. (2016), the index model provides a good linear fit up to $12 + \log(\text{O}/\text{H}) \sim 9.05$ dex.

The uncertainties in oxygen abundances are derived from the propagation of line fitting errors from the spectra. We note, however, that each calibration index has intrinsic uncertainties of $\sim 0.1 - 0.2$ dex, as shown by Marino et al. (2013) and Dopita et al. (2016). Such uncertainties might affect the comparison between the different distributions and indicators, and are taken into account in our conclusions.

H α emission

Tracing of H α emission is a well established method to look for correlations between SN locations and the star forming regions in a galaxy (e.g., Leloudas et al., 2011; Anderson et al., 2012; Kuncarayakti et al., 2013a; Kuncarayakti et al., 2013b; Kangas et al., 2017). As demonstrated by Kennicutt (1998b), the H α luminosity alone can be used as an estimate of the recent star formation rate (SFR). Here, we use the conversion given by Kennicutt (1998b) to obtain the SFR in $\text{M}_{\odot} \text{yr}^{-1}$ from the extinction corrected H α luminosity: $\text{SFR}(\text{M}_{\odot} \text{yr}^{-1}) \simeq 7.9 \times 10^{-42} L(\text{H}\alpha)$. Because the galaxies in our sample have different sizes, we use the star formation rate surface density (ΣSFR) in order to estimate the SF intensity normalized by the physical size of each HII region, dividing the SFR at each location by the area, as reported in Table 2.2. We report the uncertainty in SFR propagated from the H α line fitting. We do not correct the H α luminosities by the host galaxy inclination. We also do not take into account the dependence of the conversion factor on the properties of the stellar populations (for example, age, metallicity, and single vs binary stars; see Eldridge et al. 2017).

The H α EW gives a measurement of the strength of the line relative to the continuum. Assuming a stellar population born at the same epoch, the contribution to the stellar population light of young and massive stars will decrease with time, decreasing the ionization of the HII region and therefore the line strength relative to the continuum emission. Consequently, the EW can be used as a tracer of the age and indicator of the level of the current SFR in an

HII region (Leitherer et al., 1999; Xiao et al., 2019). It is important to note that H α EW is subject to the photon-leakage effect and contamination from older stellar populations, which might input uncertainties in our conclusions (Xiao, Stanway, and Eldridge, 2018; Schady et al., 2019; Sun et al., 2021). We use the H α EW measurements from the Gaussian fits to the line in Section 3.5.

Extinction

We use the Balmer decrement as an indicator of the dust extinction at the line of sight, $E(B - V)_{host}$. We estimate it using Equation 3 from Domínguez et al. (2013), assuming $(H\alpha/H\beta) = 2.86$ for Case B recombination, and $k(\lambda)$ parameters obtained from a fitting to the Cardelli, Clayton, and Mathis (1989) extinction law. The extinction is extracted only from HII regions coincident with the SN position.

The values of $E(B - V)_{host}$ for the different SN host HII regions also are related to the extinction suffered by the SNe themselves. We therefore compare the values of extinction for the different CCSN types and analyze which subtype environment is more reddened, and therefore more affected by the presence of preexisting dust.

2.6 Results

In this section, we present the normalized cumulative distributions for the physical parameters of the HII regions at the SN positions. To estimate the measured errors associated to each normalized cumulative distribution, we have performed a resampling of 3×10^4 trials of each distribution, using the uncertainty associated to each parameter as one sigma of a Gaussian distribution. We also show the Kolmogorov-Smirnov (KS) statistic matrix and report the results from the Anderson-Darling (AD) tests for the combination of the different SN types at each distribution. The p -value of these tests express the statistical significance of two distributions being drawn from the same parent population. While a KS test is more sensitive to the center of the distributions, the AD test is a modification more sensitive to the tail ends of the distributions. We consider a $p \leq 0.05$ as indicating a statistically significant result. We show the measured fluxes for the different emission lines and the resulting physical parameter values in Appendix 2.10.4, and the statistics, KS and AD results for these parameters in

Appendix 2.10.5.

We first separate the CCSNe into types II, IIb, Ib, Ic (including SNe Ic-BL), IIn (including ASASSN-16jt, classified as a SN 2009ip-like event), and Ibn, based on their spectroscopic classification from Table 2.1. In order to make a more statistically significant analysis, we also group the CCSNe into three different groups: SNe II, consisting of the 78 II; SESNe, including the four Ic, two Ic-BL, seven IIb, seven Ib, plus SN 2017gax, classified as an ambiguous SN Ibc; and IIn/Ibn SNe, including the nine IIn and three Ibn

Because SN 2015bn is classified as a SLSN, it does not belong to any of the other subtypes. As it is one single event, it cannot be included in the statistical analyses used for the other groups. Therefore, we present an analysis of its environment in Appendix 2.10.6, and make a comparison with the results for the other subtypes of CCSNe presented in this section.

2.6.1 Oxygen abundance

Figure 2.4 shows the cumulative distributions of the oxygen abundances for the HII regions. In Appendix 2.10.5, Tables 2.7, 2.8, and 2.9 present the median and average values, the KS test results, and the AD test results, respectively. SNe Ic, IIb, and Ibn have the highest median metallicity values for all three indicators, while SNe II have the lowest median value for the D16 index, SNe IIn for the N2 index, and SNe Ib for the O3N2 index. The D16 indicator leads to the largest range of oxygen abundance values (going from $12 + \log(\text{O}/\text{H}) \sim 7.6$ dex to ~ 9.2 dex). This index also provides a KS p -value ~ 0.05 between SNe Ic and II, suggesting a statistically significant difference. The other comparisons between the CCSN distributions do not show statistically significant differences. No comparisons between the different types show statistically significant difference for the N2 and O3N2 indexes.

In Figure 2.5, we show the cumulative distributions the CCSNe grouped into SNe II, SESNe, and IIn/Ibn. The SESN events have the higher median metallicities for all three indexes. None of the indicators show any statistically significant differences.

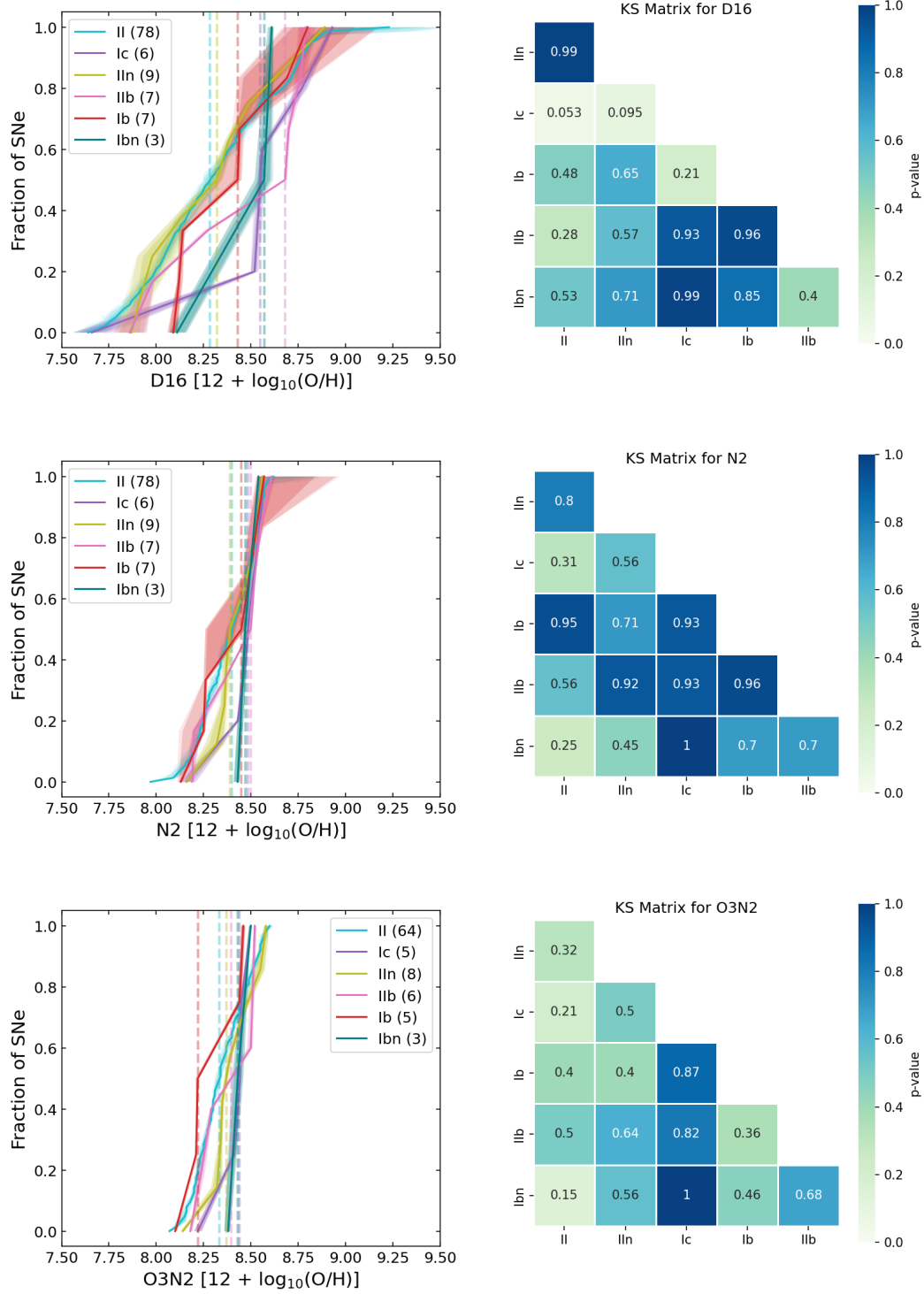


Figure 2.4: Cumulative distributions for the D16, N2, and O3N2 oxygen abundance indicators of the different types of CCSNe. The right column shows the Kolmogorov-Smirnov (KS) statistic matrix for the combination of the different SN types. The legend gives the number of SNe used in each distribution and the median oxygen abundance is marked as the dashed line. The color scale and the matrix values report the KS p-values.

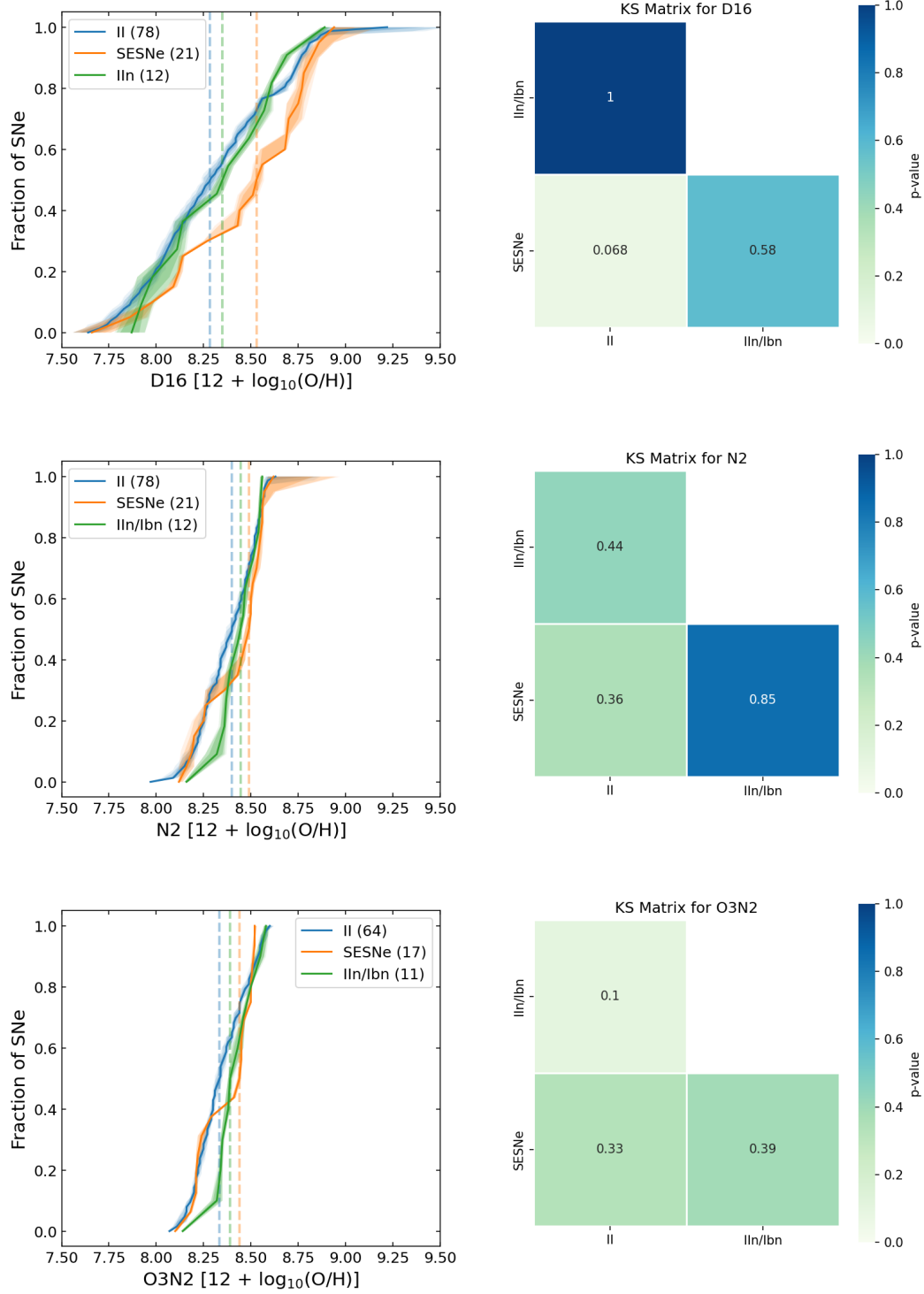


Figure 2.5: Cumulative distributions for the D16, N2, and O3N2 oxygen abundance estimates of the CCSNe grouped as SNe II, SESNe, and IIIn/Ibn. The right column shows the Kolmogorov-Smirnov (KS) statistic matrix for the combination of the different SN types.

2.6.2 H α equivalent width

Figure 2.6 shows the cumulative distributions of the H α EW for the different CCSN types. The median and the average of each distribution, their KS test and AD test values are in Tables 2.10, 2.11, and 2.12, respectively. In the top panel of Figure 2.6, we see that SNe Ic have the highest median H α EW (221 ± 9 Å), followed by SNe IIb and Ib (139.8 ± 8 Å and 87.2 ± 12 Å, respectively). SNe Ibn show the lowest median H α EW (45 ± 11 Å), although only three events are considered in the analysis and chance alignment with older stellar populations cannot be excluded. The KS test values between the different distributions are not statistically significant, with the resulting KS test p-value between the SNe II and Ic being ~ 0.1 . However, the AD test shows a significance value of ~ 0.03 between the SNe II and Ic, suggesting a statistically significant difference between the distributions.

When we group the different types as SNe II, SESNe, and IIn/Ibn, in the bottom panel of Figure 2.6, SESNe show a higher median of H α EW (109 ± 5 Å) than the other subtypes. The KS test shows a statistically significant difference between SNe II and SESNe, with a p-value ~ 0.03 . The AD test also shows a statistically significant difference between SNe II and SESNe, with a significance value of ~ 0.005 .

As can be seen in Figure 2.6, one event has a very large H α EW: SN 2016cdd, a SN Ib, with an H α EW of 995 ± 20 Å. SN 2016cdd is a regular SN Ib, with He I absorption features and is similar to the prototypical SN 1999dn (Qiu et al., 1999; Hosseinzadeh et al., 2016). Although this appears to be a common example of a SN Ib, it is associated to a very high value of H α EW, suggesting an association with very young stars and very recent episodes of star formation. Finally, a chance alignment of the SN with a very recent star-forming region cannot be excluded.

2.6.3 Star formation rate

The top panel of Figure 2.7 shows the cumulative distributions of Σ SFR for the different CCSN types. The median and the average of each distribution, their KS test and AD test values are reported in Tables 2.13, 2.14, and 2.15, respectively. The SNe Ic have the highest median $\log_{10}\Sigma$ SFR (-1.11 ± 0.50 M $_{\odot}$ yr $^{-1}$ kpc $^{-2}$), with no associated HII regions having $\log_{10}\Sigma$ SFR ≤ -3 M $_{\odot}$ yr $^{-1}$ kpc $^{-2}$. SNe IIn have the smallest median value

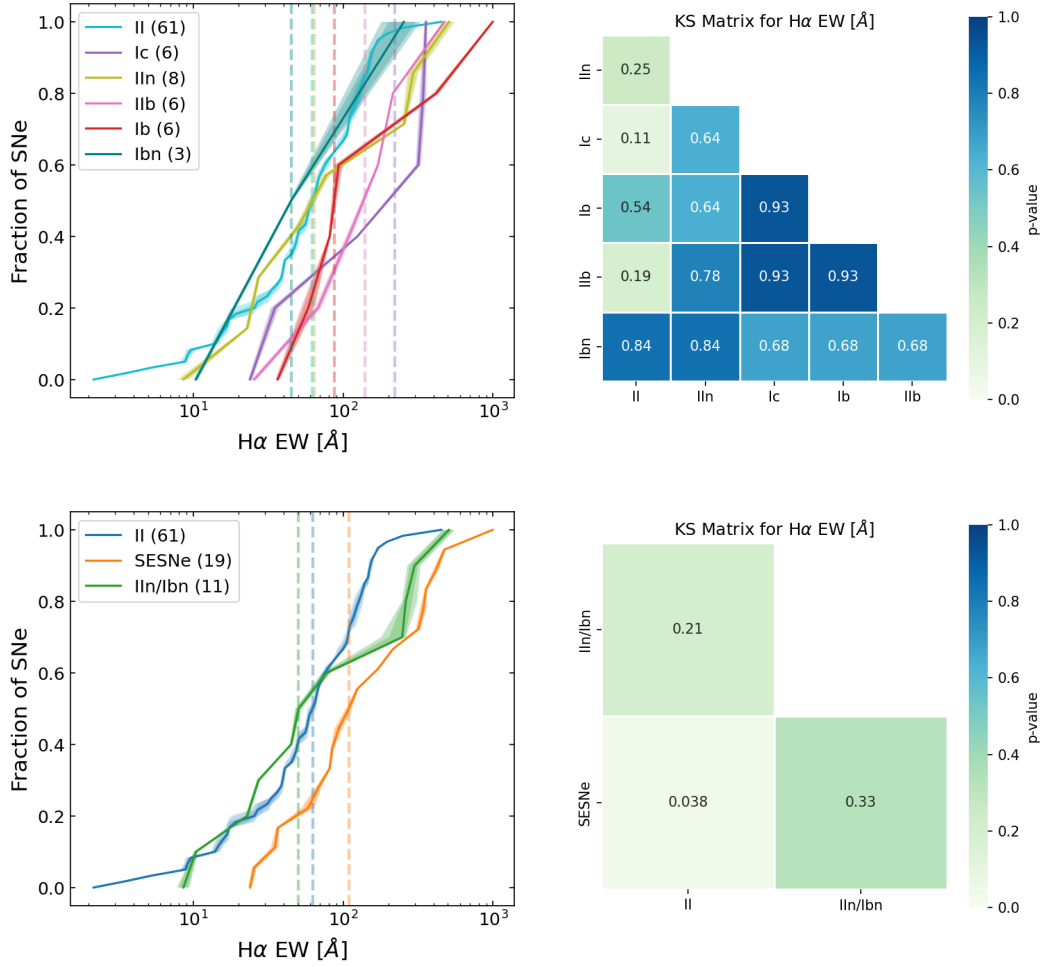


Figure 2.6: Cumulative distributions of the H α EW of the HII regions at the SN locations. The top row shows the distribution for all the SN types, while the bottom row shows the distribution for the types grouped into SNe II, SESNe, and IIn/Ibn. The Kolmogorov-Smirnov (KS) statistic matrix is shown in the right column.

($-2.13 \pm 0.17 \text{ M}_{\odot} \text{ yr}^{-1} \text{ kpc}^{-2}$), followed by SNe Ibn ($-1.97 \pm 1.0 \text{ M}_{\odot} \text{ yr}^{-1} \text{ kpc}^{-2}$). Based on the KS and AD tests the differences are not statistically significant.

The differences between SNe II, IIn/Ibn, and SESNe are clearer in the bottom panel of Figure 2.7. The SESNe have the highest values of ΣSFR , with a median of $\log_{10}\Sigma\text{SFR} = -1.27 \pm 0.23 \text{ M}_{\odot} \text{ yr}^{-1} \text{ kpc}^{-2}$. The KS and AD tests show no statistically significant difference.

2.6.4 Extinction

In the top panel of Figure 2.8 we show the cumulative distributions for the host extinction for the different CCSNe, and report the median and average of each distribution, the KS

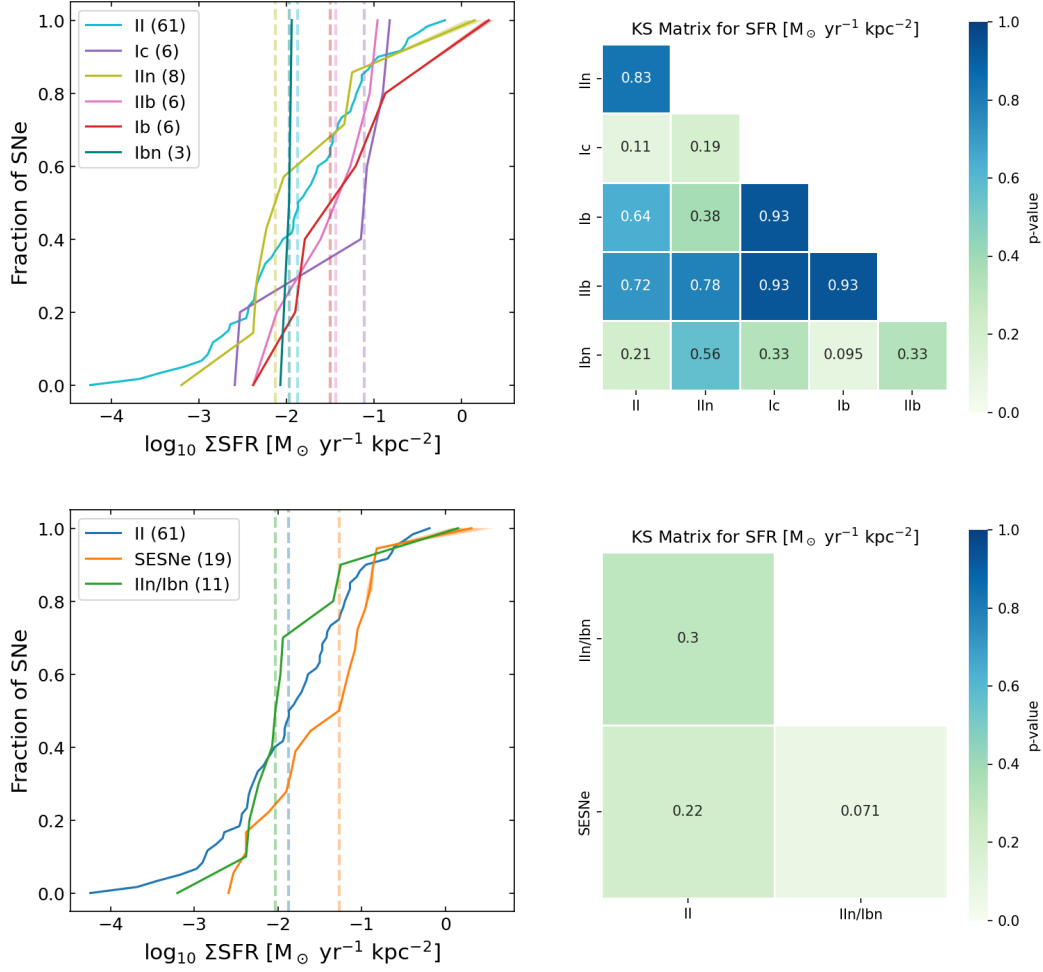


Figure 2.7: Cumulative distributions of the star formation rate surface density (ΣSFR) of HII regions at the SN locations, for the different SN types, and for the types grouped into SNe II, SESNe, and IIIn/Ibn. The right column shows the Kolmogorov-Smirnov (KS) statistic matrix.

and AD test values in Tables 2.16, 2.17, and 2.18, respectively. The extinctions have values up to ~ 1 mag, with a SN Ic having the highest value and the SNe IIb having the highest median of 0.32 ± 0.3 mag (although it has a large uncertainty associated). SNe Ib and Ic have the same median value for their distribution (~ 0.20 mag) and SNe II have a similar median (0.23 ± 0.1 mag). However, the differences are not statistically significant.

Grouping the different SN types does not produce a more statistically significant result, as it is shown in the bottom of Figure 2.8. The SNe II, SESNe, and IIIn/Ibn have very similar median values, ~ 0.23 , ~ 0.22 , and ~ 0.26 mag, respectively.

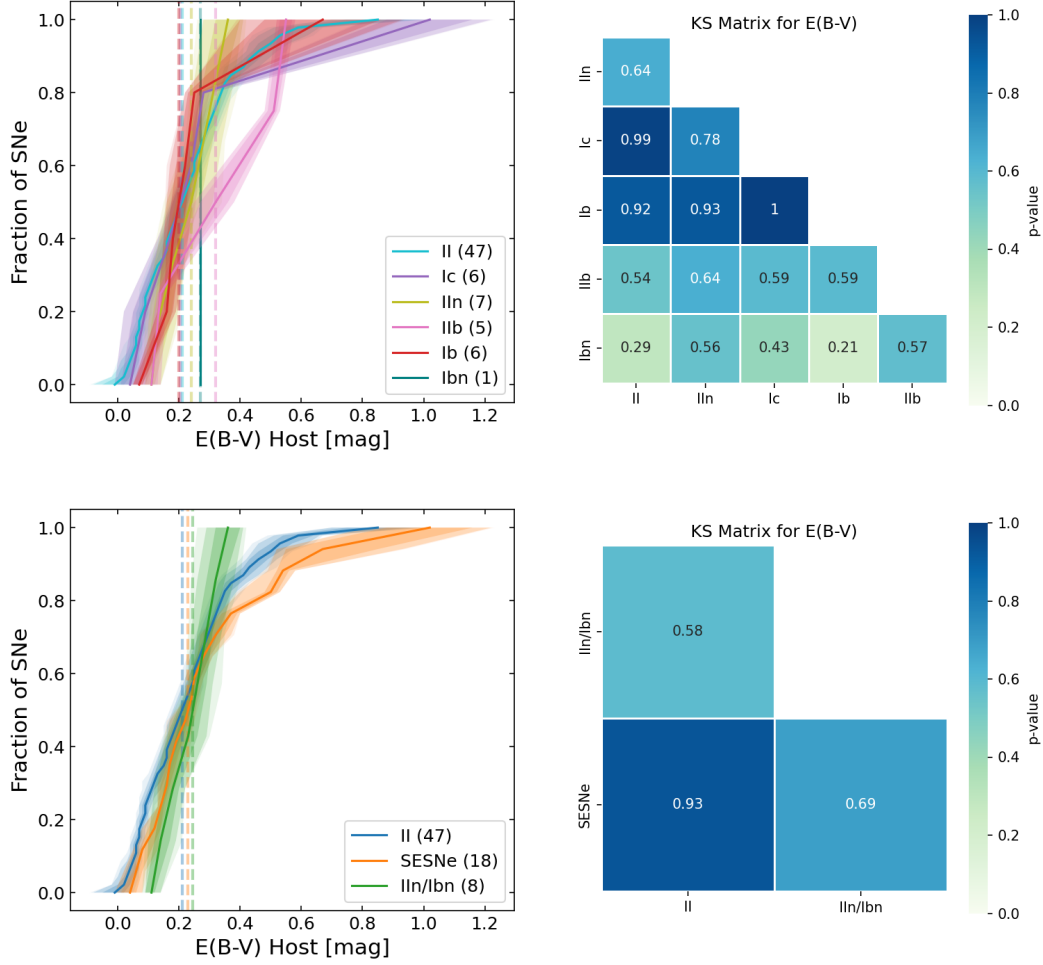


Figure 2.8: Cumulative distributions of the line of sight extinction $E(B - V)$, estimated from the Balmer decrement. The top row shows the distributions for the different types of CCSNe, while the bottom row shows the distributions for the CCSNe grouped into SNe II, SESNe, and IIn/Ibn. The right column shows the Kolmogorov-Smirnov (KS) statistic matrix.

2.7 Discussion

2.7.1 Constraints on progenitor properties

As discussed in the introduction, other studies of SN environments with larger samples have been achieved, but most of them have the major drawback of selecting SNe from targeted surveys, or selecting a sample with little or no control for systematics and biases. This might have an important effect in the final results, since these studies are focused on more massive and more metal rich galaxies, while also combining selection effects from many different SN search surveys.

We find in Section 3.5 that SESNe are associated with larger median $H\alpha$ EW, ΣSFR ,

and oxygen abundances than SNe II and II_n/Ib_n, and that SNe Ic have larger values of these parameters than SNe Ib and IIb. Although this could indicate that SESNe come from younger, more massive and more metal rich stars than SNe II and II_n/Ib_n, the differences between the distributions are not statistically significant in most cases, suggesting that any difference in progenitor properties is not large.

For the different CCSN subtypes, we see a decreasing trend in median values of H α EW and Σ SFR as Ic \rightarrow IIb/Ib \rightarrow II/Ib_n/II_n. We found a statistically significant difference only between SNe Ic and II for H α EW. This suggests that SNe Ic are associated to the youngest and more star-forming stellar populations, while SNe II and II_n are related to the oldest and less star-forming populations between the CCSNe. This relation also shows that SNe Ic are associated to younger and more star-forming stellar population than SNe IIb and Ib, pointing to differences in progenitor age and mass-loss mechanisms. Similar results were also found by other previous analyses (see, e.g., Anderson and James, 2008; Sanders et al., 2012; Anderson et al., 2012; Galbany et al., 2014; Habergham et al., 2014; Galbany et al., 2018; Kuncarayakti et al., 2018). Again, we note that the differences in H α EW and Σ SFR between the CCSN subtypes are not large, as no statistically significant result was found for most cases. We also note the large intrinsic errors in the measured Σ SFR.

In the analysis of oxygen abundance, we see a decreasing trend of median values as Ic/IIb/Ib_n \rightarrow Ib \rightarrow II/II_n in the D16 and N2 indexes, and Ic/IIb/Ib_n \rightarrow II/II_n \rightarrow Ib in the O3N2 index. These results suggests that SNe Ic are related to the more metal-rich environments, while SNe II and II_n are associated to the less metal-rich regions within CCSNe. This also suggests that SNe Ic and IIb are associated to stellar populations with higher metal content than SNe Ib. However, the only statistically significant differences found were in the D16 index between SNe II and Ic. The lack of statistically significant differences in the N2 and O3N2 indexes suggests that the metallicity differences in the environments of the different CCSN subtypes is not large. We also note that the large intrinsic errors associated to the oxygen abundance calibrators might input uncertainties in this analysis. Although previous studies found significant differences in the environment metallicity of SNe II and SESNe (see, e.g., Prantzos and Boissier, 2003; Boissier and Prantzos, 2009; Prieto, Stanek, and Beacom, 2008; Arcavi et al., 2010; Modjaz et al., 2011), recent analyses have shown that such differences might not be large. Galbany et al. (2016b) and Galbany et al. (2018) showed

that no difference in the metal content of SN environments is seen when using a targeted sample, but that significant differences arise when taking host galaxies from untargeted searches. By using the integrated properties of SN host galaxies, Schulze et al. (2021) found no significant differences in the galaxy mass (related to metallicity) and SFR for the different CCSN types, although they show that SNe Ibc prefer galaxies with slightly higher masses and SFR than SNe II and IIb.

Rotating single star models predict that SNe Ib should be generated by stars in the range of $20\text{--}40\text{ M}_{\odot}$, while SNe Ic should arise from progenitors with masses greater than 40 M_{\odot} , at solar metallicity (Georgy et al., 2009). Binary population models predict that SNe originating in such systems would require less massive progenitor stars for the envelope stripping (e.g., Eldridge, Izzard, and Tout, 2008). However, recent binary models show that a thin layer of hydrogen is still present after Roche-lobe overflow in these systems, making it hard for the stars to lose their deeper helium layer (Yoon, 2017). Other recent results propose a hybrid mass-loss mechanism, with both binary interaction and strong winds playing a role (Fang et al., 2022; Sun, Maund, and Crowther, 2023). Our results suggest that SNe Ic have a higher chance to be originated by more massive and more metal-rich stars than SNe Ib, either in single or binary systems.

We find that SNe IIb are related to slightly younger and star-forming regions than SNe II and Ib, and with values of oxygen abundance higher than these types. Previous studies either report SNe IIb environments older than (e.g., Anderson et al., 2012; Kuncarayakti et al., 2018; Maund, 2018) or similar to (e.g., Kangas et al., 2013; Sun, Maund, and Crowther, 2023) SNe Ib. The fact that the progenitors of SNe IIb are in a similar age and mass range to SNe II might suggest that their progenitors are predominantly in binary systems, as they would not be massive enough to lose their envelopes through single-star winds. Another possibility is that SNe IIb come from a mixture of progenitors with different metallicities and mass ranges.

We have shown that SNe IIn/Ibn have very similar $H\alpha$ EW, SFR, and oxygen abundances to SNe II. Given the large amount of material ejected by these events, a massive progenitor (LBVs in the case of SNe IIn and massive WRs for SNe Ibn) is expected to generate such strongly interacting transients. However, lower mass progenitors could also generate SNe IIn, such as RSG with superwinds or static CSM shells close to the star (e.g., Fransson et al.,

2002; Smith, Hinkle, and Ryde, 2009). Other analyses of the environments of SNe IIn also found no association to more metal rich or more younger stellar populations, showing very similar properties to normal SNe II (Taddia et al., 2013; Anderson et al., 2012; Kangas et al., 2017; Kuncarayakti et al., 2018). Galbany et al. (2018), however, showed that the age distributions of SNe IIn had a bimodal distribution, and Ransome et al. (2022) also found a bimodal distribution of progenitors associated to younger and older stellar populations. Recent studies of SNe Ibn also show that they could be associated to older stellar populations (e.g., Shivers et al., 2017; Sun et al., 2020), in agreement with our results (although we note the low number of SNe Ibn in our sample).

Finally, we have shown that the CCSNe have similar values of host galaxy extinctions, with a median extinction ~ 0.2 mag for most of the subtypes, although SNe Ib have a slightly larger median. This is similar to what was found by Drout et al. (2011) and Sanders et al. (2012). Kelly and Kirshner (2012) found that SNe Ib and Ic have significantly higher values of host extinction than SNe II and IIb. Galbany et al. (2017) also demonstrated that SESNe have a larger dust reddening and HII column density than SNe Ia and II. Sanders et al. (2012) showed that the hosts of SESNe do not have any significant difference in extinction between themselves, but Kelly and Kirshner (2012) found that SNe Ib and Ic have significantly higher values of host extinction than SNe II and IIb.

2.7.2 Environment versus light curve properties

CCSNe display a variety of properties in their LCs that are directly connected to the evolution of their progenitor stars and explosion properties. Properties such as the hydrogen envelope mass, progenitor radius, explosion energy and ejected ^{56}Ni affect the observed luminosity, duration and shapes of their LCs (e.g., Kasen and Woosley, 2009; Bersten, Benvenuto, and Hamuy, 2011). By analyzing 116 V-band LCs of SNe II, Anderson et al. (2014) showed that they display a large range of decline rates, and that the decline rate is directly proportional to the magnitude at peak luminosity. Their results also suggest that fast-decliner SNe II have lower ejected masses. Recently, Martinez et al. (2022) found that SNe II with higher luminosity have higher ^{56}Ni masses and that faster declining events have a more centrally concentrated ^{56}Ni distribution. Martinez et al. (2022) also concluded that the explosion energy was the property that dominates the SN LC diversity. G18 looked for correlations

between the LC parameters and the environments of SNe II in low-luminosity host galaxies, and concluded that this sample had slower declining LCs than events in higher-luminosity galaxies. G18 however found no correlation between the plateau duration or the explosion energy of the Type II SNe with the metallicity at their environments.

Recent analyses of SESNe LCs have shown that they are characterized by relatively small ejecta masses and explosion energies (Cano, 2013; Taddia et al., 2015a; Lyman et al., 2016; Prentice et al., 2016). Since the LCs of these events are powered by radioactive decay, the amount of ^{56}Ni synthesized in the explosion is directly proportional to the observed peak luminosity. In a study of 34 SESNe, Taddia et al. (2018) showed that the Δm_{15} parameter, the brightness difference between the peak and 15 days later, is correlated with the slope of the LC during its linear decay and with the peak absolute B -band magnitude.

Observations of SNe IIn have shown that they have very heterogeneous spectra and LCs (Taddia et al., 2013). Due to interaction with CSM, SNe IIn can stay bright for a much longer period than normal SNe, and the geometry of the CSM may drive further LC diversity. Taddia et al. (2015b) proposed a grouping of SNe IIn based on the similarities with the prototypical SN 1988Z (Turatto et al., 1993), SN 1994W (Sollerman, Cumming, and Lundqvist, 1998), and SN 1998S (Fassia et al., 2000), and found that 1998S-like SNe show higher metallicities than the other events. Nyholm et al. (2020) analyzed the LC parameters of a sample of 42 SNe IIn and found that they could be divided into two groups with distinct rise times, and that more luminous events are also the more long-lasting.

Here, we look for correlations between the environment and the explosion properties of the SNe in our sample. We compare the LC properties to the derived physical properties of $\text{H}\alpha$ EW, ΣSFR , and oxygen abundance. We expand the study presented in Galbany et al. (2018) and make this analysis using the LCs of 64 SNe II, eight SESNe, and ten SNe IIn (because only one SN IIn in our sample has good photometry coverage, this type is not included in this work). For most SNe, we use BVR photometry obtained by ASAS-SN or the follow-up observations obtained with the Las Cumbres Observatory (LCO) telescopes (for a in depth discussion on ASASSN photometry, see Kochanek et al., 2017). In a few cases for which ASAS-SN photometry is not available we use other published photometry, such as for ASASSN-14jb (Meza et al., 2019a), SN 2014cy, SN 2014dw, SN 2015W (Valenti et al., 2016), and SN 2017gmr (Andrews et al., 2021). We characterize the LCs of SNe II using the

magnitude at peak luminosity and the decline slope, s , similar to what was used by Anderson et al. (2014) and Galbany et al. (2016c). For SESNe, together with the magnitude at peak luminosity, we also use the Δm_{15} parameter, first defined by Phillips (1993) in the study of SNe Ia. For SNe IIn, we only characterize their LCs with the magnitude at peak luminosity. As noted before, our sample is composed of intrinsically bright SNe, due to the magnitude-limited nature of ASAS-SN. Therefore, this analysis is biased toward including brighter events at the expense of fainter events, and fainter SNe could present distinct correlations between their LCs and environments.

The LC parameters are given in Appendix 2.10.7, in Tables 2.19, 2.20, and 2.21 for SNe II, SESNe, and IIn, respectively. We show how the LCs and environment parameters are related to each other in Figures 2.9, 2.10, and 2.11. To define the possible correlation between the parameters analyzed, we use the Pearson test factor and p -value of the distributions. We find a correlation for the postmaximum decline slope, s , in the B and r bands with the H α EW for SNe II. The resulting Pearson test factors for these correlations were $(B, V, r) = (0.63, 0.33, 0.86)$ (p -value = 0.06, 0.07, 0.004). However, only a few SNe II could have the s parameters derived from their LCs in the B and r bands, leading to low-number statistics. In contrast to Galbany et al. (2018), no significant correlation is found between the SFR and the V -band postmaximum decline slope for SNe II.

For SESNe, correlations are found between the B -band magnitude at maximum luminosity and H α EW, with a Pearson correlation factor of ~ 0.99 (p -value ~ 0.06) and small correlations are found between the B -band Δm_{15} parameter to Σ SFR and H α EW, with Pearson correlation factors ~ 0.97 (although with a nonstatistically significant p -value ~ 0.1) and 0.98 (p -value ~ 0.09), respectively. Small correlations are also found between M_{peak} and the oxygen abundance, with Pearson test factors of $(B, V, r) = (0.5, 0.5, 0.76)$ (p -value = 0.1, 0.4, 0.2) for the D16 index. This suggests that the production of synthesized ^{56}Ni in these explosions might be connected to the age of their parent stellar population, with events that produce more ^{56}Ni occurring in the oldest and less star-forming regions. This also suggests a connection of their metal abundance to ^{56}Ni production, with events in lower metallicity regions producing more ^{56}Ni than events in higher metallicity environments. We also note that low-number statistics bring a significant caveat to this analysis. A similar result was found for SNe Ia, as higher metallicity leads to more production of ^{58}Ni instead of ^{56}Ni (for

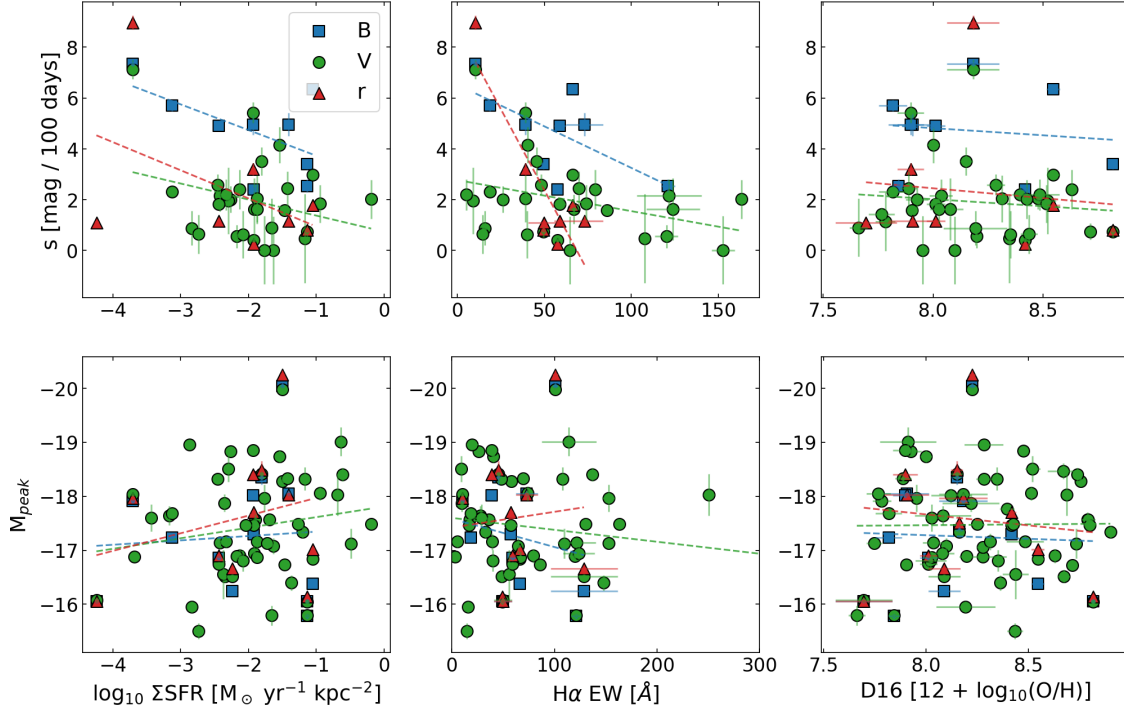


Figure 2.9: SNe II postmaximum brightness decline rate (s) and absolute magnitude at peak (M_{peak}) in B , V , and r bands, as a function of ΣSFR (left), $\text{H}\alpha$ EW (middle), and the oxygen abundance given by the D16 indicator (right).

a recent description on SNe Ia modeling, see e.g., Bravo, Badenes, and Martínez-Rodríguez, 2019). However, we note that all of these results suffer from low-number statistics, and thus additional events are required to test the robustness of any correlations observed.

For SNe IIn, no correlation is found between M_{peak} and the environment. Again, such an analysis might be suffering from small number statistics, and more observations of SNe IIn are required to enable stronger conclusions.

2.8 Conclusions

In this work, we analyzed 112 CCSN environments observed with the MUSE instrument on the VLT. By using a untargeted sample of galaxies that hosted CCSNe detected by the ASAS-SN survey, we were able to make a minimally target-biased analysis of their environments, with a larger control of survey selection systematics than previous studies. We used the HII regions centered at the SN positions to derive physical properties of their environments, such as $\text{H}\alpha$ EW, ΣSFR , oxygen abundance, and host extinction. Our main results can be summarized as follows:

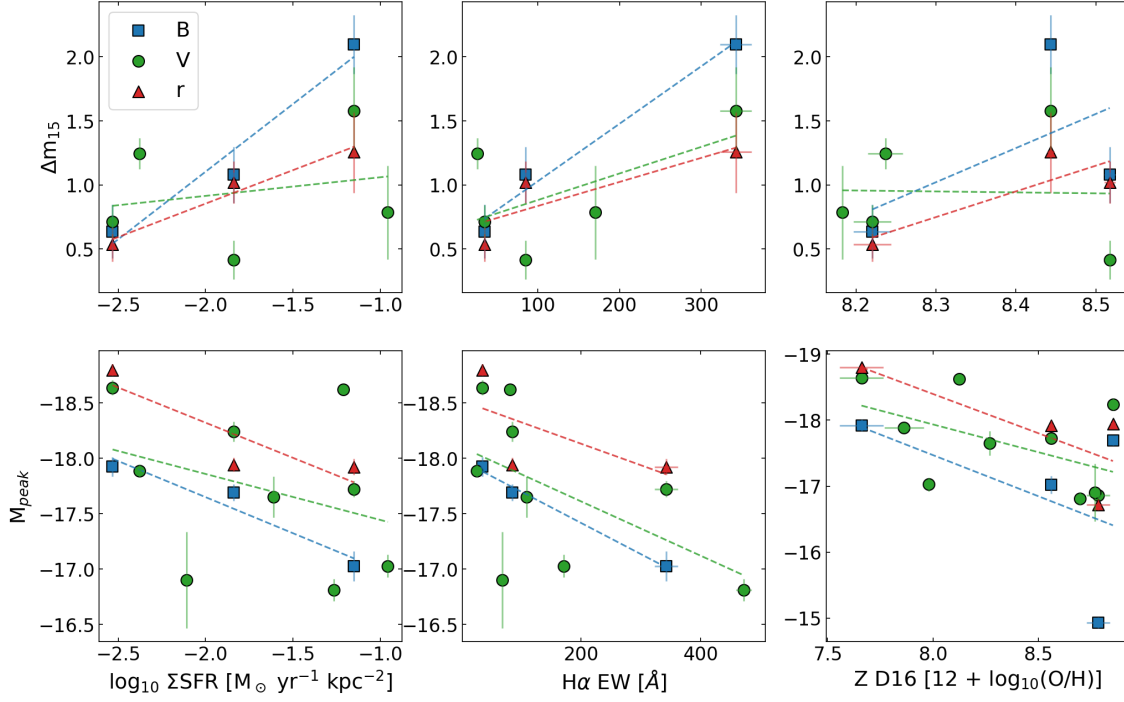


Figure 2.10: Brightness difference between peak and 15 days later and absolute magnitude at peak (M_{peak}) for SESNe in B , V , and r bands, as a function of ΣSFR (left), H α EW (middle), and the oxygen abundance given by the D16 indicator (right).

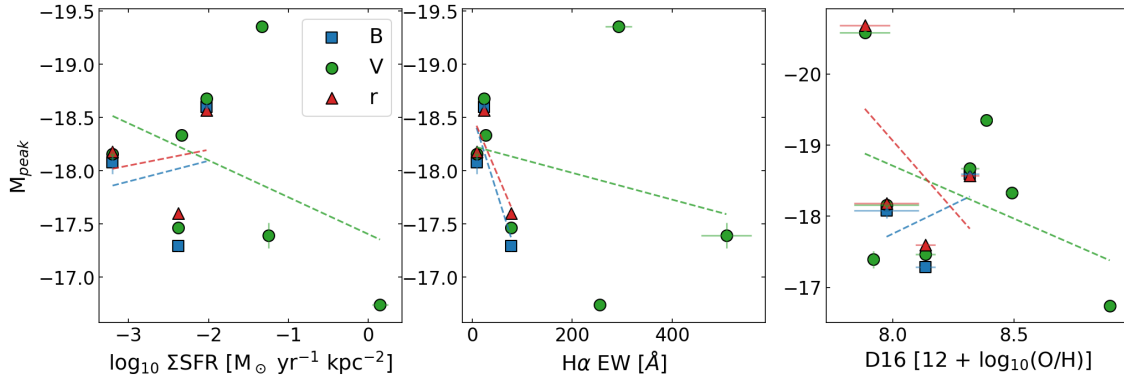


Figure 2.11: SNe IIn absolute magnitude at peak (M_{peak}) in B , V , and r bands, as a function of ΣSFR (left), H α EW (middle), and the oxygen abundance given by the D16 indicator (right).

- SESNe occur in environments with higher median H α EW, ΣSFR , and oxygen abundance than SNe II and IIn/Ibn. However, a statistically significant difference between the cumulative distributions is found only for H α EW between SNe II and SESNe and for oxygen abundances in the D16 index between SNe II and Ic.
- Within SESNe, SNe Ic show higher median SFR, H α EW, and oxygen abundance than SNe Ib, although no statistically significant difference between the distributions is

found. This could suggest that SNe Ic are produced by higher mass and more metal rich progenitors than SNe Ib.

- The environments of SNe IIb have similar median $H\alpha$ EW and SFR to SNe Ib SNe, and similar oxygen abundance medians to SNe Ic.
- The properties of SNe Ic are consistent with higher mass and higher metallicity progenitors, while SNe Ib might be connected to lower mass and lower metallicity populations. SNe IIb are consistent with relatively lower mass progenitors in higher metallicity environments, but a mixture of single stars and binary systems might be possible.
- SNe IIn have similar distributions to SNe II, suggesting that they occur in environments with similar physical properties. SNe Ibn have a median oxygen abundance similar to SNe IIb and Ic, and Σ SFR similar to SNe IIn.
- The distributions of host-galaxy extinctions are very similar for the different CCSN types, suggesting that different CCSN types suffer from similar degrees of host extinction.
- For SNe II, a correlation was found between the postmaximum decline rate in B and r bands to $H\alpha$ EW, with faster-declining events happening in environments with lower $H\alpha$ EW. However only a few points are used in this analysis. No further correlation of LC properties of SNe II to their environments was found.
- For SESNe, weak correlations are found between B -band peak magnitude and Δm_{15} to $H\alpha$ EW and Σ SFR. Brighter events seem to occur in environments with lower $H\alpha$ EW and Σ SFR, and SESNe with higher Δm_{15} are connected to higher $H\alpha$ EW and Σ SFR. The BVr peak luminosity of SESNe is also weakly correlated to the oxygen abundance at their environments, with brighter events happening in locations with less oxygen content. This suggests an intrinsic relation between the metal content, the star formation intensity, and stellar age at the environments of SESNe and the amount of synthesized ^{56}Ni .

Although some contrasts to previous results are found in this work, this represents the most homogeneous sample of CCSN host galaxies to date. The low number statistics in

our sample (specially for SESNe) might also have contributed to such differences. We aim to complement this analysis with new observations of SESN and SNe IIn/Ibn host galaxies obtained with MUSE, which will give more statistical significance to the study of the environments of these events.

As a legacy of this work, all the resultant physical parameter maps derived for the analyzed galaxies are available online¹² or under request to the corresponding author.

Following the results presented here, Paper II will present a global analysis and characterization of all star-forming regions within the CCSN host galaxies within our sample. Comparing SN host HII region environment properties to all other HII regions within their galaxies - and indeed the full sample of galaxies - one can ask whether different SN types prefer to explode from, for example, lower or higher metallicity star forming regions. As a future work, we aim to use the data and physical quantities derived here to estimate the relative rates of the different CCSN types as a function of their environment properties, which will help in constraining the mass ranges of their progenitor stars.

2.9 Acknowledgements

Based on observations collected at the European Southern Observatory under ESO programme(s): 096.D-0296 (A), 0103.D-0440 (A), 096.D-0263 (A), 097.B-0165 (A), 097.D-0408 (A), 0104.D-0503 (A), 60.A-9301 (A), 096.D-0786 (A), 097.D-1054 (B), 0101.C-0329 (D), 0100.D-0341 (A), 1100.B-0651 (A), 094.B-0298 (A), 097.B-0640 (A), 0101.D-0748 (A), 095.D-0172 (A), 1100.B-0651 (A), 0100.D-0649 (F), 096.B-0309 (A).

This work makes use of the following softwares: ESO reduction pipeline (Weilbacher et al., 2014), EsoReflex (Freudling et al., 2013), CosmicFlows (Carrick et al., 2015), Astropy (Astropy Collaboration et al., 2013), SciPy (Virtanen et al., 2020), HyperLEDA (Makarov et al., 2014), VizieR Queries (Ginsburg et al., 2019), and IFUanal (Lyman et al., 2018).

This research has made use of the NASA/IPAC Extragalactic Database (NED), which is funded by the National Aeronautics and Space Administration and operated by the California Institute of Technology. T.P. acknowledges the support by ANID through the Beca Doctorado Nacional 202221222222. J.L.P. acknowledges support by ANID through the Fonde-

¹²<https://sites.google.com/view/theamusingasassnsample>

cyt regular grant 1191038 and through the Millennium Science Initiative grant ICN12_009, awarded to The Millennium Institute of Astrophysics, MAS. L.G. acknowledges financial support from the Spanish Ministerio de Ciencia e Innovación (MCIN), the Agencia Estatal de Investigación (AEI) 10.13039/501100011033, and the European Social Fund (ESF) "Investing in your future" under the 2019 Ramón y Cajal program RYC2019-027683-I and the PID2020-115253GA-I00 HOSTFLOWS project, from Centro Superior de Investigaciones Científicas (CSIC) under the PIE project 20215AT016, and the program Unidad de Excelencia María de Maeztu CEX2020-001058-M. E.J.J. acknowledges support from FONDECYT Iniciación en investigación 2020 Project 11200263. J.D.L. acknowledges support from a UK Research and Innovation Fellowship(MR/T020784/1). S.D. acknowledge support from the National Natural Science Foundation of China (grant No. 12133005) and the XPLOER PRIZE. H.K. was funded by the Academy of Finland projects 324504 and 328898. F.F. acknowledges the Chilean Ministry of Economy, Development, and Tourism's Millennium Science Initiative through grant ICN12 12009, awarded to the Millennium Institute of Astrophysics National Agency for Research and Development (ANID) grants: BASAL Center of Mathematical Modelling Grant PAI AFB-170001 FONDECYT Regular 1200710. Support for T.W.-S.H. was provided by NASA through the NASA Hubble Fellowship grant HST-HF2-51458.001-A awarded by the Space Telescope Science Institute (STScI), which is operated by the Association of Universities for Research in Astronomy, Inc., for NASA, under contract NAS5-26555. We thank the referee for the very detailed and constructive report.

2.10 Appendix

2.10.1 BPT analysis

Figure 2.12 shows a BPT diagram of all HII regions (blue circles) extracted from the galaxies in our sample. The dashed line marks the active galactic nucleus (AGN) ionization region defined by Kewley et al. (2001) while the solid line shows the composite region limit defined by Kauffmann et al. (2003). The orange circles in Figure 2.12 show the position of the CCSNe in our sample and the green circles mark the SNe that fall above the composite region line: ASASSN-14ha (NGC 1566), SN 2014eh (NGC 6907), and SN 2016bev (ESO 560-G013). Since we are interested in the properties of regions that are ionized only by star

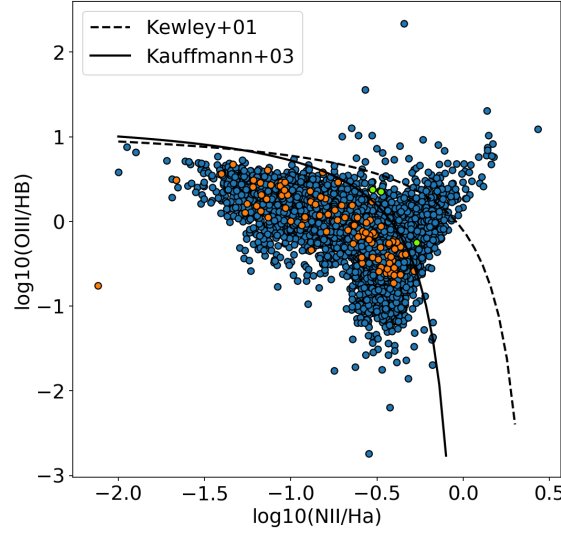


Figure 2.12: BPT diagram of the HII regions in our sample. The blue circles show all the HII regions, while the orange circles mark the position of the HII regions associated to the CCSNe. The green circles show the SNe that are above the composite region (solid line) defined by Kauffmann et al. (2003). We also show the AGN ionization region as the dashed line, as defined by Kewley et al. (2001).

formation, we exclude these three SNe of our analysis as they might be contaminated by other ionizing sources. In Paper II we will present an analysis of all HII regions in detail, and compare the SN host HII regions to all the other star-forming regions within their galaxies.

2.10.2 Parameter tests

We tested IFUanal in three galaxies in order to estimate how the selected HII segmentation parameters could affect the final result for the physical parameters. The galaxies (ESO 381-IG048/ASASSN-15bb, NGC 0988/SN 2017gmr, and NGC 2466/ASASSN-14dd) were selected to be representative of the full sample: one galaxy with a small projected size; one nearby spiral galaxy; and one spiral galaxy with a large projected size. We performed five runs of the code for each galaxy, varying the maximum bin radius, the minimum $\text{H}\alpha$ flux threshold to define the seed peaks, and the maximum flux threshold to where the region will expand. We compare the extracted results for all the selected bins in each galaxy in Figure 2.13, where we show the normalized cumulative distributions for $\text{H}\alpha$ flux and EW, the oxygen abundance given by the D16 indicator, and the estimated host extinction.

Table 2.4 lists the different sets of parameters used for the tests. Sets 1 and 2 have fixed values for the minimum and maximum $\text{H}\alpha$ flux thresholds, relative to the standard

Table 2.4: IFUanal parameters used in the tests.

Set	R_{max} [px]	$F_{H\alpha,min}$ [$\times\sigma$]	$F_{H\alpha,max}$ [$\times\sigma$]
1	6	3	10
2	12	3	10
3	6	1.5	8
4	6	4.5	12
5	Var.	Var.	Var.

deviation of the $H\alpha$ flux in a empty region of the cube, while the maximum radii are set to 6 or 10 pixels, respectively. The sets 3 and 4 have a maximum radius of 6 pixels, while the maximum $H\alpha$ flux threshold varies between 8σ and 12σ , respectively, and the minimum $H\alpha$ flux threshold varies between 1.5σ and 4.5σ , respectively. We also used the HII region segmentation obtained through pyHII extractor (Lugo-Aranda et al., 2022), which allows the bin regions to expand with no predefined maximum radius or threshold in the flux. We show the results from this segmentation as the set of parameters 5 in Figure 2.13, and report them as varying parameters in Table 2.4.

Figure 2.13 shows the cumulative distributions for $H\alpha$ flux. The galaxy ESO 381-IG048 presents the largest scatter between the distributions, with the set of parameters 3 showing the lowest median. This is also true for the oxygen abundance and the $H\alpha$ EW, shown in the second and third panels, respectively. Lowering the $H\alpha$ flux thresholds includes more pixels with lower values of $H\alpha$ flux, EW, and oxygen abundance. The results for NGC 0988 and NGC 2466, on the other hand, do not show significant differences between the distinct tests. These tests show that the input parameters in IFUanal might have a larger effect on the final analysis in smaller galaxies, where less HII regions are selected. This should be taken as a caveat for the analyses presented in this work and for the conclusions taken from them.

We set an intermediate minimum threshold of 10 times the standard deviation of the $H\alpha$ flux in a background region of the datacube, and a limiting threshold of three times the standard deviation of the $H\alpha$ flux to where the region can expand. Given our results, varying these parameters around the chosen values do not produce significant differences in the output for the majority of the galaxies.

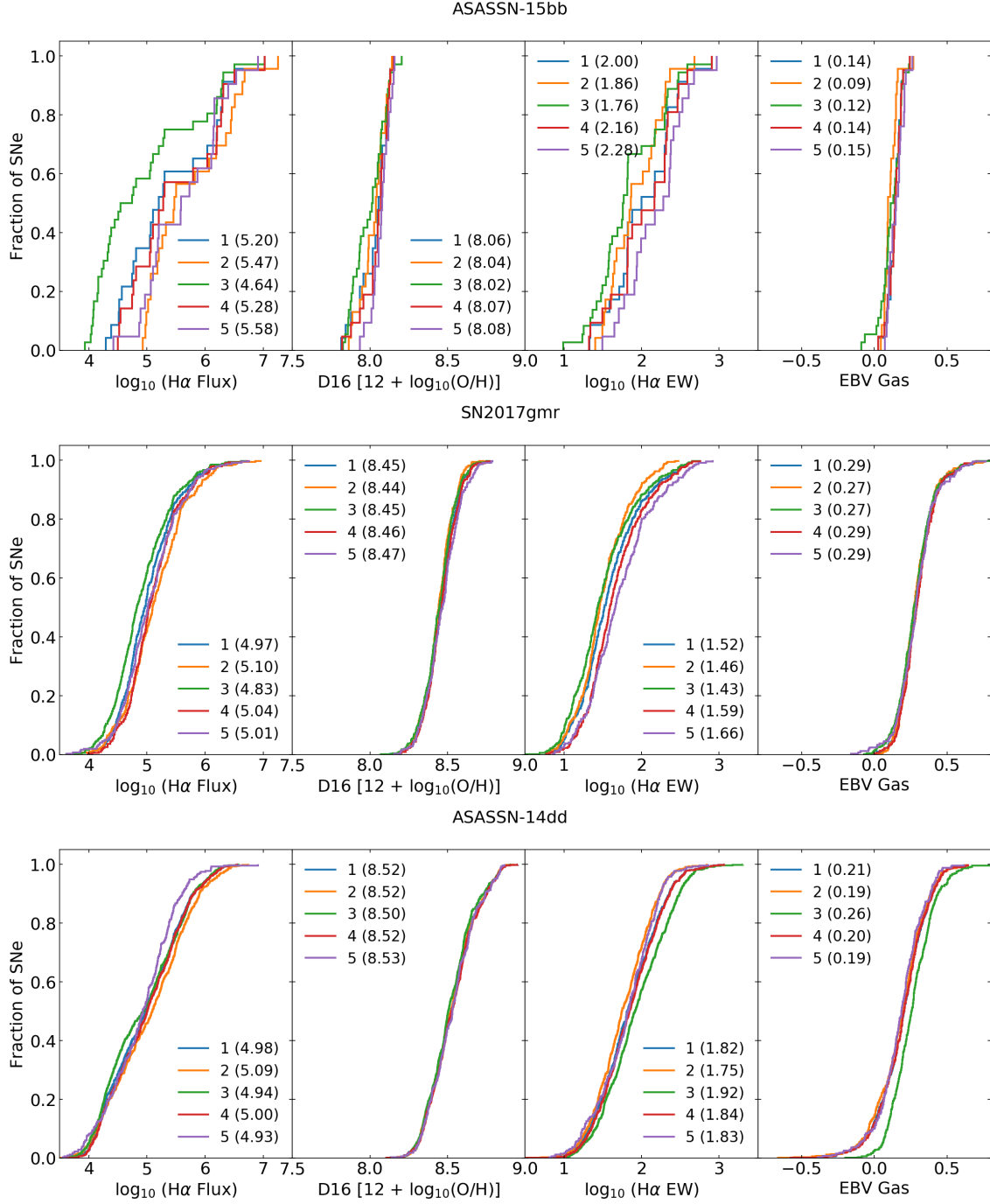


Figure 2.13: Cumulative distributions for the different tests with the objects ESO 381-IG048/ASASSN-15bb (top), NGC 0988/SN 2017gmr (middle), and NGC 2466/ASASSN-14dd (bottom). The tests were run using the parameters described in 2.4.

2.10.3 Metallicity gradients

In Figure 2.14 we show an example of the oxygen abundance gradient fit for ASASSN-16ba (hosted by MCG-03-25-015). The same method was applied for all the SNe where the nearest HII region was at a projected distance greater than 1×10^3 pc: ASASSN-15jp, SN2018yo,

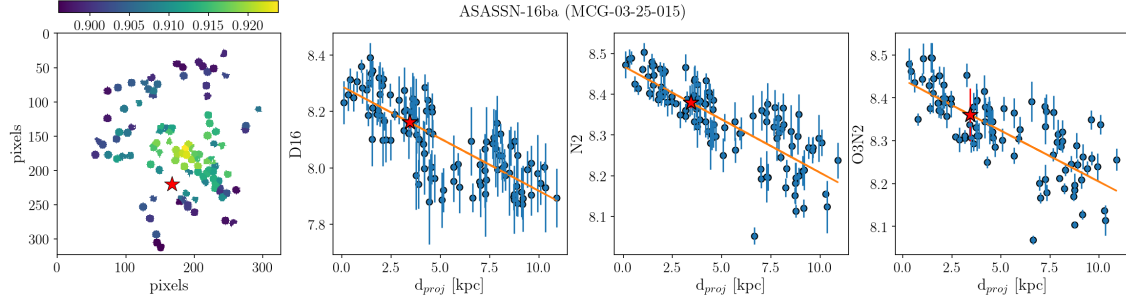


Figure 2.14: Oxygen abundances fit for ASASSN-16ba, hosted by MCG-03-25-015. The same method was applied for all the SNe where the extracted spectrum at their position has a SNR of < 3 . The Left panel shows the spatial distribution in pixels of the HII regions extracted in the galaxy, where the color gradient indicates the oxygen abundance given by the D16 index. The spatial coordinates of the SN in relation to the HII regions is given by the red star. The other three panels show, respectively from left to right, the resulting fit to the oxygen abundance gradient in the D16, N2, and O3N2 indexes. The resulting value for the SN is given by the red star. The x-axis show the deprojected distance from the nucleus in kpc for each HII region.

ASASSN-17oj, SN2017gbv, ASASSN-16ba, ASASSN-16al, LSQ15xp, SN2015W, and ASASSN-18ou. A straight line is fit to all the oxygen abundances obtained from the HII regions. The line fitting is weighted by the measured uncertainties from the oxygen abundance measurements. We note that systematic uncertainties from each index could input a larger error in the gradient fittings. We use pixel deprojected distances from the center of the galaxy following the method from Hakobyan et al. (2009). Values of position angle (PA) and inclination angle (i) of each galaxy are taken from HyperLeda (Makarov et al., 2014). The resulting oxygen abundances in the D16, N2 and O3N2 indexes are reported in Table 2.6.

2.10.4 Measured fluxes and physical parameters

In Table 2.5, we report the measured fluxes of $H\alpha$, $H\beta$, $[OIII] \lambda 5007$, $[NII] \lambda 6584$, and $[SII] \lambda 6716$ for the HII region related to each SN. The individual line fluxes were corrected for Galactic, and host galaxy reddening. Table 2.6 reports the resulting $H\alpha$ EW, oxygen abundances, ΣSFR , and host galaxy extinction for the HII region related to each SN.

2.10.5 Statistics results, KS, and AD tests.

In Table 2.7 we show the number of events, median, and average values for each distribution used in the analysis for oxygen abundance. In Tables 2.8 and 2.9 we report, respectively, the

Table 2.5: Measured fluxes of different emission lines at the nearest HII region to each SN.

SN Name	H α	H β	[OIII] λ 5007	[NII] λ 6584	[SII] λ 6716
SN2018eog	19.92 (1.12)	6.97 (2.02)	3.80 (1.34)	4.58 (1.05)	5.73 (0.90)
SN2018ant	61.91 (3.94)	11.90 (24.92)	12.46 (7.27)	17.76 (3.58)	17.35 (3.25)
ASASSN-18oa	189.38 (3.61)	66.22 (5.17)	45.88 (4.45)	57.99 (2.66)	46.54 (2.31)
SN2018bl	382.70 (5.33)	133.82 (6.65)	89.50 (5.41)	98.01 (3.10)	70.51 (3.34)
SN2018evy	2398.58 (24.23)	838.73 (35.76)	157.37 (25.65)	941.54 (16.49)	348.78 (12.82)
SN2018cho	140.11 (2.43)	48.99 (6.81)	19.77 (6.65)	61.52 (2.10)	27.41 (1.62)
SN2018ie	629.83 (5.17)	220.18 (6.65)	150.08 (5.14)	164.01 (2.83)	111.36 (2.39)
SN2018yo	-	-	35.18 (4.04)	42.77 (2.60)	33.53 (2.10)
...					

¹³ The entire table is available in the online version of the article and in Appendix 2.10.8. Flux units are given in $10^{-17} \text{ erg s}^{-1} \text{ cm}^{-2} \text{ \AA}^{-1}$.

Table 2.6: Physical properties of the HII region related to each SN.

SN Name	H α EW (Å)	D16 (12 + log(O/H))	N2 (12 + log(O/H))	O3N2 (12 + log(O/H))	Σ SFR (log M $_{\odot}$ yr $^{-1}$ kpc $^{-2}$)	E(B - V) (mag)
SN2018eog	3.45 (0.26)	8.28 (0.12)	8.45 (0.05)	-	-3.68 (-0.00)	-
SN2018ant	8.94 (0.75)	8.37 (0.11)	8.49 (0.04)	-	-2.90 (-0.02)	-
ASASSN-18oa	27.22 (0.79)	8.49 (0.03)	8.51 (0.01)	8.46 (0.01)	-2.34 (-0.05)	0.16 (0.07)
SN2018bl	171.54 (5.87)	8.54 (0.02)	8.47 (0.01)	8.44 (0.01)	-1.47 (-0.52)	0.24 (0.05)
SN2018evy	108.29 (3.37)	8.86 (0.01)	8.56 (0.00)	8.60 (0.02)	-1.22 (-1.09)	0.44 (0.04)
SN2018cho	17.32 (0.52)	8.79 (0.02)	8.58 (0.01)	-	-1.90 (-0.15)	0.27 (0.13)
SN2018ie	342.46 (19.46)	8.56 (0.01)	8.47 (0.00)	8.44 (0.00)	-1.15 (-1.35)	0.28 (0.03)
SN2018yo	-	8.28 (0.03)	8.36 (0.05)	8.36 (0.05)	-	-
...						

¹⁴ The entire table is available in the online version of the article and in Appendix 2.10.8. Some CCSNe could not have their oxygen abundance in the O3N2 index and extinction estimated due to the low SNR (< 3) of H β or [OIII] λ 5007 in their spectra.

results for the KS and AD tests for oxygen abundance. The KS and AD tests were performed through SciPy (version 1.0 Virtanen et al., 2020). The same is reported for $H\alpha$ EW in Tables 2.10, 2.11, and 2.12, Σ SFR in Tables 2.13, 2.14, and 2.15, and for $E(B - V)_{host}$ in Tables 2.16, 2.17, and 2.18.

2.10.6 The SLSN 2015bn

The SN 2015bn is a well studied Type I superluminous supernova (SLSN), located at a redshift ~ 0.1136 and is one of the closest events of this type (Nicholl et al., 2016; Nicholl et al., 2018). Since SN 2015bn is part of the ASAS-SN catalog (Holoien et al., 2017a) and is the only SLSN event in the sample, we make a brief analysis of its environment in this section for a comparison with the other SN types described in this work. The transient was observed with the MUSE instrument on 2016 January 17, ~ 390 days after discovery and ~ 296 days after reaching peak brightness (see upper panel of Figure 2.15).

We extracted the spectrum of SN 2015bn in a circular region with a 6 pixel radius centered at the SN coordinates, and show it in the bottom panel of Figure 2.15. The spectrum is dominated by emission from the SN, but a few emission lines originating from the underlying HII region can be identified, such as $H\alpha$, $H\beta$, $O[III]\lambda 5007$, and $N[II]\lambda 6584$. We fit these lines using a Gaussian model with a local continuum and estimate the physical parameters using the methods described in Section 2.5.

We measured an integrated flux for $H\alpha$ of $5.96 \pm 0.05 \times 10^{-18} \text{ erg s}^{-1} \text{ cm}^{-2} \text{ \AA}^{-1}$, a luminosity of $2.42 \pm 0.12 \times 10^{38} \text{ erg s}^{-1}$, and an EW $\sim 110 \text{ \AA}$. We note that the EW value in this case is a lower limit, as the SN elevates the continuum level of the spectrum. The value for the $H\alpha$ EW is similar to the median for the SESNe distribution, and slightly higher than the median for most of the CCSN distributions. This value is also similar to the distribution of $H\alpha$ EW of SLSNe-I found by Leloudas et al. (2015).

We use the measured fluxes of $H\alpha$, $H\beta$, $[OIII] \lambda 5007$, and $[NII] \lambda 6584$ to estimate the oxygen abundance through the N2 and O3N2 indicators. We find $12 + \log(O/H) = 8.25 \pm 0.12 \text{ dex}$ for the N2 index, and $12 + \log(O/H) = 8.20 \pm 0.19 \text{ dex}$ for the O3N2 index. The values found for SN 2015bn are similar to the oxygen abundance of the H-poor SLSN reported by Leloudas et al. (2015), and to the values in these two indicators of the environment around PTF12dam ($12 + \log(O/H) \sim 8.00 \text{ dex}$, Thone et al., 2015). Our results agree with the

Table 2.7: Oxygen abundance statistics.

SN Type	D16 N	D16 Median	D16 Average	O3N2 N	O3N2 Median	O3N2 Average	N2 N	N2 Median	N2 Average
II	78	8.28 (0.41)	8.31 (0.33)	78	8.34 (0.45)	8.34 (0.36)	78	8.41 (0.41)	8.38 (0.33)
II n	9	8.35 (1.19)	8.30 (0.95)	9	8.39 (1.29)	8.39 (1.03)	9	8.38 (1.21)	8.41 (0.96)
Ic	6	8.55 (1.46)	8.50 (1.16)	6	8.44 (1.62)	8.40 (1.29)	6	8.49 (1.47)	8.45 (1.18)
Ib	7	8.43 (1.39)	8.39 (1.11)	7	8.22 (1.62)	8.29 (1.29)	7	8.46 (1.38)	8.38 (1.10)
IIb	7	8.68 (1.36)	8.43 (1.09)	7	8.40 (1.48)	8.37 (1.18)	7	8.50 (1.37)	8.42 (1.09)
IIbn	3	8.57 (2.10)	8.43 (1.67)	3	8.43 (2.10)	8.43 (1.68)	3	8.47 (2.10)	8.48 (1.68)
II	78	8.28 (0.41)	8.31 (0.33)	78	8.34 (0.45)	8.34 (0.36)	78	8.41 (0.41)	8.38 (0.33)
II n/IIbn	9	8.32 (1.04)	8.30 (0.83)	9	8.39 (1.10)	8.39 (0.87)	9	8.44 (1.05)	8.43 (0.84)
SESNe	6	8.55 (0.80)	8.50 (0.64)	6	8.44 (0.88)	8.40 (0.70)	6	8.49 (0.80)	8.42 (0.64)

Table 2.8: Oxygen abundance KS values.

KS test	D16 D-value	D16 p-value	O3N2 D-value	O3N2 p-value	N2 D-value	N2 p-value
II x IIIn	0.34	0.32	0.21	0.80	0.34	0.32
II x Ic	0.46	0.21	0.38	0.31	0.46	0.21
II x Ib	0.40	0.35	0.18	0.95	0.40	0.35
II x IIb	0.33	0.50	0.29	0.56	0.33	0.50
II x IIn	0.61	0.15	0.55	0.25	0.61	0.15
IIn x Ic	0.42	0.50	0.39	0.56	0.42	0.50
IIn x Ib	0.47	0.40	0.32	0.71	0.47	0.40
IIn x IIb	0.38	0.64	0.24	0.92	0.38	0.64
IIn x IIn	0.50	0.56	0.56	0.45	0.50	0.56
Ic x Ib	0.40	0.87	0.26	0.93	0.40	0.87
Ic x IIb	0.33	0.82	0.26	0.93	0.33	0.82
Ic x IIn	0.27	1.00	0.17	1.00	0.27	1.00
Ib x IIb	0.50	0.36	0.29	0.96	0.50	0.36
Ib x IIn	0.60	0.46	0.43	0.70	0.60	0.46
Ib x IIn	0.50	0.68	0.43	0.70	0.50	0.68
II x IIn/IIn	0.38	0.10	0.26	0.44	0.38	0.10
II x SESNe	0.24	0.33	0.22	0.36	0.24	0.33
IIn/IIn x SESNe	0.32	0.33	0.20	0.85	0.32	0.39

Table 2.9: Oxygen abundance AD values.

AD test	D16 Statistic	D16 Significance	O3N2 Statistic	O3N2 Significance	N2 Statistic	N2 Significance
II x IIn	-1.10	0.25	-0.91	0.25	-0.26	0.25
II x Ic	1.24	0.10	-0.27	0.25	-0.04	0.25
II x Ib	-0.56	0.25	-1.07	0.25	-0.15	0.25
II x IIb	-0.28	0.25	-0.47	0.25	-0.67	0.25
II x IIn	-0.43	0.25	-0.15	0.25	0.24	0.25
IIn x Ic	0.71	0.17	-0.59	0.25	-0.65	0.25
IIn x Ib	-0.64	0.25	-0.81	0.25	-0.05	0.25
IIn x IIb	-0.59	0.25	-0.92	0.25	-0.55	0.25
IIn x IIn	-0.67	0.25	-0.40	0.25	-0.54	0.25
Ic x Ib	-0.01	0.25	-1.06	0.25	0.11	0.25
Ic x IIb	-0.89	0.25	-1.06	0.25	-0.39	0.25
Ic x IIn	-1.04	0.25	-1.32	0.25	-1.39	0.25
Ib x IIb	-0.57	0.25	-1.01	0.25	0.25	0.25
Ib x IIn	-1.02	0.25	-0.90	0.25	-0.00	0.25
IIb x IIn	-0.32	0.25	-0.77	0.25	-0.35	0.25
II x IIn/IIn	-1.04	0.25	-0.37	0.25	0.54	0.20
II x SESNe	1.39	0.09	0.13	0.25	-0.17	0.25
IIn/IIn x SESNe	-0.18	0.25	-0.67	0.25	-0.40	0.25

Table 2.10: H α EW statistics.

SN Type	N	Median (\AA)	Average (\AA)
II	61	62.32 (1.75)	80.55 (1.40)
IIIn	8	63.76 (8.63)	155.24 (6.88)
Ic	6	220.80 (8.93)	199.77 (7.12)
Ib	6	87.27 (11.82)	280.30 (9.43)
IIb	6	139.80 (8.56)	176.73 (6.83)
Ibn	3	44.94 (11.43)	103.07 (9.12)
II	61	62.32 (1.75)	80.55 (1.40)
IIIn/Ibn	11	50.28 (6.77)	141.01 (5.40)
SESNe	19	109.04 (5.67)	211.86 (4.53)

Table 2.11: H α EW KS values.

KS test	D -value	p -value
II x IIIn	0.36	0.25
II x Ic	0.48	0.11
II x Ib	0.32	0.54
II x IIb	0.43	0.19
II x Ibn	0.32	0.84
IIIn x Ic	0.38	0.64
IIIn x Ib	0.38	0.64
IIIn x IIb	0.33	0.78
IIIn x Ibn	0.38	0.84
Ic x Ib	0.33	0.93
Ic x IIb	0.33	0.93
Ic x Ibn	0.50	0.68
Ib x IIb	0.33	0.93
Ib x Ibn	0.50	0.68
IIb x Ibn	0.50	0.68
II x IIIn/Ibn	0.33	0.21
II x SESNe	0.36	0.04
IIIn/Ibn x SESNe	0.33	0.33

Table 2.12: H α EW AD values.

AD test	Statistic	Significance
II x IIn	0.74	0.16
II x Ic	2.45	0.03
II x Ib	0.95	0.13
II x IIb	2.05	0.05
II x IIn	-0.38	0.25
IIn x Ic	-0.44	0.25
IIn x Ib	-0.19	0.25
IIn x IIb	-0.62	0.25
IIn x IIn	-0.95	0.25
Ic x Ib	-0.23	0.25
Ic x IIb	-0.92	0.25
Ic x IIn	-0.17	0.25
Ib x IIb	-0.94	0.25
Ib x IIn	-0.19	0.25
IIb x IIn	-0.40	0.25
II x IIn/IIn	0.43	0.22
II x SESNe	4.48	0.0054
IIn/IIn x SESNe	0.67	0.17

Table 2.13: Σ SFR statistics.

SN Type	N	Median ($M_{\odot} \text{ yr}^{-1} \text{ kpc}^{-2}$)	Average ($M_{\odot} \text{ yr}^{-1} \text{ kpc}^{-2}$)
II	61	-1.87 (0.11)	-1.87 (0.09)
IIn	8	-2.13 (0.17)	-1.83 (0.14)
Ic	6	-1.11 (0.50)	-1.51 (0.40)
Ib	6	-1.50 (0.30)	-1.31 (0.24)
IIb	6	-1.44 (0.57)	-1.56 (0.45)
IIn	3	-1.97 (1.02)	-1.99 (0.81)
II	61	-1.87 (0.11)	-1.87 (0.09)
IIn/IIn	11	-2.03 (0.15)	-1.87 (0.12)
SESNe	19	-1.27 (0.23)	-1.48 (0.18)

Table 2.14: Σ SFR KS values.

KS test	D -value	p -value
II x II _n	0.22	0.83
II x I _c	0.49	0.11
II x I _b	0.29	0.64
II x II _b	0.27	0.72
II x I _b _n	0.57	0.21
II _n x I _c	0.54	0.19
II _n x I _b	0.46	0.38
II _n x II _b	0.33	0.78
II _n x I _b _n	0.50	0.56
I _c x I _b	0.33	0.93
I _c x II _b	0.33	0.93
I _c x I _b _n	0.67	0.33
I _b x II _b	0.33	0.93
I _b x I _b _n	0.83	0.10
II _b x I _b _n	0.67	0.33
II x II _n /I _b _n	0.30	0.30
II x SESNe	0.26	0.22
II _n /I _b _n x SESNe	0.46	0.07

Table 2.15: Σ SFR AD values.

AD test	Statistic	Significance
II x II _n	-0.73	0.25
II x I _c	0.58	0.19
II x I _b	0.23	0.25
II x II _b	-0.45	0.25
II x I _b _n	0.21	0.25
II _n x I _c	-0.03	0.25
II _n x I _b	-0.03	0.25
II _n x II _b	-0.65	0.25
II _n x I _b _n	-0.32	0.25
I _c x I _b	-0.59	0.25
I _c x II _b	-0.23	0.25
I _c x I _b _n	0.21	0.25
I _b x II _b	-0.91	0.25
I _b x I _b _n	1.26	0.10
II _b x I _b _n	0.21	0.25
II x II _n /I _b _n	-0.39	0.25
II x SESNe	1.11	0.11
II _n /I _b _n x SESNe	1.00	0.13

Table 2.16: Extinction statistics.

SN Type	N	Median (mag)	Average (mag)
II	47	0.23 (0.10)	0.23 (0.08)
II _n	7	0.25 (0.24)	0.23 (0.19)
Ic	6	0.20 (0.39)	0.31 (0.31)
Ib	6	0.20 (0.35)	0.26 (0.28)
IIb	5	0.32 (0.32)	0.32 (0.26)
Ib _n	1	0.27 (0.65)	0.27 (0.52)
II	47	0.23 (0.10)	0.23 (0.08)
II _n /Ib _n	8	0.26 (0.22)	0.23 (0.18)
SESNe	18	0.22 (0.21)	0.30 (0.16)

Table 2.17: Extinction KS values.

KS test	<i>D</i> -value	<i>p</i> -value
II x II _n	0.28	0.64
II x Ic	0.17	0.99
II x Ib	0.22	0.92
II x IIb	0.34	0.54
II x Ib _n	0.64	0.29
II _n x Ic	0.33	0.78
II _n x Ib	0.26	0.93
II _n x IIb	0.40	0.64
II _n x Ib _n	0.57	0.56
Ic x Ib	0.17	1.00
Ic x IIb	0.43	0.59
Ic x Ib _n	0.67	0.43
Ib x IIb	0.43	0.59
Ib x Ib _n	0.83	0.21
IIb x Ib _n	0.60	0.57
II x II _n /Ib _n	0.28	0.58
II x SESNe	0.14	0.93
II _n /Ib _n x SESNe	0.28	0.69

Table 2.18: Extinction AD values.

AD test	Statistic	Significance
II x II _n	-0.61	0.25
II x I _c	-0.79	0.25
II x I _b	-0.81	0.25
II x II _b	0.07	0.25
II x I _{bn}	nan	nan
II _n x I _c	-0.60	0.25
II _n x I _b	-0.93	0.25
II _n x II _b	-0.32	0.25
II _n x I _{bn}	nan	nan
I _c x I _b	-1.11	0.25
I _c x II _b	-0.45	0.25
I _c x I _{bn}	nan	nan
I _b x II _b	-0.71	0.25
I _b x I _{bn}	nan	nan
II _b x I _{bn}	nan	nan
II x II _n /I _{bn}	-0.41	0.25
II x SESNe	-0.58	0.25
II _n /I _{bn} x SESNe	-0.66	0.25

occurrence of these types of events in regions with a lower abundance of oxygen, a strong indication of the preference of H-poor SLSN for metal-poorer environments.

2.10.7 Photometry and light curve parameters

In Tables 2.19, 2.20, and 2.21 we present the LC derived parameters for the SNe II, SESNe, and SNe II_n, respectively. In most events, the BVr photometry was retrieved from the ASAS-SN archive (for a in depth discussion on ASASSN photometry, see Kochanek et al., 2017), but in some cases data was obtained from the literature, such as for ASASSN-14jb (Meza et al., 2019a), SN 2014cy, SN 2014dw, SN 2015W (Valenti et al., 2016), and SN 2017gmr (Andrews et al., 2021). A second order polynomial was used for fit the peak time and the magnitude at peak luminosity, as is shown in Figure 2.16 for the SN II ASASSN-14jb. The absolute magnitude is corrected by Galactic extinction. For SNe II, a linear fitting between peak and 30 days after was used to obtain the postmaximum decline rate. For SESNe the second order fit was used to obtain the Δm_{15} values.

The relation between the LC parameters and the physical parameters derived at the SN position are shown in Figures 2.9, 2.10, and 2.11. The straight dashed lines represent linear fits obtained from the scatter of the values in each photometric band. Pearson correlation

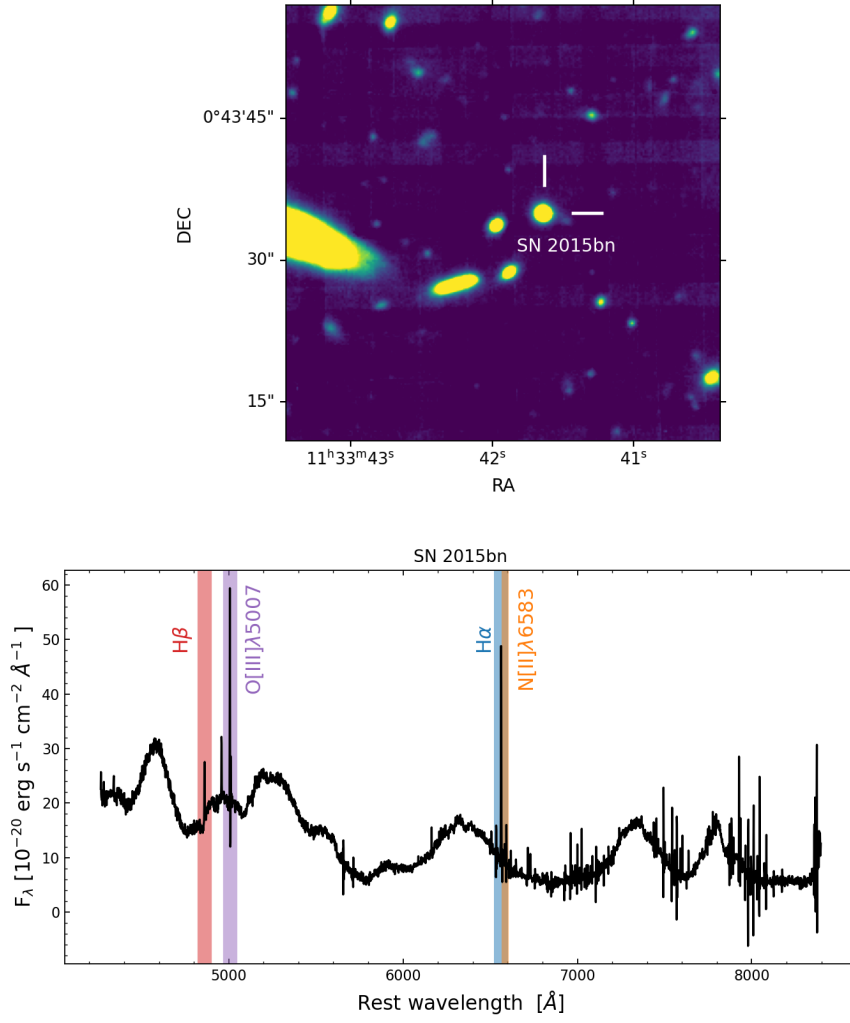


Figure 2.15: Spectrum fitting for the SLSN 2015bn. Top panel: Position of SN 2015bn in the MUSE image of the observed field. Bottom panel: Extracted spectrum for SN 2015bn, where the broad emission lines of the SN are still clearly present. Emission lines of H α , H β , O[III] λ 5007, and N[II] λ 6583 belonging to the underlying HII region can be identified.

tests are performed through SciPy to obtain the significance from each possible correlation.

Table 2.19: LC parameters of the SNe II.

SN	V		B		r	
	M_{peak} (mag)	s (mag/days)	M_{peak} (mag)	s (mag/days)	M_{peak} (mag)	s (mag/days)
SN2018eog	-16.88 (0.06)	-	-	-	-	-
SN2018cho	-17.56 (0.14)	-	-	-	-	-
SN2018yo	-17.06 (0.09)	-	-	-	-	-
AT2018cuf	-16.52 (0.12)	-	-	-	-	-
ASASSN-18eo	-18.83 (0.08)	0.0201 (0.0053)	-	-	-	-
ASASSN-18cb	-16.72 (0.07)	0.0075 (0.0032)	-	-	-	-
SN2017bjj	-16.55 (0.45)	-	-	-	-	-
SN2017grn	-17.57 (0.09)	-	-	-	-	-
Gaia17chn	-18.28 (0.10)	-	-	-	-	-
SN2017gmr	-17.47 (0.03)	0.0042 (0.0007)	-17.30 (0.04)	0.0239 (0.0016)	-17.70 (0.03)	0.0025 (0.0007)
SN2017fem	-17.12 (0.27)	-	-	-	-	-
SN2017faf	-19.01 (0.27)	-	-	-	-	-
ATLAS17hpc	-18.84 (0.08)	0.0205 (0.0041)	-	-	-	-
...						

^aThe entire table is available in the online version of the article and in Appendix 2.10.8.

Table 2.20: LC parameters of the SESNe.

SN	V		B		r	
	M_{peak} (mag)	Δm_{15} (mag)	M_{peak} (mag)	Δm_{15} (mag)	M_{peak} (mag)	Δm_{15} (mag)
SN2018ie	-17.72 (0.07)	1.58 (0.34)	-17.02 (0.13)	2.09 (0.23)	-17.92 (0.07)	1.26 (0.32)
SN2018dfg	-16.81 (0.10)	-	-	-	-	-
SN2017gax	-18.24 (0.09)	0.41 (0.15)	-17.69 (0.08)	1.08 (0.22)	-17.94 (0.06)	1.02 (0.16)
SN2017gat	-18.64 (0.07)	0.72 (0.13)	-17.92 (0.09)	0.64 (0.21)	-18.80 (0.05)	0.54 (0.13)
ASASSN-14az	-17.89 (0.06)	1.25 (0.12)	-	-	-	-
SN2016gkg	-16.86 (0.06)	1.15 (0.20)	-14.93 (0.09)	0.53 (0.25)	-16.72 (0.08)	0.92 (0.14)
PSNJ1828582	-16.90 (0.44)	-	-	-	-	-
ASASSN-15tu	-17.65 (0.19)	-	-	-	-	-
ASASSN-15ta	-18.62 (0.04)	-	-	-	-	-
ASASSN-15bd	-17.03 (0.10)	0.79 (0.36)	-	-	-	-

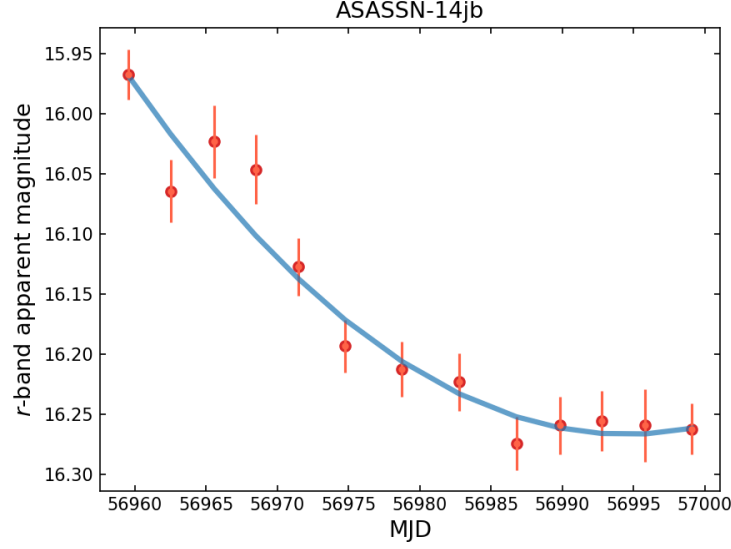


Figure 2.16: Example of a second order polynomial fitting in r -band for ASASSN-14jb. The y -axis shows the apparent magnitude and x -axis gives the phase as modified Julian date (MJD).

Table 2.21: LC parameters of the SNe IIn.

SN	V	B	r
	M_{peak} (mag)	M_{peak} (mag)	M_{peak} (mag)
ASASSN-18oa	-18.33 (0.03)	-	-
ATLAS17lsn	-20.59 (0.03)	-	-20.69 (0.03)
ASASSN-16jt	-18.68 (0.04)	-18.60 (0.04)	-18.57 (0.04)
ASASSN-16in	-18.16 (0.03)	-18.08 (0.11)	-18.18 (0.04)
SN2016aiy	-17.47 (0.04)	-17.29 (0.04)	-17.60 (0.03)
ASASSN-15hs	-16.74 (0.03)	-	-
ASASSN-15ab	-19.35 (0.03)	-	-
ASASSN-15lx	-17.39 (0.12)	-	-

2.10.8 Entire tables

Tables 2.22, 2.23, 2.24, 2.25, and 2.26 show, respectively, the complete version of Tables 2.1, 2.2, 2.5, 2.6, and 2.19.

Table 2.22: Entire version of Table 2.1.

Name	Type	RA	DEC	Host Galaxy Name	z_{host}	$A_{v,MW}$	$M_{B,host}$
SN2018eog	II	20 28 11.970	-03 08 13.47	2MASS J20281135-0308096	0.01886	-	-
SN2018ant	II	08 36 31.450	-11 49 40.73	MCG-2-22-22	0.019784	0.192	-20.67
ASASSN-18oa	II	01 30 27.120	-26 47 05.98	ESO476-G16	0.019744	0.055	-20.94
SN2018bl	II	08 24 11.590	-77 47 16.55	ESO18-G9	0.017773	0.357	-20.94
SN2018evy	IIn	18 22 38.170	+15 41 47.66	NGC6627	0.017647	0.611	-20.94
SN2018cho	IIn	00 13 26.515	+17 29 19.57	IC4	0.016558	0.173	-20.72

SN2018ie	II	10 54 01.060	-16 01 21.40	NGC3456	0.013954	0.211	-20.76
SN2018yo	II	12 41 11.140	-01 35 20.40	UGC7840	0.013429	0.1	-18.58
AT2018cuf	II	21 16 11.570	-64 28 57.27	IC5092	0.010513	0.099	-20.46
ASASSN-18eo	II	03 58 01.498	-65 30 24.50	GALEXASC J035801.64-653024.6	0.024752	-	-
SN2018dfg	IIP	14 06 34.700	-05 27 02.90	NGC5468	0.009443	0.076	-20.64
ASASSN-18cb	IIP	12 55 31.252	-50 03 16.95	IC3896A	0.006857	0.653	-20.44
AT2018bbl	Ic	22 56 54.610	-37 20 20.90	NGC7421	0.005979	0.045	-19.51
SN2017bjj	Ic	00:48:5.42	-02:47:22.40	NGC 0259	0.013613	0.14	-20.98
LCRSB1107092	II	11:09:39.52	-12:35:18.34	LCRS B110709.2-121854	0.036932	0.156	-20.60
ATLAS17lsn	IIP	00:03:50.58	-11:28:28.78	GALEX 2674128878581058535	0.016818	0.102	-
SN2017grn	II	23:31:53.6	-05:00:43.40	IC 1498	0.017271	0.141	-21.13
Gaia17chn	II	03:28:7.94	-56:34:41.99	ESO 155-G36	0.019377	0.081	-19.53
SN2017gmr	II	02:35:30.15	-09:21:14.95	NGC 988	0.00504	0.084	-20.87
SN2017gax	II	04:45:49.43	-59:14:42.56	NGC 1672	0.004723	0.072	-20.80
SN2017fem	IIB	14:32:27.32	+27:25:36.75	IC 4452	0.014254	0.066	-18.93
SN2017faf	IIB	17:34:39.98	+26:18:22.00	GALEXASC J173440.11+261818.0	0.028779	0.172	-
ATLAS17hpc	II	13:19:03.90	-02:30:45.81	IC 4224	0.018455	0.103	-20.54
SN2017cjd	II	11:50:30.17	-18:35:44.96	GALEXASC J115030.27-183545.2	0.02261	0.111	-
SN2017bzb ₂	II	22:57:17.3	-41:00:57.60	NGC 7424	0.002895	0.033	-19.78
SN2017bif	II	17:26:27.12	-60:32:39.73	2MASX J17262669-6032500	0.018942	0.312	-20.01
ASASSN-17qp	II	20:28:49.80	-04:22:57.29	GALEXASC J202849.46-042255.5 (?)	0.00559	-	-
ASASSN-17oj	II	21:44:22.94	-29:54:59.29	ESO 466-G 004	0.018712	0.139	-19.82
ASASSN-17ny	Ic-BL	08:15:43.38	-28:51:19.84	AM 0813-284	0.005625	1.224	-17.25
SN2017gat	Ic-BL	23:53:17.03	-32:46:32.84	GALEXASC J235316.77-324634.3	0.022951	0.042	-17.61
SN2017fqk	IIn	02:54:02.09	+02:58:07.72	NGC 1137	0.010214	0.331	-20.53
SN2017ffq	IIn	17:40:14.50	-58:25:57.11	2MASX J17401447-5825586	0.012619	0.268	-18.56
SN2017fbu	II	02:11:06.94	+03:50:36.64	IC 0211	0.010892	0.125	-20.04
SN2017ecp	II	14:14:48.93	-29:33:37.01	PGC 727891	0.022857	-	-
SN2017auf	IIP	05:02:19.58	-10:21:22.75	MCG -02-13-038	0.01336	0.274	-
ASASSN-14at	IIP	17 55 05.31	+18 15 27.4	UGC 11037	0.010484	0.255	-18.76
ASASSN-14az	II	23 44 48.05	-02 07 02.1	GALEXASC J234448.27-020653.4	0.00706	0.099	-16.51
ASASSN-14dd	II	07 45 14.64	-71 24 14.4	NGC 2466	0.017821	0.512	-21.37
SN2014dw	Ib/c	11 10 48.41	-37 27 02.2	NGC 3568	0.008195	0.334	-20.71
NGC7742	Ib/c	23 44 16.03	+10 46 12.5	NGC 7742	0.005435	0.171	-19.96
SN2014cw	IIP	22 15 26.55	-10 28 34.6	KDG 236	0.009149	0.18	-
SN2014ce	IIP	23 27 40.86	+23 35 21.4	NGC 7673	0.011353	0.135	-21.18
ASASSN-14ma	II	23 55 09.13	+10 12 54.2	2MASX J23551001+1013281	0.013197	0.318	-19.19
ASASSN-14kp	II	00 39 52.58	-38 03 52.2	GALEXASC J003952.48-380347.3	0.02265	0.041	-16.79
ASASSN-14dl	II	12 21 51.38	-24 09 54.0	ESO 506-G004	0.013416	0.239	-21.29
ASASSN-14dp	II	11 21 58.33	-37 54 24.6	ESO 319-G15	0.00918	0.375	-18.57
ASASSN-14iz	Ic	20 21 49.84	-31 17 06.8	ESO 462-G009	0.019209	0.213	-20.49
ASASSN-14jb	Ic	22 23 16.12	-28 58 30.8	ESO 467-G051	0.006013	0.058	-19.26

SN2016iae	II	04 12 05.53	-32 51 44.8	NGC 1532	0.004	0.047	-21.54
SN2016hvu	II	22 35 55.56	+20 19 12.6	NGC 7316	0.018532	0.148	-21.33
SNhunt327	II	01 22 11.73	+00 57 07.8	NGC 493	0.007618	0.101	-20.08
SN2016gkg	II	01 34 14.46	-29 26 25.0	NGC 613	0.00492	0.06	-21.48
SN2016bmi	II	18 34 32.19	-58 31 44.8	IC 4721	0.007455	0.245	-20.63
SN2016bas	II	07 38 05.53	-55 11 47.0	ESO 163-G011	0.009451	0.46	-20.38
SN2016P	II	13 57 31.10	+06 05 51.0	NGC 5374	0.014558	0.084	-20.69
SN2016C	II	13 38 05.30	-17 51 15.3	NGC 5247	0.004571	0.276	-21.31
SN2016jga	II	02 05 38.33	-59 47 58.2	AM 0204-600	0.024365	0.088	-20.14
SN2016iyd	II	07 37 09.92	-52 19 03.9	SSTSL2 J073710.03-521905.6	0.034731	0.666	-
SN2016hwn	Ic	12 04 16.91	+21 48 01.8	KUG 1201+220	0.021585	0.071	-18.77
SN2016hpt	Ic	21 54 36.59	-42 51 02.9	GALEXASC J215436.98-425103.9	0.026605	0.05	-18.77
ASASSN-16jt	II	22 19 49.42	-40 40 04.6	ESO 344-G021	0.010762	0.039	-19.05
ASASSN-16in	II	04 59 30.07	-28 51 39.4	ESO 422-G019	0.015902	0.041	-19.11
SN2016egz	II	00 04 03.85	-34 48 51.8	GALEXASC J000403.88-344851.6	0.023162	0.048	-16.36
ASASSN-16go	II	13 02 44.26	-26 56 26.8	2MASX J13024397-2656276	0.016065	0.245	-19.28
NGC3627 ₃	II	11 20 19.09	+12 58 57.2	M66	0.002743	0.103	-21.21
SN2016cdd	II	12 31 53.64	-51 44 50.8	ESO 218-G008	0.008646	0.572	-19.73
ASASSN-16eh	Ibn	15 40 29.23	+00 54 36.4	SDSS J154029.29+005437.4	0.011736	0.318	-17.56
ASASSN-16dm	Ibn	11 37 20.64	-04 54 36.8	2MASX J11372059-0454450	0.018019	0.162	-19.70
SN2016ase	II	11 42 34.66	-25 54 45.1	ESO 504-G009	0.014086	0.146	-
ASASSN-16cc	II	05 46 23.80	-52 05 18.5	NGC 2101	0.003956	0.17	-17.66
SN2016aiy	II	13 08 25.40	-41 58 50.1	ESO 323-G084	0.010017	0.401	-
ASASSN-16bm	II	11 51 56.24	-13 25 03.1	GALEXASC J115155.68-132459.3	0.006838	0.133	-
ASASSN-16ba	IIb	09 42 29.22	-16 58 26.9	MCG -03-25-015	0.013944	0.203	-
ASASSN-16at	IIb	12 55 15.50	+00 05 59.7	UGC 08041	0.004114	0.069	-18.53
ASASSN-16al	Ibn	15 00 27.47	-13 33 09.0	UGCA 397	0.009295	0.312	-
ASASSN-16ai	Ibn	14 39 44.77	+23 23 42.5	UGC 09450	0.015058	0.1	-18.60
ASASSN-16ab	II	11 55 04.20	+01 43 07.2	CGCG 012-116	0.004373	0.066	-16.48
SN2015bf	II	23 24 49.03	+15 16 52.0	NGC 7653	0.014295	0.207	-20.99
PSNJ0919528	IIP	09 19 52.86	-68 54 41.9	ESO 061-G008	0.011291	0.369	-21.20
SN2015ay	IIP	01 09 46.77	+13 18 28.9	UGC 00722	0.014123	0.085	-18.75
SN2015ap	II	02 05 13.32	+06 06 08.4	IC 1776	0.011348	0.131	-19.48
PSNJ2241147	II	22 41 14.79	-21 47 42.1	NGC 7349	0.015054	0.091	-19.43
2015ah	II	23 00 24.63	+01 37 36.8	UGC 12295	0.016122	0.25	-19.27
PSNJ2246050	II	22 46 05.04	-10 59 48.4	NGC 7371	0.009007	0.191	-20.58
PSNJ1828582	IIP	18 28 58.23	+22 54 10.6	NGC 6641	0.013873	0.349	-18.47
LSQ15xp	IIP	11 32 42.79	-16 44 01.2	MCG -03-30-002	0.012231	0.12	-
SN2015W	II	06 57 43.03	+13 34 45.7	UGC 03617	0.013337	0.43	-18.62
ASASSN-15tw	II	12 50 28.05	-10 50 29.2	DDO 151	0.008228	0.139	-20.36
ASASSN-15tu	II	22 34 02.58	-32 23 53.6	2MASX J22340166-3223490	0.012229	0.043	-23.48
ASASSN-15ta	II	20 29 33.03	-61 57 03.4	GALEXASC J202933.17-615703.5	0.014591	0.153	-

ASASSN-15rp	II	00 03 37.27	-34 33 23.9	GALEXASC J000337.23-343323.1	0.028621	0.049	-
ASASSN-15qh	II	22 45 13.22	-22 43 39.8	ESO 534-G024	0.010229	0.093	-20.17
ASASSN-15ln	IIP	00 53 41.40	+18 05 29.0	UGC 00546	0.015092	0.147	-19.29
ASASSN-15kz	IIP	13 37 18.67	-28 39 23.6	IC 4303	0.007957	0.186	-18.06
ASASSN-15kj	IIP	01 58 11.53	-39 32 49.7	ESO 297-G037	0.01845	0.062	-21.05
ASASSN-15jp	IIP	10 11 38.99	-31 39 04.0	NGC 3157	0.009483	0.311	-20.15
ASASSN-15hs	Ic	15 33 34.31	-78 07 23.5	ESO 022-G010	0.009058	0.336	-19.55
ASASSN-15fz	Ic	13 35 25.14	+01 24 33.0	NGC 5227	0.01746	0.076	-20.84
ASASSN-15fi	IIP	16 31 48.80	+20 24 38.5	MRK 0884	0.017222	0.177	-19.52
ASASSN-15bd	IIP	15 54 38.33	+16 36 38.1	SDSS J155438.39+163637.6	0.007971	0.107	-15.92
ASASSN-15bb	II	13 01 06.38	-36 36 00.2	ESO 381-IG048	0.016032	0.147	-19.72
ASASSN-15ab	II	14 03 06.24	-38 28 29.9	ESO 325-G045	0.017683	0.34	-20.72
ASASSN-15lx	IIb	20 36 05.24	-73 06 32.4	ESO 047-G004	0.012622	0.176	-18.28
ASASSN-15ng	IIb	13 51 31.65	-48 04 33.7	ESO 221-G012	0.009998	0.454	-20.62
ASASSN-15oz	II	19 19 33.49	-33 46 02.0	HIPASS J1919-33	0.006929	0.281	-
SN2015bm	II	12 08 00.10	+19 44 26.7	SDSS J120759.79+194434.9	-	0.095	-
ASASSN-16gy	IIb	02 21 22.77	+16 33 54.6	UGC 01814	-	0.454	-
ASASSN-18ou	IIb	05 11 33.411	-21 16 10.47	ESO553-G19	-	0.113	-
SN2017ewx	Ic-BL	14:02:16.52	+07:40:44.21	NGC 5418	-	0.083	-
SN2017ivu	Ic-BL	15:36:32.7	+16:36:19.40	NGC 5962	-	0.168	-
SN2016afa	IIP	15 36 32.47	+16 36 36.7	NGC 5962	-	0.168	-

Table 2.23: Entire version of Table 2.2.

Name	z_{cmb}	D_L	d_{proj}	r_{HII}	$Area_{HII}$
SN2018eog	0.0180	79.1	0.0	460.2	5.99
SN2018ant	0.0207	91.9	0.0	534.6	3.29
ASASSN-18oa	0.0190	86.8	0.0	504.8	2.94
SN2018bl	0.0181	80.2	0.0	466.3	0.68
SN2018evy	0.0173	77.1	0.0	448.6	1.90
SN2018cho	0.0155	68.1	0.0	396.3	0.49
SN2018ie	0.0151	67.7	0.0	393.6	0.49
SN2018yo	0.0145	60.8	2004.2	353.5	0.39
AT2018cuf	0.0102	42.6	0.0	247.7	1.73
ASASSN-18eo	0.0247	106.9	0.0	622.0	3.65
SN2018dfg	0.0103	43.6	0.0	253.9	0.20
ASASSN-18cb	0.0077	23.9	819.2	139.0	0.18
AT2018bbl	0.0060	29.3	0.0	283.7	0.25
SN2017jbj	0.0126	53.5	0.0	311.5	0.30
LCRSB1107092	0.0382	169.3	0.0	985.1	9.15
ATLAS17lsn	0.0157	69.3	889.6	336.0	2.06
SN2017grn	0.0161	72.0	0.0	418.7	0.55

Gaia17chn	0.0192	85.2	0.0	495.4	0.77
SN2017gmr	0.0044	21.7	0.0	126.1	0.25
SN2017gax	0.0048	23.2	0.0	224.8	0.16
SN2017fem	0.0148	63.0	0.0	366.4	0.42
SN2017faf	0.0286	126.1	331.2	733.8	1.69
ATLAS17hpc	0.0195	82.2	599.0	398.7	1.70
SN2017cjd	0.0237	104.7	0.0	608.9	1.16
SN2017bzb ₂	0.0021	11.5	0.0	66.7	0.04
SN2017bif	0.0190	89.8	0.0	522.6	4.86
ASASSN-17qp	0.0048	25.7	0.0	149.6	0.30
ASASSN-17oj	0.0179	79.2	3774.5	383.9	1.57
ASASSN-17ny	0.0064	25.9	363.2	125.7	0.17
SN2017gat	0.0221	95.6	0.0	556.2	0.97
SN2017fqk	0.0096	40.3	0.0	234.6	0.52
SN2017ffq	0.0127	47.5	0.0	184.1	0.53
SN2017fbu	0.0101	42.6	0.0	247.7	0.71
SN2017ecp	0.0236	101.9	0.0	593.0	1.10
SN2017auf	0.0134	58.6	0.0	341.1	0.37
ASASSN-14at	0.0103	46.6	0.0	270.9	0.23
ASASSN-14az	0.0059	29.1	0.0	281.9	0.25
ASASSN-14dd	0.0182	79.3	902.3	461.2	0.67
SN2014dw	0.0092	31.1	0.0	180.6	0.10
NGC7742	0.0043	22.7	0.0	219.7	0.15
SN2014cw	0.0079	38.0	558.7	221.1	0.15
SN2014ce	0.0102	44.3	0.0	257.7	0.21
ASASSN-14ma	0.0121	52.4	0.0	304.7	0.29
ASASSN-14kp	0.0217	95.4	2654.1	555.2	5.49
ASASSN-14dl	0.0147	64.9	423.4	377.5	0.45
ASASSN-14dp	0.0103	39.9	0.0	232.1	0.73
ASASSN-14iz	0.0186	80.1	847.8	466.2	0.68
ASASSN-14jb	0.0049	24.7	1434.6	143.6	0.45
SN2016iae	0.0038	18.0	0.0	174.8	0.10
SN2016hvu	0.0174	77.7	0.0	452.0	0.64
SNhunt327	0.0066	30.5	0.0	177.4	0.10
SN2016gkg	0.0041	21.8	209.6	126.8	0.19
SN2016bmi	0.0074	27.3	0.0	158.6	0.24
SN2016bas	0.0100	45.1	0.0	437.1	0.60
SN2016P	0.0154	64.2	0.0	373.4	0.44
SN2016C	0.0056	15.3	0.0	89.1	0.02
SN2016jga	0.0240	105.1	0.0	611.6	3.52
SN2016iyd	0.0353	148.8	0.0	865.9	8.64
SN2016hwn	0.0226	92.5	1619.6	538.3	0.91

SN2016hpt	0.0258	110.6	0.0	643.7	1.30
ASASSN-16jt	0.0100	46.5	0.0	270.6	1.00
ASASSN-16in	0.0160	70.5	0.0	410.1	1.94
SN2016egz	0.0222	96.3	0.0	560.3	0.99
ASASSN-16go	0.0171	75.2	0.0	437.3	0.60
NGC3627 ₃	0.0039	10.4	0.0	100.6	0.03
SN2016cdd	0.0095	32.4	0.0	188.3	0.11
ASASSN-16eh	0.0117	51.6	0.0	300.0	0.28
ASASSN-16dm	0.0180	75.8	0.0	440.9	0.61
SN2016ase	0.0154	69.9	0.0	406.5	0.52
ASASSN-16cc	0.0042	18.6	0.0	180.8	0.10
SN2016aiy	0.0110	35.9	0.0	208.8	0.68
ASASSN-16bm	0.0080	31.3	0.0	182.3	0.31
ASASSN-16ba	0.0150	67.1	1560.7	390.5	0.48
ASASSN-16at	0.0052	15.5	0.0	150.4	0.07
ASASSN-16al	0.0100	41.9	4074.9	243.5	0.19
ASASSN-16ai	0.0157	66.1	0.0	384.4	0.46
ASASSN-16ab	0.0055	18.2	0.0	105.8	0.04
SN2015bf	0.0131	58.0	0.0	337.4	1.07
PSNJ0919528	0.0118	51.4	0.0	299.1	0.28
SN2015ay	0.0131	55.4	0.0	322.1	0.33
SN2015ap	0.0105	44.2	0.0	257.4	0.21
PSNJ2241147	0.0141	63.7	0.0	370.5	0.43
2015ah	0.0150	67.4	0.0	392.3	0.48
PSNJ2246050	0.0079	37.8	0.0	219.7	0.15
PSNJ1828582	0.0135	58.5	0.0	340.4	0.36
LSQ15xp	0.0134	57.6	1429.0	334.9	0.35
SN2015W	0.0139	61.4	4317.5	357.0	0.40
ASASSN-15tw	0.0093	36.8	0.0	214.2	0.14
ASASSN-15tu	0.0114	52.2	0.0	303.7	0.29
ASASSN-15ta	0.0144	64.5	0.0	375.1	0.44
ASASSN-15rp	0.0276	122.1	0.0	710.3	1.59
ASASSN-15qh	0.0092	43.7	0.0	254.4	0.20
ASASSN-15ln	0.0141	60.3	796.2	351.0	0.39
ASASSN-15kz	0.0089	29.7	0.0	172.7	0.09
ASASSN-15kj	0.0179	79.1	0.0	460.4	0.67
ASASSN-15jp	0.0105	44.2	2275.8	257.3	0.21
ASASSN-15hs	0.0094	36.5	0.0	212.6	0.14
ASASSN-15fz	0.0184	76.5	0.0	445.2	1.87
ASASSN-15fi	0.0174	75.6	0.0	440.0	0.61
ASASSN-15bd	0.0083	39.1	0.0	227.6	0.16
ASASSN-15bb	0.0170	76.7	0.0	445.9	0.62

ASASSN-15ab	0.0186	83.6	0.0	486.4	0.74
ASASSN-15lx	0.0125	54.7	0.0	318.2	0.32
ASASSN-15ng	0.0108	36.4	0.0	211.6	0.14
ASASSN-15oz	0.0065	28.2	2153.2	164.1	0.08
SN2015bm	0.0256	118.5	1534.2	689.6	1.49
ASASSN-16gy	0.0129	54.1	0.0	314.6	0.31
ASASSN-18ou	0.0141	62.3	2143.2	362.4	1.79
SN2017ewx	0.0159	66.3	0.0	385.5	0.47
SN2017ivu	0.0070	33.9	0.0	197.1	0.12
SN2016afa	0.0070	33.9	0.0	197.1	0.12

Table 2.24: Entire version of Table 2.5.

SN Name	H α	H β	[OIII] λ 5007	[NII] λ 6584	[SII] λ 6716
SN2018eog	19.92 (1.12)	6.97 (2.02)	3.80 (1.34)	4.58 (1.05)	5.73 (0.90)
SN2018ant	61.91 (3.94)	11.90 (24.92)	12.46 (7.27)	17.76 (3.58)	17.35 (3.25)
ASASSN-18oa	189.38 (3.61)	66.22 (5.17)	45.88 (4.45)	57.99 (2.66)	46.54 (2.31)
SN2018bl	382.70 (5.33)	133.82 (6.65)	89.50 (5.41)	98.01 (3.10)	70.51 (3.34)
SN2018evy	2398.58 (24.23)	838.73 (35.76)	157.37 (25.65)	941.54 (16.49)	348.78 (12.82)
SN2018cho	140.11 (2.43)	48.99 (6.81)	19.77 (6.65)	61.52 (2.10)	27.41 (1.62)
SN2018ie	629.83 (5.17)	220.18 (6.65)	150.08 (5.14)	164.01 (2.83)	111.36 (2.39)
SN2018yo	-	-	35.18 (4.04)	42.77 (2.60)	33.53 (2.10)
AT2018cuf	452.06 (8.04)	158.06 (12.31)	78.73 (9.75)	149.76 (8.62)	83.08 (4.52)
ASASSN-18eo	156.28 (2.04)	54.64 (3.92)	144.63 (3.89)	13.31 (1.43)	28.54 (1.50)
SN2018dfg	1330.07 (13.75)	465.02 (16.70)	175.33 (9.74)	395.10 (7.27)	196.41 (4.58)
ASASSN-18cb	51120.30 (1552.38)	466.34 (17.08)	81.25 (9.13)	390.52 (6.45)	188.40 (4.39)
AT2018bbl	33.10 (1.58)	11.57 (2.26)	2.85 (2.21)	11.84 (1.21)	10.62 (1.01)
SN2017bjj	52.55 (1.72)	18.37 (4.14)	28.58 (3.62)	11.94 (1.30)	10.18 (1.17)
LCRSB1107092	88.11 (1.15)	30.81 (1.44)	22.69 (1.24)	26.49 (0.97)	20.35 (0.72)
ATLAS17lsn	14.89 (0.74)	5.21 (1.28)	3.94 (1.42)	2.40 (0.51)	7.83 (0.87)
SN2017grn	227.51 (4.83)	79.59 (14.06)	21.40 (13.65)	90.96 (4.07)	40.58 (3.42)
Gaia17chn	401.03 (5.41)	140.19 (12.81)	39.68 (9.79)	159.41 (4.13)	75.16 (2.90)
SN2017gmr	742.20 (11.92)	259.54 (14.92)	83.39 (11.97)	191.68 (7.68)	179.02 (6.36)
SN2017gax	451.15 (4.18)	157.75 (6.01)	76.65 (4.69)	184.85 (2.91)	70.75 (1.74)
SN2017fem	2888.48 (49.43)	1009.98 (50.53)	291.67 (35.31)	958.27 (26.92)	455.45 (16.37)
SN2017faf	345.84 (9.08)	137.25 (12.96)	421.88 (15.54)	20.93 (6.05)	40.93 (5.76)
ATLAS17hpc	312.45 (2.52)	109.26 (2.66)	148.16 (2.46)	56.19 (1.23)	41.30 (0.95)
SN2017cjd	978.49 (16.14)	342.13 (16.30)	271.02 (13.47)	209.76 (7.96)	136.37 (9.17)
SN2017bzb ₂	126.69 (2.83)	44.30 (4.55)	20.40 (3.49)	16.60 (1.79)	30.68 (1.59)
SN2017bif	321.82 (7.17)	112.53 (14.19)	63.75 (11.47)	94.56 (5.99)	73.54 (5.07)
ASASSN-17qp	59.89 (1.41)	20.94 (1.80)	21.17 (1.58)	5.96 (1.18)	5.75 (0.79)
ASASSN-17oj	-	-	37.62 (2.53)	3.16 (0.71)	7.88 (0.80)

ASASSN-17ny	118.02 (3.17)	41.26 (6.08)	70.82 (5.20)	34.91 (2.34)	35.16 (2.01)
SN2017gat	33.04 (0.62)	11.55 (1.13)	18.62 (1.06)	1.84 (0.41)	6.62 (0.49)
SN2017fqk	258.78 (3.93)	90.50 (11.18)	79.72 (9.29)	86.15 (3.09)	52.03 (2.50)
SN2017ffq	2819.09 (32.53)	985.69 (48.70)	680.45 (42.40)	805.78 (20.86)	610.30 (15.93)
SN2017fbu	280.27 (3.16)	98.00 (3.22)	225.16 (3.65)	36.32 (1.50)	46.25 (1.35)
SN2017ecp	71.37 (1.58)	24.95 (3.31)	27.87 (2.83)	14.63 (1.28)	27.06 (1.81)
SN2017auf	712.21 (10.19)	249.10 (23.96)	99.77 (22.20)	259.15 (8.08)	87.31 (4.67)
ASASSN-14at	160.31 (2.41)	56.05 (4.97)	21.02 (4.21)	41.08 (1.80)	48.31 (1.56)
ASASSN-14az	110.60 (1.71)	38.67 (4.07)	59.21 (3.24)	6.99 (1.40)	15.87 (1.13)
ASASSN-14dd	121.43 (4.10)	42.46 (9.54)	32.76 (7.78)	31.68 (2.69)	19.95 (2.10)
SN2014dw	986.57 (24.92)	344.80 (62.02)	207.24 (59.80)	388.33 (20.08)	289.66 (17.74)
NGC7742	2387.71 (25.68)	834.88 (28.68)	345.60 (26.70)	1103.17 (18.12)	476.78 (10.62)
SN2014cw	18.77 (1.09)	6.56 (2.00)	25.06 (2.54)	2.87 (0.83)	4.96 (0.73)
SN2014ce	7349.78 (86.15)	2569.84 (76.02)	3993.94 (84.51)	1451.09 (30.38)	1208.06 (24.14)
ASASSN-14ma	242.18 (1.97)	84.68 (3.69)	151.92 (3.35)	31.67 (1.14)	51.10 (1.12)
ASASSN-14kp	34.04 -	-	11.71 (1.92)	2.67 (0.63)	2.66 (0.48)
ASASSN-14dl	29.02 (0.70)	3.69 (1.92)	1.86 (1.53)	12.55 (0.60)	6.31 (0.48)
ASASSN-14dp	32.97 (1.27)	11.53 (2.82)	12.30 (2.71)	3.97 (1.14)	6.47 (0.90)
ASASSN-14iz	18.35 (1.01)	6.42 (1.98)	1.58 (4.04)	6.94 (0.77)	4.22 (0.68)
ASASSN-14jb	5.05 (0.21)	1.76 (0.24)	2.32 (0.22)	0.34 (0.10)	1.12 (0.12)
SN2016iae	3977.43 (82.08)	1390.61 (343.34)	798.24 (288.85)	1638.44 (69.65)	767.29 (51.70)
SN2016hvu	2392.35 (25.80)	836.46 (30.04)	816.21 (24.61)	653.60 (12.81)	326.62 (8.68)
SNhunt327	477.84 (3.05)	167.08 (5.86)	173.04 (4.85)	88.63 (1.77)	85.19 (1.48)
SN2016gkg	10.35 (0.51)	2.38 (0.98)	0.62 (0.86)	5.36 (0.41)	2.29 (0.32)
SN2016bmi	48.96 (3.07)	7.64 (6.00)	22.12 (6.43)	9.15 (2.68)	13.22 (2.29)
SN2016bas	2786.94 (14.12)	974.81 (27.96)	346.59 (21.44)	897.35 (8.62)	477.67 (6.05)
SN2016P	1769.39 (12.72)	618.70 (12.81)	331.21 (8.83)	655.16 (7.16)	200.12 (3.89)
SN2016C	20.56 (0.76)	7.19 (0.94)	3.43 (0.81)	8.22 (0.59)	8.21 (0.51)
SN2016jga	2512.82 (23.89)	878.60 (29.65)	792.58 (26.17)	576.53 (13.30)	571.66 (15.09)
SN2016iyd	1304.56 (9.70)	456.13 (20.43)	855.39 (18.34)	206.57 (6.29)	266.37 (6.65)
SN2016hwn	14.93 (1.52)	-	2.44 (1.19)	3.41 (0.60)	4.92 (0.67)
SN2016hpt	160.84 (1.80)	56.24 (2.32)	97.13 (2.29)	20.93 (1.19)	28.37 (1.28)
ASASSN-16jt	507.33 (12.14)	177.40 (17.82)	198.98 (17.97)	123.06 (9.04)	142.22 (7.67)
ASASSN-16in	24.06 (0.93)	8.41 (1.94)	9.55 (1.41)	2.90 (0.83)	6.23 (0.71)
SN2016egz	304.61 (2.41)	106.51 (3.59)	289.14 (3.83)	23.23 (1.37)	41.12 (1.57)
ASASSN-16go	2821.05 (29.12)	986.53 (32.89)	252.35 (21.45)	910.03 (16.75)	424.21 (11.00)
NGC3627 ₃	1765.41 (33.08)	617.33 (48.80)	170.43 (38.01)	640.88 (22.17)	292.66 (15.02)
SN2016cdd	23160.74 (433.15)	8098.06 (271.53)	38441.12 (758.30)	1067.26 (54.98)	1285.52 (50.66)
ASASSN-16eh	380.90 (3.38)	133.18 (7.90)	246.10 (7.26)	27.47 (2.24)	62.50 (2.19)
ASASSN-16dm	36.34 (2.94)	12.71 (3.86)	9.37 (2.85)	9.88 (2.69)	15.34 (2.99)
SN2016ase	32.76 (0.83)	11.46 (1.78)	12.85 (1.50)	2.42 (0.56)	5.26 (0.54)
ASASSN-16cc	1434.55 (10.04)	501.59 (17.33)	1285.95 (17.74)	86.43 (5.25)	205.09 (4.93)

SN2016aiy	235.18 (4.04)	82.24 (8.88)	96.99 (7.49)	34.55 (2.96)	52.96 (2.50)
ASASSN-16bm	814.23 (6.84)	284.71 (6.31)	877.06 (8.70)	17.57 (1.52)	47.87 (1.66)
ASASSN-16ba	-	-	8.46 (1.25)	2.95 (0.55)	4.79 (0.48)
ASASSN-16at	114.11 (2.17)	39.90 (4.23)	63.46 (3.84)	15.79 (1.39)	31.57 (1.42)
ASASSN-16al	-	-	110.05 (3.22)	9.88 (1.09)	19.22 (1.06)
ASASSN-16ai	241.35 (2.23)	84.39 (2.38)	310.40 (3.54)	9.53 (0.76)	24.49 (0.87)
ASASSN-16ab	396.43 (2.92)	138.61 (3.48)	199.33 (3.48)	36.85 (1.42)	85.26 (1.42)
SN2015bf	289.96 (7.19)	101.40 (12.13)	32.54 (9.08)	107.74 (5.49)	58.46 (4.16)
PSNJ0919528	93.17 (1.49)	32.58 (2.39)	29.47 (2.02)	21.70 (0.98)	22.47 (0.88)
SN2015ay	116.04 (2.09)	40.57 (4.42)	117.67 (4.54)	10.21 (1.21)	15.58 (1.17)
SN2015ap	1342.52 (8.10)	469.40 (10.19)	1242.37 (12.55)	116.78 (3.26)	154.68 (3.02)
PSNJ2241147	224.14 (2.24)	78.38 (4.42)	48.33 (3.76)	63.53 (1.59)	55.83 (1.36)
2015ah	147.37 (2.93)	51.53 (4.19)	33.79 (3.55)	36.16 (1.91)	32.14 (1.91)
PSNJ2246050	101.22 (5.02)	35.40 (11.45)	13.61 (9.11)	38.39 (4.03)	20.13 (3.36)
PSNJ1828582	243.11 (3.79)	85.00 (6.30)	49.18 (5.12)	94.23 (2.71)	43.91 (2.07)
LSQ15xp	8.44 (0.88)	-	-	-	8.30 (1.01)
SN2015W	8.19 -	-	-	-	14.24 (1.47)
ASASSN-15tw	64.83 (2.09)	22.67 (3.50)	20.35 (3.14)	7.50 (1.18)	11.77 (1.22)
ASASSN-15tu	275.89 (2.13)	96.47 (3.62)	187.18 (3.54)	41.10 (1.23)	46.36 (1.12)
ASASSN-15ta	743.30 (5.22)	259.90 (5.47)	756.50 (7.20)	68.86 (2.07)	95.40 (1.84)
ASASSN-15rp	65.18 (0.86)	22.79 (1.43)	47.35 (1.40)	4.38 (0.56)	8.86 (0.54)
ASASSN-15qh	36.19 (2.35)	11.43 (5.16)	6.11 (4.38)	13.39 (2.09)	11.69 (2.02)
ASASSN-15ln	47.54 (1.29)	16.62 (2.69)	33.93 (2.75)	4.22 (0.82)	5.82 (0.71)
ASASSN-15kz	153.16 (2.54)	53.55 (2.71)	111.21 (3.13)	14.67 (1.27)	25.87 (1.21)
ASASSN-15kj	146.92 (1.63)	51.36 (2.45)	28.31 (2.05)	54.15 (1.17)	36.12 (0.94)
ASASSN-15jp	39.42 (1.09)	-	6.87 (1.86)	8.83 (0.80)	10.50 (0.71)
ASASSN-15hs	15767.86 (421.61)	5513.47 (350.94)	1282.76 (202.79)	6264.71 (215.37)	2051.17 (107.20)
ASASSN-15fz	303.57 (6.13)	106.14 (14.76)	25.19 (13.19)	131.33 (5.25)	59.01 (4.26)
ASASSN-15fi	4688.63 (57.17)	1639.39 (52.35)	6631.22 (93.16)	343.12 (16.48)	483.71 (17.64)
ASASSN-15bd	1163.62 (6.06)	406.86 (7.44)	1164.92 (9.23)	77.21 (2.23)	136.93 (2.21)
ASASSN-15bb	191.62 (2.33)	67.00 (2.85)	156.91 (3.17)	17.59 (1.11)	36.40 (1.17)
ASASSN-15ab	519.60 (5.93)	181.67 (10.49)	220.93 (9.47)	85.34 (3.34)	73.49 (4.12)
ASASSN-15lx	636.47 (4.69)	222.55 (6.85)	837.83 (8.44)	35.04 (1.77)	67.29 (1.74)
ASASSN-15ng	605.14 (4.23)	211.61 (5.52)	348.63 (6.04)	92.29 (2.00)	109.26 (1.95)
ASASSN-15oz	-	-	204.08 (4.11)	10.70 (1.36)	28.04 (1.29)
SN2015bm	-	-	-	-	-
ASASSN-16gy	2431.28 (14.92)	850.06 (24.78)	-	-	-
ASASSN-18ou	111.83 (5.59)	-	-	-	-
SN2017ewx	-	-	-	-	-
SN2017ivu	-	-	-	-	-
SN2016afa	-	-	-	-	-

Table 2.25: Entire version of Table 2.6.

SN Name	H α EW	D16	N2	O3N2	Σ SFR	$E(B - V)$
SN2018eog	3.45 (0.26)	8.28 (0.12)	8.45 (0.05)	-	-3.68 (-0.00)	- (0.27)
SN2018ant	8.94 (0.75)	8.37 (0.11)	8.49 (0.04)	-	-2.90 (-0.02)	- (1.94)
ASASSN-18oa	27.22 (0.79)	8.49 (0.03)	8.51 (0.01)	8.46 (0.01)	-2.34 (-0.05)	0.16 (0.07)
SN2018bl	171.54 (5.87)	8.54 (0.02)	8.47 (0.01)	8.44 (0.01)	-1.47 (-0.52)	0.24 (0.05)
SN2018evy	108.29 (3.37)	8.86 (0.01)	8.56 (0.00)	8.60 (0.02)	-1.22 (-1.09)	0.44 (0.04)
SN2018cho	17.32 (0.52)	8.79 (0.02)	8.58 (0.01)	-	-1.90 (-0.15)	0.27 (0.13)
SN2018ie	342.46 (19.46)	8.56 (0.01)	8.47 (0.00)	8.44 (0.00)	-1.15 (-1.35)	0.28 (0.03)
SN2018yo	-	8.28 (0.03)	8.36 (0.05)	8.36 (0.05)	-	-
AT2018cuf	48.97 (1.36)	8.67 (0.03)	8.52 (0.01)	8.50 (0.01)	-2.35 (-0.04)	0.25 (0.07)
ASASSN-18eo	26.37 (0.85)	7.93 (0.05)	8.25 (0.02)	8.21 (0.01)	-2.27 (-0.05)	0.04 (0.07)
SN2018dfg	472.64 (12.91)	8.70 (0.01)	8.50 (0.00)	8.51 (0.01)	-1.27 (-0.95)	0.55 (0.03)
ASASSN-18cb	-	8.71 (0.01)	8.50 (0.00)	8.58 (0.01)	0.18 (213.32)	0.39 (0.04)
AT2018bbi	14.17 (1.08)	8.49 (0.06)	8.54 (0.02)	-	-2.97 (-0.01)	0.24 (0.19)
SN2017bjj	55.85 (6.32)	8.44 (0.06)	8.45 (0.02)	8.35 (0.03)	-2.37 (-0.05)	0.23 (0.21)
LCRSB1107092	23.91 (0.76)	8.52 (0.02)	8.50 (0.01)	8.45 (0.01)	-2.59 (-0.02)	0.06 (0.04)
ATLAS17lsn	-	7.88 (0.10)	8.38 (0.04)	-	-3.34 (-0.00)	0.25 (0.23)
SN2017grn	35.96 (1.32)	8.79 (0.03)	8.56 (0.01)	-	-1.69 (-0.28)	0.52 (0.16)
Gaia17chn	58.14 (1.71)	8.75 (0.02)	8.56 (0.01)	8.56 (0.02)	-1.50 (-0.47)	0.49 (0.09)
SN2017gmr	57.65 (2.35)	8.42 (0.02)	8.47 (0.01)	8.51 (0.01)	-1.92 (-0.14)	0.32 (0.06)
SN2017gax	84.55 (2.48)	8.85 (0.01)	8.56 (0.00)	8.52 (0.01)	-1.84 (-0.17)	0.36 (0.04)
SN2017fem	109.43 (3.12)	8.73 (0.02)	8.52 (0.01)	8.55 (0.01)	-0.49 (-15.10)	0.35 (0.05)
SN2017faf	114.12 (26.56)	7.91 (0.14)	8.15 (0.06)	8.16 (0.03)	-0.64 (-8.94)	0.06 (0.09)
ATLAS17hpc	-	8.48 (0.01)	8.40 (0.00)	8.35 (0.00)	-1.93 (-0.13)	0.23 (0.02)
SN2017cjd	124.31 (2.99)	8.54 (0.03)	8.43 (0.01)	8.41 (0.01)	-1.08 (-1.78)	0.17 (0.05)
SN2017bzb ₂	121.74 (18.71)	8.04 (0.05)	8.34 (0.02)	8.42 (0.02)	-2.43 (-0.04)	0.07 (0.10)
SN2017bif	9.07 (0.22)	8.52 (0.04)	8.50 (0.01)	8.47 (0.02)	-2.30 (-0.05)	- (0.12)
ASASSN-17qp	62.32 (6.13)	8.30 (0.10)	8.28 (0.04)	8.32 (0.02)	-2.66 (-0.02)	0.06 (0.08)
ASASSN-17oj	-	7.78 (0.05)	8.15 (0.03)	8.17 (0.05)	-	-
ASASSN-17ny	-	8.39 (0.04)	8.50 (0.01)	8.37 (0.02)	-2.34 (-0.05)	0.21 (0.14)
SN2017gat	34.97 (2.25)	7.66 (0.10)	8.16 (0.04)	8.22 (0.02)	-2.53 (-0.03)	0.07 (0.09)
SN2017fqk	79.26 (3.84)	8.63 (0.02)	8.52 (0.01)	8.44 (0.02)	-2.13 (-0.08)	0.42 (0.12)
SN2017ffq	74.11 (1.91)	8.51 (0.01)	8.49 (0.01)	8.45 (0.01)	-0.95 (-2.65)	0.32 (0.05)
SN2017fbu	120.19 (6.59)	8.20 (0.02)	8.33 (0.01)	8.27 (0.01)	-2.17 (-0.07)	0.07 (0.03)
SN2017ecp	10.39 (0.39)	8.11 (0.05)	8.43 (0.02)	8.38 (0.02)	-2.07 (-0.10)	- (0.12)
SN2017auf	32.68 (0.90)	8.90 (0.02)	8.54 (0.01)	8.52 (0.02)	-1.20 (-1.18)	0.57 (0.09)
ASASSN-14at	39.25 (1.17)	8.31 (0.02)	8.47 (0.01)	8.50 (0.02)	-1.87 (-0.16)	0.36 (0.08)
ASASSN-14az	25.48 (1.08)	7.86 (0.09)	8.19 (0.04)	8.24 (0.02)	-2.38 (-0.04)	- (0.10)
ASASSN-14dd	253.86 (76.40)	8.57 (0.05)	8.47 (0.02)	8.43 (0.03)	-1.97 (-0.14)	0.41 (0.21)
SN2014dw	66.22 (2.27)	8.55 (0.03)	8.56 (0.01)	8.49 (0.03)	-1.06 (-2.02)	0.85 (0.17)

NGC7742	49.39 (1.32)	8.82 (0.01)	8.59 (0.00)	8.54 (0.01)	-1.14 (-1.43)	0.24 (0.03)
SN2014cw	-	8.09 (0.14)	8.37 (0.06)	8.23 (0.04)	-2.82 (-0.02)	0.28 (0.29)
SN2014ce	163.38 (2.33)	8.43 (0.01)	8.42 (0.00)	8.34 (0.00)	-0.19 (-74.80)	0.28 (0.03)
ASASSN-14ma	64.85 (2.31)	8.10 (0.02)	8.33 (0.01)	8.29 (0.01)	-1.64 (-0.31)	0.15 (0.04)
ASASSN-14kp	10.52 -	8.18 (0.12)	8.31 (0.05)	-	-3.71 -	-
ASASSN-14dl	-	8.74 (0.03)	8.57 (0.01)	-	-2.61 (-0.02)	- (0.48)
ASASSN-14dp	28.01 (4.24)	8.08 (0.14)	8.32 (0.06)	8.33 (0.04)	-3.17 (-0.01)	- (0.23)
ASASSN-14iz	-	8.67 (0.08)	8.55 (0.02)	-	-2.79 (-0.02)	0.08 (0.29)
ASASSN-14jb	49.84 (9.01)	7.70 (0.14)	8.20 (0.06)	8.26 (0.03)	-4.24 (-0.00)	0.07 (0.13)
SN2016iae	317.28 (13.39)	8.77 (0.03)	8.57 (0.01)	-	-0.90 (-3.34)	1.02 (0.23)
SN2016hvu	250.41 (5.51)	8.69 (0.01)	8.48 (0.00)	8.41 (0.00)	-0.69 (-6.56)	0.14 (0.03)
SNhunt327	148.06 (5.33)	8.36 (0.01)	8.40 (0.00)	8.37 (0.00)	-1.37 (-0.68)	0.26 (0.03)
SN2016gkg	-	8.78 (0.06)	8.61 (0.02)	-	-3.60 (-0.00)	- (0.38)
SN2016bmi	15.88 (1.93)	8.19 (0.14)	8.41 (0.06)	-	-2.84 (-0.02)	- (0.73)
SN2016bas	214.71 (2.82)	8.68 (0.01)	8.52 (0.00)	8.52 (0.01)	-1.05 (-1.86)	0.51 (0.03)
SN2016P	355.72 (8.83)	8.93 (0.01)	8.54 (0.00)	8.50 (0.00)	-0.82 (-4.05)	0.24 (0.02)
SN2016C	14.69 (1.16)	8.43 (0.04)	8.56 (0.02)	8.52 (0.03)	-2.74 (-0.02)	- (0.13)
SN2016jga	107.78 (2.52)	8.35 (0.01)	8.45 (0.01)	8.41 (0.00)	-1.17 (-1.28)	0.21 (0.03)
SN2016iyd	100.70 (2.66)	8.22 (0.02)	8.37 (0.01)	8.30 (0.01)	-1.50 (-0.46)	0.15 (0.04)
SN2016hwn	19.86 (5.77)	8.28 (0.09)	8.46 (0.04)	-	-2.87 (-0.02)	-
SN2016hpt	45.68 (1.87)	8.15 (0.03)	8.33 (0.01)	8.29 (0.01)	-1.81 (-0.19)	0.09 (0.04)
ASASSN-16jt	22.83 (0.67)	8.32 (0.04)	8.46 (0.02)	8.39 (0.01)	-2.03 (-0.11)	0.33 (0.10)
ASASSN-16in	8.59 (0.84)	7.97 (0.13)	8.32 (0.06)	8.32 (0.04)	-3.20 (-0.01)	- (0.22)
SN2016egz	40.32 (0.87)	8.00 (0.03)	8.23 (0.01)	8.20 (0.01)	-1.54 (-0.41)	0.05 (0.03)
ASASSN-16go	136.74 (2.74)	8.74 (0.01)	8.52 (0.00)	8.55 (0.01)	-0.61 (-8.86)	0.33 (0.03)
NGC3627 ₃	92.78 (2.93)	8.77 (0.02)	8.54 (0.01)	8.56 (0.02)	-1.25 (-1.05)	0.48 (0.08)
SN2016cdd	994.94 (20.23)	8.09 (0.03)	8.13 (0.01)	8.10 (0.01)	0.31 (152.18)	0.25 (0.04)
ASASSN-16eh	69.73 (2.00)	7.89 (0.04)	8.22 (0.02)	8.23 (0.01)	-1.42 (-0.58)	0.29 (0.06)
ASASSN-16dm	9.60 (1.02)	8.22 (0.14)	8.48 (0.06)	8.44 (0.05)	-2.36 (-0.08)	- (0.29)
SN2016ase	73.07 (10.69)	7.91 (0.11)	8.22 (0.05)	8.28 (0.03)	-1.41 (-0.67)	0.04 (0.15)
ASASSN-16cc	121.12 (4.16)	7.84 (0.03)	8.18 (0.01)	8.18 (0.01)	-1.14 (-1.40)	0.10 (0.03)
SN2016aiy	77.24 (5.07)	8.13 (0.04)	8.36 (0.02)	8.34 (0.01)	-2.38 (-0.04)	0.31 (0.10)
ASASSN-16bm	451.89 (14.53)	7.66 (0.04)	7.97 (0.02)	8.07 (0.01)	-1.66 (-0.29)	0.06 (0.02)
ASASSN-16ba	-	8.16 (0.02)	8.38 (0.01)	8.36 (0.06)	-	-
ASASSN-16at	58.98 (3.41)	8.01 (0.04)	8.35 (0.02)	8.31 (0.01)	-2.44 (-0.03)	0.20 (0.10)
ASASSN-16al	-	8.02 (0.08)	8.27 (0.04)	8.22 (0.04)	-	-
ASASSN-16ai	152.74 (5.02)	7.75 (0.04)	8.09 (0.02)	8.11 (0.01)	-1.72 (-0.24)	0.08 (0.03)
ASASSN-16ab	86.01 (2.30)	7.90 (0.02)	8.27 (0.01)	8.28 (0.00)	-1.47 (-0.51)	0.08 (0.02)
SN2015bf	50.28 (2.60)	8.69 (0.03)	8.54 (0.01)	8.55 (0.03)	-2.23 (-0.06)	0.25 (0.11)
PSNJ0919528	40.11 (1.91)	8.35 (0.02)	8.45 (0.01)	8.41 (0.01)	-2.08 (-0.09)	0.20 (0.07)
SN2015ay	123.99 (15.40)	8.08 (0.06)	8.26 (0.02)	8.21 (0.02)	-1.92 (-0.15)	0.24 (0.10)
SN2015ap	417.45 (19.67)	8.14 (0.01)	8.25 (0.01)	8.22 (0.00)	-0.87 (-3.39)	0.17 (0.02)

PSNJ2241147	36.48 (1.15)	8.44 (0.01)	8.49 (0.01)	8.46 (0.01)	-1.79 (-0.20)	0.19 (0.05)
2015ah	93.34 (6.27)	8.43 (0.03)	8.46 (0.01)	8.44 (0.01)	-1.90 (-0.16)	0.20 (0.08)
PSNJ2246050	58.37 (6.31)	8.74 (0.08)	8.55 (0.02)	-	-2.38 (-0.05)	0.67 (0.30)
PSNJ1828582	67.99 (3.49)	8.77 (0.02)	8.55 (0.01)	8.50 (0.01)	-2.11 (-0.08)	0.32 (0.07)
LSQ15xp	29.12 (12.41)	8.03 (0.03)	8.25 (0.02)	8.24 (0.05)	-3.44 (-0.01)	-
SN2015W	18.81 -	7.82 (0.06)	8.16 (0.04)	8.14 (0.05)	-3.12 -	-
ASASSN-15tw	128.80 (32.65)	8.09 (0.08)	8.31 (0.03)	8.34 (0.03)	-2.24 (-0.07)	0.20 (0.15)
ASASSN-15tu	109.04 (5.26)	8.27 (0.02)	8.36 (0.01)	8.29 (0.00)	-1.61 (-0.33)	0.11 (0.04)
ASASSN-15ta	81.20 (1.60)	8.12 (0.01)	8.27 (0.01)	8.21 (0.00)	-1.21 (-1.11)	0.07 (0.02)
ASASSN-15rp	39.10 (1.72)	7.90 (0.06)	8.20 (0.03)	8.21 (0.01)	-1.94 (-0.13)	0.05 (0.06)
ASASSN-15qh	5.28 (0.38)	8.48 (0.09)	8.54 (0.03)	-	-2.33 (-0.07)	- (0.42)
ASASSN-15ln	-	8.12 (0.10)	8.26 (0.04)	8.24 (0.02)	-2.34 (-0.05)	0.20 (0.15)
ASASSN-15kz	67.00 (2.33)	8.03 (0.04)	8.27 (0.02)	8.25 (0.01)	-1.87 (-0.16)	0.04 (0.05)
ASASSN-15kj	44.94 (1.14)	8.61 (0.01)	8.54 (0.00)	8.50 (0.01)	-1.94 (-0.13)	0.27 (0.05)
ASASSN-15jp	48.08 (3.20)	8.28 (0.04)	8.41 (0.02)	8.39 (0.08)	-2.46 (-0.04)	0.42 -
ASASSN-15hs	254.64 (8.26)	8.90 (0.02)	8.56 (0.01)	8.58 (0.02)	0.15 (235.26)	0.29 (0.06)
ASASSN-15fz	16.84 (0.59)	8.80 (0.03)	8.57 (0.01)	-	-2.04 (-0.10)	0.26 (0.13)
ASASSN-15fi	147.13 (2.44)	8.08 (0.02)	8.22 (0.01)	8.16 (0.01)	-0.39 (-23.51)	0.19 (0.03)
ASASSN-15bd	170.56 (3.62)	7.98 (0.01)	8.20 (0.01)	8.18 (0.00)	-0.96 (-2.51)	0.14 (0.02)
ASASSN-15bb	152.82 (6.75)	7.95 (0.03)	8.26 (0.01)	8.23 (0.01)	-1.77 (-0.22)	0.07 (0.04)
ASASSN-15ab	292.89 (26.36)	8.39 (0.03)	8.38 (0.01)	8.35 (0.01)	-1.34 (-0.77)	0.16 (0.05)
ASASSN-15lx	508.26 (50.47)	7.92 (0.02)	8.16 (0.01)	8.14 (0.01)	-1.25 (-1.00)	0.11 (0.03)
ASASSN-15ng	130.49 (3.25)	8.25 (0.01)	8.37 (0.00)	8.31 (0.00)	-1.27 (-0.93)	0.23 (0.02)
ASASSN-15oz	-	7.77 (0.06)	8.11 (0.03)	8.16 (0.01)	-	-
SN2015bm	-	8.10 (0.49)	8.28 (0.10)	8.30 (0.04)	-	-
ASASSN-16gy	196.10 (5.39)	8.55 (0.01)	8.43 (0.00)	8.44 (0.00)	-1.02 (-2.02)	0.17 (0.03)
ASASSN-18ou	2.16 (0.11)	8.14 (0.06)	8.32 (0.04)	8.30 (0.06)	-2.64 (-0.03)	-
SN2017ewx	-	8.75 (0.44)	8.54 (0.43)	-	-	-
SN2017ivu	-	9.09 (0.45)	8.45 (0.42)	-	-	-
SN2016afa	-	8.99 (0.45)	8.45 (0.42)	-	-	-

Table 2.26: Entire version of Table 2.19.

SN	V		B		r	
	M_{peak}	s	M_{peak}	s	M_{peak}	s
SN2018eog	-16.88 (0.06)	-	-	-	-	-
SN2018ant	-	-	-	-	-	-
SN2018bl	-	-	-	-	-	-
SN2018evy	-	-	-	-	-	-
SN2018cho	-17.56 (0.14)	-	-	-	-	-
SN2018fit	-	-	-	-	-	-
SN2018yo	-17.06 (0.09)	-	-	-	-	-

AT2018cuf	-16.52 (0.12)	-	-	-	-	-
ASASSN-18eo	-18.83 (0.08)	0.0201 (0.0053)	-	-	-	-
ASASSN-18cb	-16.72 (0.07)	0.0075 (0.0032)	-	-	-	-
AT2018bbl	-	-	-	-	-	-
SN2017jbj	-16.55 (0.45)	-	-	-	-	-
SN2017grn	-17.57 (0.09)	-	-	-	-	-
Gaia17chn	-18.28 (0.10)	-	-	-	-	-
SN2017gmr	-17.47 (0.03)	0.0042 (0.0007)	-17.30 (0.04)	0.0239 (0.0016)	-17.70 (0.03)	0.0025 (0.0007)
SN2017fem	-17.12 (0.27)	-	-	-	-	-
SN2017faf	-19.01 (0.27)	-	-	-	-	-
ATLAS17hpc	-18.84 (0.08)	0.0205 (0.0041)	-	-	-	-
SN2017bzb ₂	-17.14 (0.10)	0.0216 (0.0063)	-	-	-	-
SN2017bif	-18.51 (0.24)	0.0196 (0.0131)	-	-	-	-
ASASSN-17qp	-	-	-	-	-	-
ASASSN-17oj	-17.91 (0.12)	0.0114 (0.0115)	-	-	-	-
ASASSN-17ny	-17.77 (0.08)	0.0221 (0.0029)	-	-	-	-
SN2017fqk	-16.90 (0.13)	0.0240 (0.0077)	-	-	-	-
SN2017ffq	-18.06 (0.13)	0.0184 (0.0074)	-	-	-	-
SN2017fbu	-16.90 (0.08)	0.0056 (0.0046)	-	-	-	-
SN2017auf	-17.34 (0.11)	-	-	-	-	-
ASASSN-14at	-17.16 (0.15)	0.0205 (0.0092)	-	-	-	-
SN2014dw	-16.84 (0.04)	0.0298 (0.0015)	-16.38 (0.04)	0.0633 (0.0015)	-17.02 (0.04)	0.0178 (0.0010)
NGC7742	-16.04 (0.04)	0.0073 (0.0021)	-16.06 (0.04)	0.0340 (0.0021)	-16.14 (0.03)	0.0081 (0.0008)
SN2014cw	-	-	-	-	-	-
SN2014ce	-17.48 (0.09)	0.0202 (0.0077)	-	-	-	-
ASASSN-14ma	-17.07 (0.15)	0.0000 (0.0133)	-	-	-	-
ASASSN-14kp	-18.04 (0.06)	0.0712 (0.0038)	-17.91 (0.03)	0.0734 (0.0012)	-17.97 (0.05)	0.0897 (0.0027)
ASASSN-14dl	-	-	-	-	-	-
ASASSN-14dp	-17.64 (0.18)	-	-	-	-	-
ASASSN-14iz	-18.47 (0.15)	-	-	-	-	-
ASASSN-14jb	-16.08 (0.03)	-	-16.06 (0.04)	-	-16.05 (0.04)	0.0110 (0.0011)
SN2016hvu	-18.03 (0.38)	-	-	-	-	-
SNhunt327	-16.40 (0.14)	-	-	-	-	-
SN2016bmi	-15.95 (0.11)	0.0088 (0.0067)	-	-	-	-
SN2016C	-15.50 (0.15)	0.0064 (0.0076)	-	-	-	-
SN2016jga	-18.32 (0.22)	0.0048 (0.0175)	-	-	-	-
SN2016iyd	-19.98 (0.06)	-	-20.04 (0.07)	-	-20.25 (0.08)	-
SN2016hwn	-18.96 (0.06)	-	-	-	-	-
SN2016hpt	-18.42 (0.08)	0.0350 (0.0056)	-18.35 (0.13)	-	-18.49 (0.16)	-
SN2016egz	-18.74 (0.12)	0.0415 (0.0070)	-	-	-	-
ASASSN-16go	-18.41 (0.13)	-	-	-	-	-
NGC3627 ₃	-	-	-	-	-	-

ASASSN-16eh	-18.33 (0.10)	0.0244 (0.0068)	-	-	-	-
ASASSN-16dm	-17.88 (0.16)	-	-	-	-	-
SN2016ase	-	-	-18.05 (0.06)	0.0496 (0.0046)	-18.02 (0.04)	0.0117 (0.0019)
ASASSN-16cc	-15.80 (0.05)	-	-15.78 (0.05)	0.0254 (0.0026)	-	-
ASASSN-16bm	-15.79 (0.18)	0.0090 (0.0114)	-	-	-	-
ASASSN-16ba	-17.34 (0.04)	-	-17.38 (0.05)	-	-17.51 (0.04)	-
ASASSN-16at	-16.74 (0.03)	0.0182 (0.0009)	-16.86 (0.04)	0.0490 (0.0016)	-16.90 (0.03)	0.0117 (0.0009)
ASASSN-16al	-16.81 (0.18)	-	-	-	-	-
ASASSN-16ai	-17.13 (0.10)	-	-	-	-	-
ASASSN-16ab	-16.73 (0.04)	0.0158 (0.0012)	-	-	-	-
PSNJ0919528	-16.80 (0.20)	0.0064 (0.0093)	-	-	-	-
SN2015ay	-16.95 (0.13)	0.0163 (0.0122)	-	-	-	-
LSQ15xp	-17.60 (0.25)	-	-	-	-	-
SN2015W	-17.69 (0.04)	0.0231 (0.0014)	-17.23 (0.05)	0.0570 (0.0022)	-	-
ASASSN-15tw	-16.51 (0.04)	-	-16.24 (0.05)	-	-16.66 (0.03)	-
ASASSN-15rp	-18.85 (0.06)	0.0541 (0.0041)	-18.02 (0.05)	0.0494 (0.0040)	-18.41 (0.04)	0.0320 (0.0024)
ASASSN-15qh	-17.16 (0.11)	0.0220 (0.0061)	-	-	-	-
ASASSN-15ln	-18.01 (0.13)	-	-	-	-	-
ASASSN-15kz	-16.87 (0.10)	0.0162 (0.0057)	-	-	-	-
ASASSN-15jp	-18.32 (0.07)	0.0259 (0.0040)	-	-	-	-
ASASSN-15fz	-17.47 (0.08)	-	-	-	-	-
ASASSN-15fi	-	-	-	-	-	-
ASASSN-15bb	-17.97 (0.25)	0.0002 (0.0135)	-	-	-	-
ASASSN-15ng	-17.49 (0.10)	-	-	-	-	-
ASASSN-15oz	-18.05 (0.05)	0.0143 (0.0027)	-	-	-	-
SN2015bm	-	-	-	-	-	-
ASASSN-16gy	-	-	-	-	-	-
ASASSN-18ou	-	-	-	-	-	-
SN2017ivu	-	-	-	-	-	-
SN2016afa	-	-	-	-	-	-

Chapter 3

A metallicity dependence on the occurrence of core-collapse supernovae

Direis agora: "Tresloucado amigo!

Que conversas com elas? Que sentido

Tem o que dizem, quando estão contigo?"

3.1 Context

This chapter is composed by the article Pessi et al. (2023b), which was accepted for publication at the The Astrophysical Journal Letters on 30 August 2023 and published online on 26 September 2023 (doi: 10.3847/2041-8213/acf7c6). The authors of this work are Thallis Pessi, Joseph P. Anderson, Joseph D. Lyman, Jose L. Prieto, Lluís Galbany, Christopher S. Kochanek, Sebastian F. Sánchez, and Hanindyo Kuncarayakti.

3.2 Abstract

Core-collapse supernovae (CCSNe) are widely accepted to be caused by the explosive death of massive stars with initial masses $\gtrsim 8 M_{\odot}$. There is, however, a comparatively poor understanding of how properties of the progenitors – mass, metallicity, multiplicity, rotation

etc. — manifest in the resultant CCSN population. Here we present a minimally biased sample of nearby CCSNe from the ASAS-SN survey whose host galaxies were observed with integral-field spectroscopy using MUSE at the VLT. This dataset allows us to analyze the explosion sites of CCSNe within the context of global star formation properties across the host galaxies. We show that the CCSN explosion site oxygen abundance distribution is offset to lower values than the overall HII region abundance distribution within the host galaxies. We further split the sample at $12 + \log_{10}(\text{O}/\text{H}) = 8.6$ dex and show that within the sub-sample of low-metallicity host galaxies, the CCSNe unbiasedly trace the star-formation with respect to oxygen abundance, while for the sub-sample of higher-metallicity host galaxies, they preferentially occur in lower-abundance star-forming regions. We estimate the occurrence of CCSNe as a function of oxygen abundance per unit star formation, and show that there is a strong decrease as abundance increases. Such a strong and quantified metallicity dependence on CCSN production has not been shown before. Finally, we discuss possible explanations for our result and show that each of these has strong implications not only for our understanding of CCSNe and massive star evolution, but also star-formation and galaxy evolution.

3.3 Introduction

Core-collapse supernovae (CCSNe) are generated by the explosive death of massive stars, and are important for the formation of new elements and the evolution of galaxies (Woosley and Weaver, 1995; Scannapieco et al., 2008; Johnson, 2019). Because the delay between star formation (SF) and death for massive stars is relatively short, CCSNe are expected to be associated with the SF regions of galaxies. Indeed, the connection between CCSNe and young and massive stars has been demonstrated by direct progenitor detections and by a large number of previous environment studies (see, e.g., Smartt, 2015; Anderson et al., 2015, and references therein). Massive stars produce strong ionising fluxes that excite the local ISM, producing HII regions. The latter are thus strong tracers of massive star formation within galaxies – specifically H α emission can be used as a direct tracer of the star formation rate (SFR) within galaxies (e.g., Kennicutt, 1998a).

A CCSN explosion happens either by the collapse of an ONeMg core, for progenitor stars

with initial masses $\approx 8 - 10 M_{\odot}$ (also known as electron-capture SNe, Miyaji et al., 1980; Nomoto et al., 1982), or the collapse of an Fe core for $\gtrsim 10 M_{\odot}$ (Bethe et al., 1979; Bethe, 1990)¹. Theoretical models and simulations have demonstrated that the mass ranges of stars above these initial values that produce a CCSN explosion (i.e., that do not collapse directly to a black hole) is not continuous, with many regions of “explodability” (see, e.g., Pejcha and Thompson, 2015; Sukhbold et al., 2016; Ebinger et al., 2020; Zapartas et al., 2021).

Stellar evolution models and CCSN simulations suggest that black hole formation should be more common at low metallicity (Heger et al., 2003; Eldridge and Tout, 2004; Pejcha and Thompson, 2015), however, stellar population modelling suggests there is no strong dependence on the CCSN rate with metallicity (e.g., Briel et al., 2022). Previous observational analyzes of CCSN production found only small (e.g., Li et al., 2011b; Graur et al., 2017; Frohmaier et al., 2021) or no dependence (e.g., Schulze et al., 2021) on metallicity (although these previous works used heterogeneous samples and metallicities derived from global galaxy properties).

In this work, we take advantage of a homogeneous CCSN host galaxy sample from the All-Sky Automated Survey for Supernovae (ASAS-SN) survey (Shappee et al., 2014; Kochanek et al., 2017; Holoien et al., 2017; Holoien et al., 2017a; Holoien et al., 2017b; Holoien et al., 2019; Neumann et al., 2023a) and the large field of view and fine spatial resolution of the integral-field spectrograph MUSE (Bacon et al., 2014) to analyze how progenitor metallicity affects CCSN production. Using this sample, in Pessi et al. (2023a, Paper I), we analyzed the differences in the local environment of the different CCSN types and in Pessi et al. (2023, in prep.; Paper II) we analyzed the CCSN environments in the context of the properties of all HII regions within their host galaxies. Here, we present the results of comparing the local CCSN environment metallicity to the overall metallicity distributions of the SF regions in their host galaxies, and discuss the implications of the metallicity dependence on CCSN occurrence that we find. This letter is organized as follows: In Section 3.4 we present our sample and methods and in Section 3.5 we show the results of comparing the local CCSN environment to the overall SF across their host galaxies. In Section 3.6 we discuss the implications of these results and in Section 3.7 the conclusions are summarized.

¹Although the exact dividing initial mass remains uncertain.

3.4 Data and Methods

We analyze 98 galaxies that hosted 99 CCSNe detected by the ASAS-SN survey (Holoien et al., 2017; Holoien et al., 2017a; Holoien et al., 2017b; Holoien et al., 2019; Neumann et al., 2023a) and were observed by MUSE, mostly in the context of the All-weather MUSE Supernova Integral field Nearby Galaxies (AMUSING) survey (Galbany et al., 2016a, Galbany et al., in prep.). MUSE has a spatial sampling of 0.2×0.2 arcsec, a field of view of 1 arcmin^2 (in Wide Field Mode), and a mean spectroscopic resolution of $R \sim 3000$ with wide wavelength coverage (480 – 930 nm), enabling a detailed spectroscopic analysis of all HII regions within the observed galaxies. The CCSN sample was detected by ASAS-SN between 2014 and 2018, and was reported in Holoien et al. (2017a), Holoien et al. (2017b), and Holoien et al. (2019) and Neumann et al. (2023a). Using a homogeneous sample from ASAS-SN minimizes biases in host properties because it is an untargeted and almost spectroscopically complete survey (see e.g., Shappee et al., 2014; Kochanek et al., 2017, for technical details on the survey). A description of the sample selection, data reduction and calibration is given in Paper I. From the 111 host galaxies in the initial AMUSING/ASAS-SN sample², we selected 78 that hosted Type II SNe (hereafter SNe II) and 21 that hosted stripped-envelope SNe (SESNe, 7 SNe IIb, 7 SNe Ib, 4 SN Ic, 2 SN Ic-BL and 1 ambiguous SN Ibc)³ The CCSN host galaxies are nearby, with luminosity distances of $10 \lesssim D_L \text{ (Mpc)} \lesssim 169$.

We characterize the CCSN host galaxies through HII region segmentation, by combining the observed H α signal of adjacent spaxels into one region. We use IFUanal⁴ (Lyman et al., 2018) and the “nearest bin” method to perform the segmentation and obtain emission line and stellar continuum fits for each HII region in addition to that of the SN. Stellar continuum fitting is performed with STARLIGHT (Cid Fernandes et al., 2005; Mateus et al., 2006) and multiple Gaussians are then fit to the emission lines of the continuum-subtracted spectra.

For each HII region (including that of each CCSN explosion site), the oxygen abundance (hereafter $[O/H]$ - a proxy for metallicity) is estimated following Dopita et al. (2016, p. D16), using the ratios of $[NII]\lambda 6584$ to $[SII]\lambda\lambda 6717, 31$ and $[NII]\lambda 6584$ to H α . The D16 index is calibrated using photoionization models and is insensitive to reddening due to the nearby line

²<https://sites.google.com/view/theamusingasassnsample>

³We remove all interacting events (IIn, Ibn) given the less clear nature of their progenitors.

⁴<https://ifuanal.readthedocs.io/en/latest/index.html>

ratios. It has been shown that D16 removes any dependence on the inferred abundance with ionization (Krühler et al., 2017). In Appendix 3.8.1, we repeat part of our analysis using the commonly employed O3N2 and N2 diagnostics of Marino et al. (2013). We also extract the $H\alpha$ flux of each HII region and use the luminosity distance (derived from the CMB frame redshift), the host galaxy extinction correction from the Balmer decrement, and the Galactic reddening correction to estimate the $H\alpha$ luminosity ($L_{H\alpha}$) that is converted into a SFR as explained below.

Although the lifetime of an HII region (~ 10 Myr, e.g., Tremblin et al., 2014; Xiao, Stanway, and Eldridge, 2018) is shorter than the delay-time of CCSNe (up to ~ 200 Myr, when considering binary evolution, e.g., Zapartas et al., 2017; Briel et al., 2022), there should not be a significant abundance evolution in a couple generations of new SF. Therefore, the considered HII regions are a reasonable proxy for the progenitor abundance.

Given that the amount of ionizing radiation per unit SF is a function of metallicity⁵, we use a Binary Population and Spectral Synthesis (BPASS, Eldridge et al., 2017; Stanway and Eldridge, 2018) prescription to correct for this effect and obtain SFRs from HII region $H\alpha$ luminosities. We use a BPASS prescription with binary stellar populations, an initial mass function (IMF) consistent with Kroupa, Tout, and Gilmore (1993) and an upper mass limit of $300 M_{\odot}$, as described in Eldridge et al. (2017).

To characterize the star forming regions within the galaxies, we examine the cumulative distributions of SFR sorted by $[O/H]$ (for a previous use of this method, see Lyman et al., 2018). For $i = 1 \cdots N$ HII regions with SFR_i and $[O/H]_i$ sorted by the oxygen abundance, we examine the integral distribution

$$SFR(< [O/H]_i) = SFR_{tot}^{-1} \sum_{j=1}^i SFR_j \quad (3.1)$$

where $SFR_{tot} = \sum_i SFR_i$ is the total SFR of all the HII regions within our sample. This gives the fraction of SF in each region compared to the total SF of the full sample as a function of metallicity.

⁵Other effects, such as α -enhancement could affect the ionising flux as a function of oxygen abundance (e.g., Byrne et al., 2022, although in this work only colder and older stellar atmospheres were altered, with the effect being uncertain for younger stellar populations).

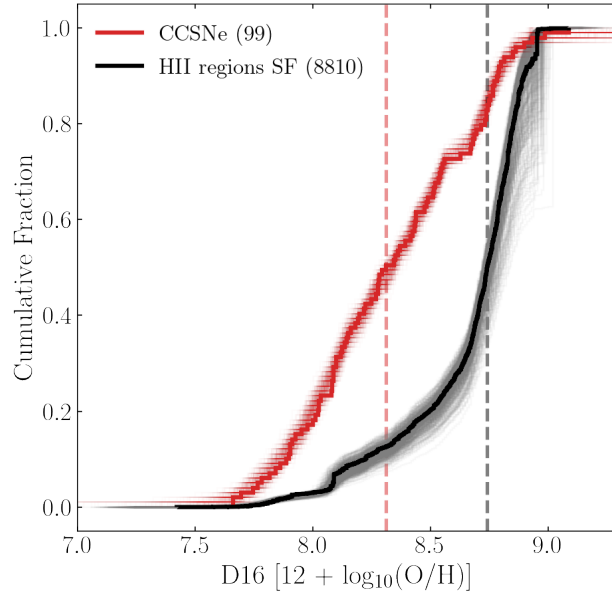


Figure 3.1: The black line shows the cumulative distribution of SFR sorted by $[O/H]$ for all the HII regions in the galaxies, while the red line shows the cumulative distribution of $[O/H]$ at CCSN sites. The shaded regions show 500 bootstrap resamplings of each distribution (using the errors on the measured parameters) and the solid lines show the median of the realizations. The black and red dashed lines show the median $[O/H]$ of the distributions for the HII regions and CCSNe, respectively.

3.5 Results

Figure 3.1 shows the overall cumulative distribution of SFR sorted by $[O/H]$ for the CCSN environments (in red) and for all the 8810 identified HII regions within the galaxies of the sample (in black), as in Equation 3.1. The shaded regions show 500 bootstrap resamplings of each distribution and the solid lines show the median of the realizations. The resampling is done by adding a Gaussian scatter on the measured errors of $[O/H]$ and SFR, with the Gaussians centered at the $[O/H]$ and SFR values, using their uncertainties for the standard deviation. The CCSNe have a median $[O/H] \sim 8.30$ dex (red dashed line), while the overall SF has a median $[O/H] \sim 8.74$ dex (black dashed line). This suggests that CCSN production does not follow the metallicity distribution of SF within all galaxies, but it is instead biased towards SF regions with lower abundance⁶.

The grey lines in Figure 3.2 show the cumulative distributions of SF as a function of $[O/H]$ for all the HII regions within each of the individual 86 CCSN host galaxies from our

⁶If older HII regions had lower oxygen abundances then this could produce some of the effect we observe. However, we do not find a correlation between age, estimated by the $H\alpha$ EW, and oxygen abundance in our sample. These results will be outlined in Paper 2.

initial sample. From the initial sample (presented in Figure 3.1), we could not estimate a $L_{H\alpha}$ for their associated HII region for six CCSNe (SN2018yo, SN2017gbv, ASASSN-17oj, ASASSN-16ba, ASASSN-16al, and SN2015W) due to the low signal-to-noise ratio, so they are excluded from the analyses presented in Figures 3.2 and 3.3. We also remove seven CCSNe (SN2015bm, ASASSN-15lv, ASASSN-16gy, ASASSN-18ou, SN2017ewx, SN2017ivu, SN2016afa) from the initial sample, where only one HII region in the host galaxy was identified. The small markers show the SF fraction rank (i.e., the y -axis position in the cumulative distribution, e.g., Galbany et al., 2016a; Galbany et al., 2018) and $[O/H]$ of each CCSN environment within each distribution, and the large markers show the median of these values for the CCSNe. A uniform distribution with a median SF fraction of 0.5 would indicate that the SNe do not show any preference for occurring in regions with higher or lower values of $[O/H]$ within their host galaxies. The $[O/H]$ values range from $12 + \log_{10}(O/H) \sim 7.4$ dex to ~ 9.0 dex, and the red circle shows the median $[O/H]$ of $12 + \log_{10}(O/H) \sim 8.35$ for the full sample. The median SF fraction of 0.46 ± 0.08 suggests an unbiased production of CCSNe as a function of metallicity (but see below). The uncertainties of the rank fractions are again estimated using bootstrap resampling.

Next, in Figure 3.2, we now split the galaxies at $12 + \log_{10}(O/H) = 8.6$ dex (nearly solar, Asplund, Amarsi, and Grevesse, 2021) based on the HII region in the galaxy with the highest abundance. The blue triangles and orange squares show the SN fraction ranks of these low and high abundance galaxies, respectively. The median SF fraction of the CCSNe in the low metallicity galaxies is 0.61 ± 0.12 , but the median SF fraction for the high metallicity galaxies is 0.24 ± 0.05 . Those SNe within higher metallicity galaxies occur in relatively lower metallicity regions within their hosts, in contrast to those in the lower metallicity galaxies.

We analyze the two distributions of SF fraction ranks through the Normalised Cumulative Rank (NCR) of the CCSNe, shown in Figure 3.3. The NCR is based on the method presented in James and Anderson (2006), but taking the rank of each CCSN in the cumulative fractions of SF as a function of $[O/H]$ for their host galaxies (see Lyman et al., 2018, for a similar application of this method). The x -axis in Figure 3.3 becomes the SF fraction that is the y -axis in Figure 3.2. A distribution of SNe that is unbiased with respect to abundance would follow the diagonal (i.e., a uniform distribution of ranks). A distribution biased to higher metallicities will lie below the diagonal and one biased to lower metallicities will lie

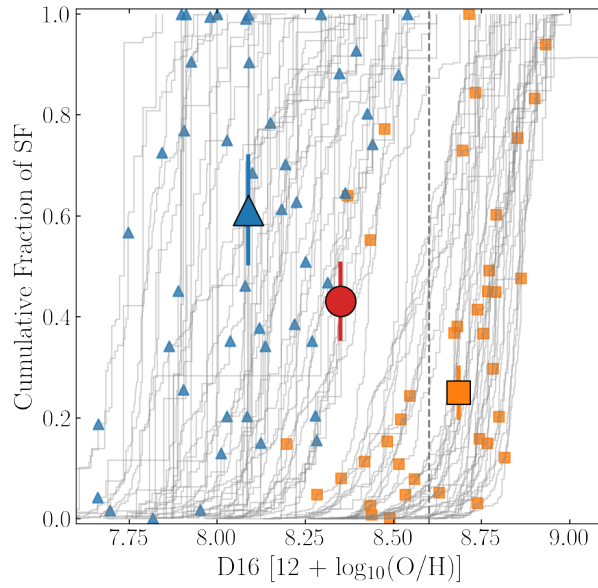


Figure 3.2: Cumulative distributions of the fraction of SF as a function of $[O/H]$ for HII regions within individual galaxies. Each gray line is the distribution for one galaxy and the small symbols are the SF fraction rank and $[O/H]$ of the CCSN environments within their host galaxy SF distributions. The median rank is given by the big markers, with uncertainties estimated by the median of the 1σ of 500 bootstrap resamplings of each distribution. The blue triangles and orange squares represent the galaxies in which the HII region with the highest $[O/H]$ has a value lower or higher than $12 + \log_{10}(O/H) = 8.6$ dex (indicated by the dashed line), respectively. The red circle shows the median values for the full sample.

above it.

The solid lines in Figure 3.3 show the median of the 500 bootstrap resamplings for the cumulative distributions, while the dashed lines show the 1σ scatter realizations. Figure 3.3 shows that for the full CCSN sample and the low metallicity galaxies, the SF fraction distribution follows the diagonal line, suggesting an unbiased dependence of these events with respect to metallicity. The Kolmogorov-Smirnov (KS) test (Chakravarti, Laha, and Roy, 1967) between the low metallicity galaxy distribution and a straight line has a p -value = 0.69, suggesting no significant metallicity bias. On the other hand, for higher metallicity galaxies the CCSN SF fractions are shifted to the left of the diagonal, with a KS-test p -value = 0.03. This suggests that they do not follow the distribution of SF as a function of metallicity in their host galaxies and are biased to SF at lower metallicities.

In Figure 3.4, we divide the HII regions into seven 0.2 dex wide bins of abundance, and

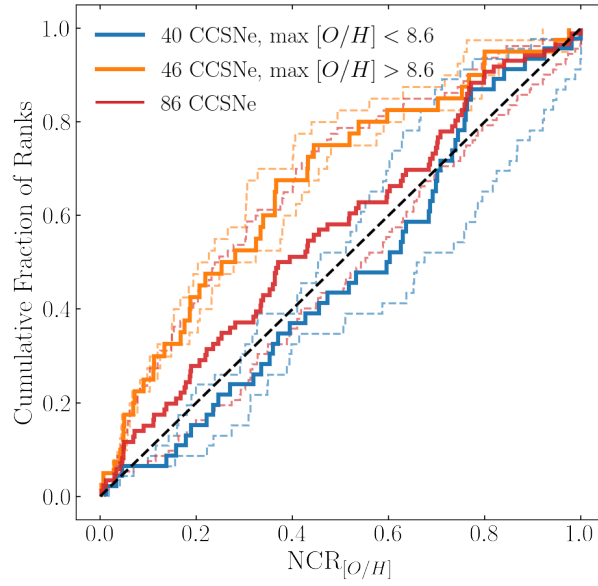


Figure 3.3: The oxygen abundance NCR for the CCSNe. The red line shows the distribution for the full sample, and the blue and orange lines show, respectively, the galaxies where the largest metallicity value of their HII regions is lower or higher than $12 + \log_{10}(\text{O}/\text{H}) = 8.6$ dex. An unbiased distribution with respect to metallicity should follow the dashed diagonal line in the plot. The solid lines show the median of 500 bootstrap resamplings of each cumulative distribution and the dashed lines show the 1σ of the realizations.

for each bin calculate

$$R_{[\text{O}/\text{H}],i} = \frac{N_{\text{CCSN},[\text{O}/\text{H}],i}}{\text{SFR}_{\text{tot},[\text{O}/\text{H}],i}} \quad (3.2)$$

where $N_{[\text{O}/\text{H}],\text{CCSN},i}$ and $\text{SFR}_{\text{tot},[\text{O}/\text{H}],i} = \sum_i \text{SFR}_{[\text{O}/\text{H}],i}$ are the numbers of CCSN and the total SFR (in units of $\text{M}_{\odot} \text{ yr}^{-1}$) associated with abundance bin i . $R_{[\text{O}/\text{H}],i}$ is proportional to the occurrence rate of CCSN per unit of SF. Figure 3.4 also shows “violin” errors from 500 bootstrap resamplings of the distributions. The median values of the resamplings, the 1σ uncertainty, the central abundance and the number of SNe in each bin are reported in Table 3.1. Figure 3.4 also presents a second order polynomial fit of

$$y = 0.11 - 2.25 x - 1.17 x^2 \quad (3.3)$$

between $12 + \log_{10}(\text{O}/\text{H}) = 7.6$ and 9.0 dex, where $y = \log_{10} R_{[\text{O}/\text{H}]}$ and $x = [\text{O}/\text{H}] - 8.69$.

Figure 3.4 shows that the occurrence of CCSNe per unit of SF at lower oxygen abundance appears to be significantly larger than at higher abundances. The occurrence rate declines

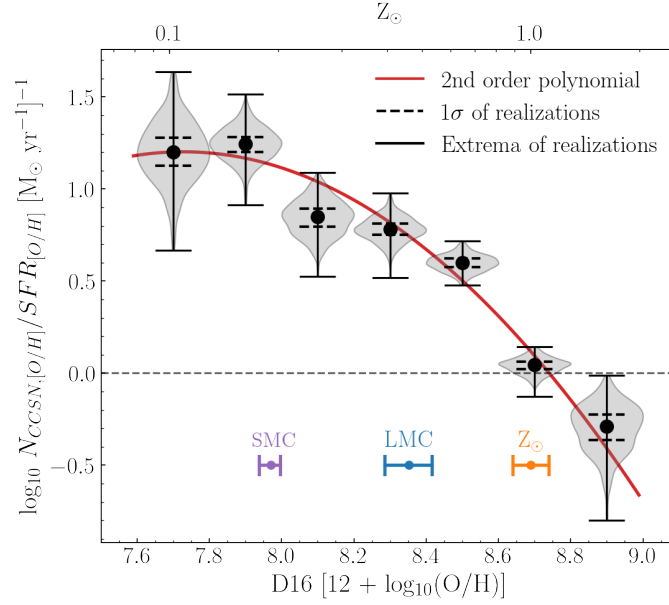


Figure 3.4: The occurrence of CCSNe per unit of SF as a function of $[O/H]$. This is estimated by dividing the number of CCSNe, $N_{[O/H],CCSN}$, by the total SFR, $SFR_{tot,[O/H],i}$, over binned intervals in the abundance axis. The violin plots show 500 bootstrap resamplings in each abundance interval of 0.2 dex. The black dots show the median of these realizations, while the dashed and solid lines show, respectively, the 1σ and the extrema of the realizations. We fit a 2nd order polynomial to the median values, weighting it by the 1σ uncertainties. A horizontal dashed line is shown at $R_{[O/H],i} = 1$. The orange dot shows the abundance for the Sun (Asplund, Amarsi, and Grevesse, 2021) and the purple and blue dots show the median abundances for, respectively, the SMC and LMC (Toribio San Cipriano et al., 2017).

as metallicity increases, with $R_{[O/H]} \approx 15.5$ at $12 + \log_{10}(O/H) \sim 7.7$ dex and $R_{[O/H]} \approx 0.5$ at $12 + \log_{10}(O/H) \sim 8.9$ dex. The latter value is nearly 25 times lower than the former, showing a large occurrence difference over metallicity. Figure 3.4 also shows the abundances for the SMC, LMC (Toribio San Cipriano et al., 2017) and the Sun (Asplund, Amarsi, and Grevesse, 2021). The occurrence of CCSNe per unit SF in abundances close to the SMC and LMC values are higher by factors of ~ 15 and ~ 5 than at abundances close to solar. We show the occurrence of CCSN per unit of SF as a function of two other oxygen abundance indicators in Appendix 3.8.1, finding consistent results.

3.6 Discussion

We have found that the CCSN production appears to be strongly dependent on metallicity, with the detected number of CCSNe relative to SF decreasing as oxygen abundances increase. CCSNe do not follow the general distribution of SF as a function of metallicity

Table 3.1: The occurrence rate of CCSN per unit of SF, as a function of abundance.

N_{SN}	$R([O/H])$	1σ	$[O/H]$
7	15.54	4.94	7.70
12	17.26	3.18	7.90
16	7.01	1.65	8.10
17	6.08	0.82	8.30
20	4.00	0.37	8.50
16	1.09	0.10	8.70
8	0.50	0.10	8.90

and tend to happen within relatively lower metallicity regions in higher metallicity galaxies. In lower metallicity galaxies, the occurrence of CCSNe seems to be unbiased with respect to metallicity. When binning SNe and SF by oxygen abundance, we find a clear decreasing occurrence of CCSNe per unit SF with increasing $[O/H]$.

Previous works have explored the metallicity dependence of the occurrence of long gamma-ray bursts (LGRBs, which are connected to SNe Ic-BL, Stanek et al., 2006; Fruchter et al., 2006; Stanek et al., 2007; Kewley et al., 2007; Modjaz et al., 2008; Mannucci, Salvaterra, and Campisi, 2011; Graham and Fruchter, 2013; Graham and Fruchter, 2017) and super-luminous (SL)SNe (Stoll et al., 2011; Chen et al., 2013; Lunnan et al., 2013; Chen et al., 2017; Frohmaier et al., 2021). Some works also discussed a metallicity effect on the rate of SNe Ia (Sullivan et al., 2006; Li et al., 2011b; Graur and Maoz, 2013; Kistler et al., 2013; Graur et al., 2017; Brown et al., 2019; Johnson, Kochanek, and Stanek, 2022). There are a number of studies of the correlations between CCSN rates and host properties. In particular, Li et al. (2011b) found that the CCSN rates per unit luminosity (either B or K band) or stellar mass decreased with galaxy luminosity or mass using the LOSS SN sample (Li et al., 2000; Filippenko et al., 2001). Indeed, the rates dropped by a factor of ~ 5 between host galaxy stellar masses of $10^9 M_\odot$ and $2 \times 10^{10} M_\odot$. Graur et al. (2017) reanalyzed those data and found changes in the CCSN rate per unit stellar mass of a factor of ~ 6 for Type II SN and a factor for ~ 4 for SESNe between galaxies oxygen abundances of ~ 8.7 to ~ 9.2 dex, which is similar to what we see in Figure 3.4. Graur et al. (2017) argue, however, that this is due to changes in the specific galaxy star formation rates rather than metallicity. Frohmaier et al. (2021) also found a drop in the CCSN rates per unit stellar mass of a factor of ~ 6 between masses of 10^9 and $10^{11} M_\odot$. Here, we are directly examining the dependence of the occurrence of CCSN per unit SF as a function of metallicity, and the driver appears to

be environment metallicity.

Our study has some significant advantages compared with previous analyzes: (1) we use a homogeneous sample of CCSNe detected by ASAS-SN and that (2) were selected in a minimally biased way to be observed by MUSE (see Paper I for a more detailed description of sample selection); and (3) we use emission-line spectroscopy of spatially resolved HII regions to measure both metallicities and SFRs across the galaxies (in contrast to central metallicities, taken, e.g., from SDSS, or global galaxy properties derived from photometry).

We now outline possible explanations for the result presented above. It is important to note that while the exact explanation of our result is currently unclear, any of the below possibilities – if confirmed – would have strong implications for our understanding of the CCSN phenomenon and/or massive SF within galaxies.

The first possibility that we discuss is that our findings are the result of selection effects and that we are missing CCSNe within higher metallicity HII regions. This could be caused by higher extinction in higher metallicity regions, or the difficulty in detecting SNe in high surface-brightness regions (which are generally of higher metallicity). While we do find that higher abundance HII regions have slightly higher $E(B - V)$ values than lower regions, this difference is not significant, neither is the overall distribution of host HII region extinction (see Paper I and Paper II). In addition, near-infrared surveys suggest that only around 20% of CCSNe are likely to be missed in the local Universe due to extinction in optical surveys – this is much less than required to explain our result (e.g. Fox et al., 2021). It has also been demonstrated that ASAS-SN has a high efficiency in detecting (and classifying) SNe towards the centers – and thus the most extinction affected regions – of galaxies (Shappee et al., 2014; Kochanek et al., 2017; Holoien et al., 2017; Holoien et al., 2017a; Holoien et al., 2017b; Holoien et al., 2019; Neumann et al., 2023a). ASAS-SN also found more tidal disruption events (TDEs) per SN than previous surveys, indicating a high efficiency for finding transients close or at the centers of galaxies (Holoien et al., 2017; Holoien et al., 2017a; Holoien et al., 2017b; Holoien et al., 2019). Finally, it should be noted, any extinction effect that biases our CCSN distribution must also affect our HII SF distribution. If SNe are being missed due to high extinction, the underlying HII regions could also be missed, thus lessening the impact of extinction in our comparative analysis.

Given that ASAS-SN is a magnitude limited survey, the number of discovered events scales

with their peak luminosity. We have made no completeness correction here and essentially we are assuming that the CCSN luminosity function is not strongly abundance dependent. If the CCSN peak luminosity were dependent on metallicity, this could affect our results. However, we have shown in Paper I that there is no strong correlation between peak luminosity and oxygen abundance at the location of CCSNe, making this explanation less compelling.

Thus, it seems unlikely that selection effects can explain our results. However, should such selection effects – together with others not considered – be responsible for our results, then this would still be a significant result. Indeed, to reproduce our observed number of CCSNe per unit SF as a function of metallicity (if no intrinsic metallicity difference exists) would require that we are missing more than a factor of 10 CCSNe at solar metallicity (per unit SF) compared to the SMC and lower metallicities (as we show in Appendix 3.8.1, the result change little if we use difference abundance estimates). This would mean that currently estimated CCSN rates are hugely underestimated, with a significant impact on our understanding of massive star evolution and death.

A second possibility is that there is a strong metallicity dependence to the IMF. Our analysis assumes that the IMF does not vary with environmental properties such as metallicity. This, however, could be the case: at low metallicity the shape of the IMF could be such that many more massive stars that will explode as CCSNe are produced per unit SF, while at high metallicity the IMF may produce many less CCSN progenitors. This scenario was explored by recent studies on the metallicity dependence of the IMF (e.g., Li et al., 2023, although any claimed dependence is much smaller than what would be required here). Such a result would also be significant, and have many implications on our current understanding of star formation and galaxy evolution.

Our third possible explanation is that $H\alpha$ is a significantly biased tracer of massive SF; as explained in Section 3.4, we used a standard prescription for converting the $H\alpha$ luminosity into an estimate of the SFR which gives less SFR per unit $H\alpha$ luminosity at low metallicity because the model stellar populations produce more ionizing radiation per unit SF. If this dependence could be made weaker or even be reversed, this would help to explain our result. However, this would imply that the real metallicity dependence on the $H\alpha$ to SFR conversion is much higher than commonly used prescriptions.

Finally, it could be that metallicity is a significant factor regulating the ‘explodability’

of massive stars. This would imply that there are many more massive stars exploding as CCSNe within lower metallicity environments than at higher metallicity (e.g. solar abundance). This result would have a significant impact in our understanding of stellar evolution and the explosion mechanism of massive stars, and the numbers of different types of compact remnants. This would go against stellar evolution studies and models that suggest that black hole formation is more common at lower progenitor metallicities (e.g., Heger et al., 2003; Eldridge and Tout, 2004; O'Connor and Ott, 2011; Ertl et al., 2016), although the metallicity dependence on the expected outcome of failed SNe has yet not been explored in depth (e.g., Kochanek et al., 2008; Piro, 2013). Some studies suggest that the lower mass limit for CCSN decreases as a function of metallicity (for those metallicity ranges probed in the current study; e.g., Eldridge and Tout, 2004; Ibeling and Heger, 2013), and that metallicity can also affect mass-loss and the populations of different SNe (for a recent analysis see, e.g., Aguilera-Dena et al., 2022; Aguilera-Dena et al., 2023). The effect of metallicity could be particularly stronger in binary systems. As demonstrated by Laplace et al. (2020), stripped stars in binaries at lower metallicity could have a higher chance of producing a SN, and Laplace et al. (2021) shows that the compactness of binary-stripped stars is lower than single stars, making their explodability higher (for previous studies on the influence of binary systems on the core structure, see e.g., Langer, 1989; Woosley, Langer, and Weaver, 1993; Vartanyan et al., 2021). Additionally, Klencki et al. (2020) shows that envelope stripping is delayed at lower metallicities, resulting in a higher final core mass, although Shenar et al. (2020) demonstrate that binary interactions might not dominate the formation of WRs in low metallicity environments. This, and the fact that stellar multiplicity might be higher at lower metallicity (which has been shown to be the case for low-mass stars, Badenes et al., 2018), could be at play in producing the effect we see in this work (although no strong evidence exists in the case of massive stars, see e.g., Sana et al., 2013; Dunstall et al., 2015).

3.7 Conclusions

We have demonstrated that the observed occurrence of CCSNe shows a strong dependence on environment metallicity. Selection effects would not seem to be able to explain such an effect; if they do, this has strong implications for the estimated rates of CCSNe. Our results

also challenge the standard assumptions of a universal IMF and the use of $H\alpha$ as a tracer of SFR; a deep analysis of how these quantities are affected by local SF properties should be further explored. Finally, our results could be explained by a strong dependence of metallicity on the explosion mechanism of massive stars; this effect has not been addressed in depth in the literature, and should be taken into account in future theoretical analyses.

3.8 Appendix

3.8.1 O3N2 and N2 Indicators

The [SII] line used in the D16 index may be affected by ionization due to supernova remnants in galaxies, making it susceptible to contamination (e.g., Kopsacheili, Zezas, and Leonidaki, 2020; Cid Fernandes et al., 2021). We therefore estimate the occurrence of CCSN per unit of SF, given by Equation 3.2, using indicators independent of [SII]. Figure 3.5 shows the resultant occurrence of CCSN per unit of SF as a function of oxygen abundance given by the O3N2 and N2 indexes, both estimated using the Marino et al. (2013) calibration. The O3N2 index uses the $H\alpha$, $H\beta$, [OIII] λ 5007 and [NII] λ 6584 emission lines, while the N2 index uses the line ratio between [NII] λ 6584 and $H\alpha$.

Figure 3.5 shows a similar behavior for the occurrence of CCSNe per unit of SF as shown in Figure 3.4, declining as metallicity increases. The $[O/H]$ values range between 8.2 and 8.56 dex, and we divide the HII regions between six 0.06 dex bins of abundance. In a similar way to Figure 3.4, we show “violin” uncertainties from 500 bootstrap resamplings of the distributions, the 1σ and extrema of the realizations given by, respectively, the dashed and solid lines. We also show a 2nd order polynomial fit to the two indicators. The O3N2 index is fit with $y = 0.5 - 3.0 x + 4.0 x^2$, and the N2 index with $y = 0.7 - 3.9 x - 4.4 x^2$, between $12 + \log_{10}(O/H) = 8.2$ and 8.56 dex, where $y = \log_{10}R_{[O/H]}$ and $x = [O/H] - 8.4$. The O3N2 index has $R_{[O/H]} \approx 18$ at $12 + \log_{10}(O/H) \sim 8.2$ dex and $R_{[O/H]} \approx 1.5$ at $12 + \log_{10}(O/H) \sim 8.5$ dex, and the N2 index has $R_{[O/H]} \approx 25$ at $12 + \log_{10}(O/H) \sim 8.2$ dex and $R_{[O/H]} \approx 1.2$ at $12 + \log_{10}(O/H) \sim 8.5$ dex. There are large systematic uncertainties between the different abundance indicators (Kewley and Ellison, 2008), which can lead to the quantitative differences seen here. However, the large difference factors seen in the three indicators suggest that the metallicity effect is not affected by these uncertainties. This

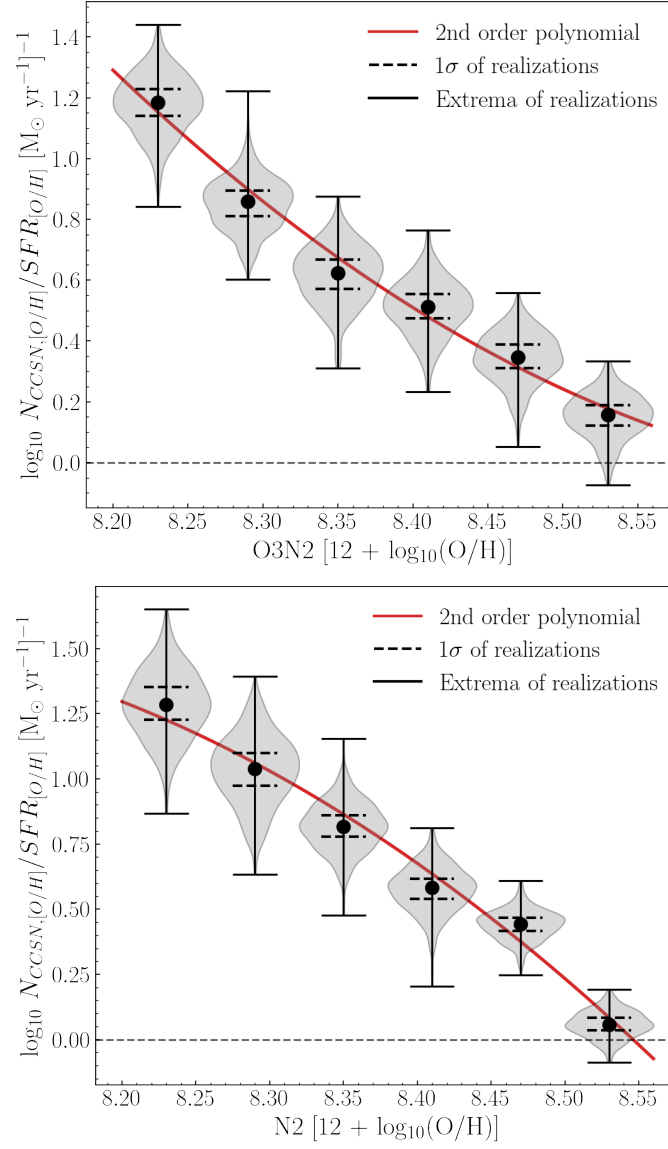


Figure 3.5: The occurrence rate of CCSNe per unit of SF as a function of $[O/H]$, given by the O3N2 (top panel) and N2 (bottom panel) indicators. The violin plots show 500 bootstrap resamplings in abundance intervals of 0.06 dex. The black dots show the median of these realizations, and the dashed and solid lines show, respectively, the 1σ and the extrema of the realizations. A 2nd order polynomial is fit to the median values of each indicator, weighting it by the 1σ uncertainties.

indicates that the metallicity dependence on CCSN occurrence is independent of the chosen oxygen abundance indicator, being also observed to a similar degree when using O3N2 and N2.

Chapter 4

Legacy of this thesis

Besides the work described in Chapters 2 and 3, other important goals were achieved during my Ph.D. During this period, I have worked with different techniques, such as photometry, spectroscopy, and integral-field data, ranging across wavelengths, from radio and to optical and X-rays. As a result, I have published four articles in major Astronomy periodic journals as lead author; I have also contributed to other projects and published five articles as a contributing author; I have presented the results of my projects at 11 conferences, both online and in person; I have participated in schools, observing training, and spent one year as part of the ESO Studentship program; I had seven accepted observing proposals as PI, with a total of 345.3 h, and conducted observations during a total of 12 nights in different telescopes. Finally, I had the chance to contribute to large collaborations of transient studies, such as ePESSTO+, AMUSING, and ASAS-SN.

Below, I summarize the most important marks and activities that contributed to my formation during these four years, and that resulted in contributions for the community.

4.1 Publications

As first author

- Pessi et al. (2023b): *A metallicity dependence on the occurrence of core-collapse supernovae*, ApJL, 955, L29.
- Pessi, Prieto, and Dessart (2023): *Very late-time spectroscopy of SN 2009ip: Constraints on the ongoing H α emission*, A&A, 677, L1.

- Pessi et al. (2023a): *A characterization of ASAS-SN core-collapse supernova environments with VLT+MUSE. I. Sample selection, analysis of local environments, and correlations with light curve properties*, A&A, 677, A28.
- Pessi et al. (2022): *Unveiling the Nature of SN 2011fh: a Young and Massive Star Gives Rise to a Luminous SN 2009ip-like Event*, ApJ, 928, 138.

As co-author

- Moriya et al. (2023): *Environmental dependence of Type IIn supernova properties*, A&A, 677, A20.
- Nicholl et al. (2023): *AT 2022aedm and a New Class of Luminous, Fast-cooling Transients in Elliptical Galaxies*, ApJL, 954, L28.
- Neumann et al. (2023a): *The ASAS-SN bright supernova catalogue - V. 2018-2020*, MNRAS, 520, 4356.
- Kilpatrick et al. (2021b): *The Gravity Collective: A Search for the Electromagnetic Counterpart to the Neutron Star-Black Hole Merger GW190814*, ApJ, 923, 258.
- Jayasinghe et al. (2021): *A unicorn in monoceros: the 3 Msun dark companion to the bright, nearby red giant V723 Mon is a non-interacting, mass-gap black hole candidate*, MNRAS, 504, 2577.

4.2 Conferences and presentations

- Transients Down Under, Swinburne University of Technology, Melbourne, Australia, Jan.-Feb. 2024, Talk: *Observational evidence for a metallicity dependence on the occurrence of core-collapse supernovae*.
- Super Virtual 2023, Virtual conference, Nov. 2023, Talk: *Observational evidence for a metallicity dependence on the occurrence of core-collapse supernovae*.
- SuperNova EXplosions Conference: Theory and observations, Israel Institute of Technology, Haifa, Israel, Aug. 2023, Talk: *Observational evidence for a metallicity dependence on the occurrence of core-collapse supernovae*.

- ESO TMT talk, ESO, Santiago, Chile, Mar. 2023, Talk: *A characterization of ASAS-SN core-collapse supernova environments with VLT+MUSE.*
- SOCHIAS XVIII Anual Meeting, Temuco, Chile, Mar. 2023, Talk: *A characterization of ASAS-SN core-collapse supernova environments with VLT+MUSE.*
- Pizza talk at IEEC, UAB, Barcelona, Spain, Nov. 2022, Talk: *SN2011fh + A characterization of ASAS-SN core-collapse supernova environments with VLT+MUSE.*
- Super Virtual 2022, Virtual conference, Nov. 2022, Poster: *A characterization of ASAS-SN core-collapse supernova environments with VLT+MUSE.*
- Primera Jornada Anual de Investigación de Estudiantes de Doctorado, Universidad Diego Portales, Santiago, Chile, Sep. 2022, Talk: *Revelando los orígenes de las supernovas con el Very Large Telescope.*
- South American Supernovae 2022, ESO, Santiago, Chile, Apr. 2022, Talk: *Unveiling the Nature of SN 2011fh: a Young and Massive Star Gives Rise to a Luminous SN 2009ip-like Event.*
- SOCHIAS XVII Anual Meeting 2022, online conference, Jan. 2022, Talk: *Unveiling the Nature of SN 2011fh: a Young and Massive Star Gives Rise to a Luminous SN 2009ip-like Event.*
- Super Virtual 2021, online conference, Nov. 2021, Poster: *Unveiling the Nature of SN 2011fh: a Young and Massive Star Gives Rise to a Luminous SN 2009ip-like Event.*

4.3 Schools, training, and other research experience

- ESO Studentship, ESO, Chile, Mar. 2022 - Mar. 2023.
- Paranal Observatory project, ESO, Chile, Feb. 2023.
- APEX observing training, APEX observatory, Chile, Oct. 2022.
- La Serena School for Data Science 2021, AURA/Chile, online school Aug. 2021.
- ALerCE Broker Tutorial, online workshop, Sep. 2020.

- GROWTH Online Astronomy School, Caltech, online school, Aug. 2020.

4.4 Observational experience

Accepted observing proposals as PI

- 2024A (P113) - VLT (MUSE): 99 h, *An ATLAS view on the occurrence of core-collapse supernovae as a function of metallicity*, ID: 113.26FT, PI: PESSI, T.
- 2023A (P111) - VLT (MUSE): 60 h, *The local environments of stripped-envelope supernovae*, ID: 111.24UM, PI: PESSI, T.
- 2021B - Magellan Baade Telescope (IMACS / FOURSTAR): 1 night, *Dead or alive? Late time observations of ongoing stellar activity in SN 2009ip and SN 2018cnf*, ID: CN2020B-51, PI: PESSI, T.
- 2021A - REM Telescope: 60 h, *Photometric and Spectroscopic Follow-up of Type IIIn Supernovae and Related Transients $z < 0.02$ ($D < 90$ Mpc)*, PI: PESSI, T.
- 2021A - LCOGT 0.4m Telescope: 50 h, *Photometric and Spectroscopic Follow-up of Type IIIn Supernovae and Related Transients $z < 0.02$ ($D < 90$ Mpc)*, PI: PESSI, T.
- 2020B - LCOGT 0.4m Telescope: 34.3 h, *Photometric Follow-up of Type IIIn Supernovae and Related Transients*, PI: PESSI, T.
- 2020B - REM Telescope: 30 h, *Photometric Follow-up of Type IIIn Supernovae and Related Transients*, PI: PESSI, T.

Accepted observing proposals as co-I

- 2023B (P112 to P114) - NTT (EFOSC2 / SOFI): 1280 h / 160 nights, *A public spectroscopic survey of transient objects*, ID: 112.25JQ, PI: INSERRA, C.
- 2023A (P111) - VLT (MUSE): 54 h, *Environment constraints on supernovae Ibn: high or low mass progenitors?*, ID: 111.24VQ, PI: KRAVTSOV, T.
- 2022A (P109) - VLT (MUSE): 17 h, *The Extreme Host Galaxy Environments of Low-Luminosity Type Ia SNe with late-time H-alpha emission*, ID:109.2399, PI: PRIETO, J.

- 2021B (P108) - VLT (MUSE): 13 h, *The Extreme Host Galaxy Environments of Low-Luminosity Type Ia SNe with late-time H-alpha emission*, ID: 108.22AV, PI: PRIETO, J.

Observing runs

- Oct. 2023 - NTT (EFOSC2): 3 nights as observer, *A public spectroscopic survey of transient objects*, ID: 112.25JQ.001, PI: INSIERRA, C.
- Apr. 2023 - NTT (EFOSC2 / SOFI): 4 nights as observer, *A public spectroscopic survey of transient objects*, ID: 111.24PR.001 / 111.24PR.007 / 111.24PR.008 , PI: INSIERRA, C.
- Oct. 2022 - APEX: 4 days as observer, Several observing programs - part of the APEX observing training as ESO student.
- Sep. 2021 - Magellan Baade Telescope (IMACS / FOURSTAR): 1 night as observer, *Dead or alive? Late time observations of ongoing stellar activity in SN 2009ip and SN 2018cnf*, ID: CN2020B-51, PI: PESSI, T.

Chapter 5

Summary and conclusions

E eu vos direi: "Amai para entendê-las!

Pois só quem ama pode ter ouvido

Capaz de ouvir e de entender estrelas.

Olavo Bilac, 1888.

This thesis presents the largest analysis to date of CCSN host galaxies observed with MUSE, a modern IFU instrument at the VLT. The high spatial resolution and spectroscopic coverage of the instrument allowed us to perform a very detailed characterization of the local environment around CCSNe. Additionally, the untargeted sample retrieved from the ASAS-SN survey allowed us to perform a very homogeneous study of CCSN host galaxies. The two articles that compose this thesis explore the differences between environment properties of CCSN subtypes, the connection between these properties and their intrinsic explosion mechanisms, and the observed occurrence effect as a function of metallicity.

In Chapter 2, I described the properties of the sample composed of 111 CCSN host galaxies. I presented the results of analysis of the local environment for the different CCSN subtypes in our sample. The main physical parameters analyzed were star formation rate (SFR), $H\alpha$ equivalent width (EW), metallicity given by the oxygen abundance, and extinction. I also analyzed how the CCSN LC parameters, such as decline rate and absolute magnitude at peak, could be related to their environments. Finally, I discussed the implications of these results for the different CCSN progenitor stars.

In Chapter 3, I showed that the CCSN explosion site metallicity distribution has lower values than the overall distribution for star-forming regions in the sample. I described how

CCSNe appear to be located in the less metal-rich regions of high-metallicity galaxies. I also discussed how the occurrence of CCSNe per unit SF changes with metallicity, and showed that this parameter is higher at lower metallicity. I then discuss the importance of these results and how the implications of this effect for our understanding of CCSN formation and massive star evolution.

In Chapter 4, I presented additional contributions that resulted from the work performed during my Ph.D. studies, such as other publications, presentations in conferences, and my participation in large transient research collaborations.

The main questions and discussions covered in this thesis can be summarized as follows:

- **What are the local environment differences between CCSN subtypes?**

I showed that the environments of SESNe have higher median values of $H\alpha$ EW, ΣSFR , and oxygen abundance than SNe II and IIn/Ibn. Between SESNe, SNe Ic show higher median values of SFR, $H\alpha$ EW, and oxygen abundance than SNe Ib. The SNe IIn in our sample have similar environment properties to SNe II, and SNe Ibn have a median oxygen abundance similar to SNe I Ib and Ic, and ΣSFR similar to SNe IIn. I also showed that the host-galaxy extinction values are similar for the different CCSN subtypes. Most of the environment comparisons between CCSN show no statistically significant differences, except for $H\alpha$ EW between SNe II and SESNe and oxygen abundances in the D16 index between SNe II and Ic.

- **What are the implications for CCSN progenitor stars?**

These results suggest that SESNe are connected to younger stellar populations, and SNe Ic to more metal-rich stellar populations, than SNe II, with a statistically significant difference between the environment properties of these subtypes. The similarities in the environments of SNe IIn to SNe II suggest connections to similar progenitor stars, although a larger sample is needed to increase the statistical significance of this result. Between SESNe, the environment properties suggest that SNe Ic are connected with higher mass and higher metallicity progenitors than SNe Ib. I also discussed that SNe I Ib might arise from relatively lower mass progenitors in higher metallicity environments. Again, a larger sample and further analysis are needed to increase the statistical significance of these results.

- **Is there a connection between LC properties and CCSN environments?**

I reported a correlation between the postmaximum decline rate in B and r bands to $H\alpha$ EW for SNe II. However, the low number of events makes this result not statistically significant. For SESNe, weak correlations were found between the peak magnitude and Δm_{15} in B -band to $H\alpha$ EW and ΣSFR . Additionally, their BVR peak luminosities are weakly correlated to the oxygen abundance. Again, further analysis with a larger number of events is needed to confirm such correlations.

- **The occurrence of CCSNe as a function of metallicity**

I reported the unexpected result that the occurrence of CCSNe in our sample appears to be dependent on metallicity. The distribution of metallicity for CCSNe presents a significantly lower median than the overall distribution of metallicity for the SF regions detected across the host galaxies. CCSNe appear to happen in the lowest metallicity regions of high metallicity galaxies but do not show a preference in metallicity for the low metallicity galaxy sample. I also showed that the occurrence of CCSNe per unit of SF is significantly dependent on metallicity. Although a similar effect was explored in previous works, this is the first time that such a significant dependence on metallicity was demonstrated.

- **What are the implications of this effect?**

Although no precise explanation was explored in our work, the possibilities seem to be significant for our understanding of CCSN formation and other areas of Astronomy. If this is caused by selection effects, a large fraction of CCSNe is being missed in higher metallicity regions. This would imply that CCSN rates are being underestimated by a large fraction. Another possible explanation is that the IMF is strongly dependent on metallicity, which would have a significant impact on our understanding of massive star formation and galaxy evolution. I also described the possibility that $H\alpha$ is a biased tracer of massive SF, which would imply that the $H\alpha$ to SFR conversion is strongly dependent on metallicity, and is being underestimated by currently used prescriptions. Finally, metallicity could be regulating the explodability of massive stars, with more CCSNe exploding at low metallicity regions. All of these possibilities should be analyzed in detail in future works, using new datasets from other transient surveys and combining

observations with theoretical modeling.

The analysis of the environments of SNe (and other transients) has been proven to be a powerful method to unveil their underlying progenitor stars and explosion mechanisms. However, it is important to note that this method does not intend to provide exact answers on the masses and evolutionary stages of individual events, as the uncertainties might be large. It has, instead, the statistical power of revealing trends and correlations to important physical parameters. Chance alignment, the physical size of the analyzed local environment, and systematic uncertainties of the estimated parameters are caveats that should be taken into account when making such a study. Biases and particular observational properties of the survey where the sample is drawn from are also to be taken into account when making a careful analysis of SN environments. Such uncertainties can be minimized when analyzing a large and homogeneous sample retrieved from an untargeted survey, as it is shown in this work.

One important caveat of this work is that our sample is composed mostly of intrinsically bright events, due to the detection limit of the ASAS-SN survey. This could be an important effect, as fainter CCSNe might have distinct explosion mechanisms. This, however, should be seen as a motivation for future studies using more complete samples derived from modern transient surveys. Finally, our study suffers from low-number statistics for subtypes other than Type II SNe. This matter should be addressed in future works, with new observations and larger samples of SN host galaxies.

As discussed above, this thesis presented the largest study to date of CCSN host galaxies observed by the MUSE instrument, and the largest analysis to be made homogeneously, by using a sample drawn from the ASAS-SN survey. The results and methodologies presented here will certainly have a significant influence on future studies of transient environments. Although many uncertainties remain and new questions were opened by this work, this should be a motivation for new studies, new observations, and more thorough analyses of CCSN environments.

Chapter 6

Perspectives and future work

A fun aspect of science is the creation of multiple new questions in an attempt to answer a problem. Instead of being frustrating, new questions should encourage for more comprehensive studies and new methods to be developed. This process allows scientists to explore new paths and advance our knowledge and understanding of nature. The work presented in this thesis created many questions that should be addressed in future works. Some of them, I plan to approach in projects to be developed in the next few years.

The question of *whether there are statistically significant environment differences between the subtypes of SESNe* was raised in this work. Due to the low number of events in our sample, no conclusive answer was found. I plan to address this by using a large sample of (~ 70) SESNe, with new observations of ASAS-SN SESN host galaxies obtained by the MUSE instrument (proposal ID: 111.24UM, PI: PESSI, T.). I plan to use this dataset to increase the statistical significance of physical parameters related to SESN environments, such as SFRs, metallicities, and stellar population ages. For this analysis I plan to use single and binary stellar population synthesis codes (e.g., BPASS + Prospector, Eldridge et al., 2017; Johnson et al., 2021) to perform continuum and emission line fitting, thus constraining better their underlying population. I will also look carefully for correlations between the LC properties of SESNe and their environments.

The robustness of the *occurrence of CCSNe as a function of metallicity* should also be analyzed in my future projects. I plan to analyze in depth the possibilities raised to explain this effect, by working together with experts in modeling and stellar evolution prescriptions. I also plan to use *volumetric CCSN rates from the ASAS-SN survey*, derived from a project

I am currently working on, to study the dependence of the environment on absolute rates. Additionally, I plan to analyze this effect using a *new sample of (~ 95) ATLAS CCSN host galaxies*, to be observed with MUSE during ESO period 113 (proposal ID: 113.26FT, PI: PESSI, T.). These observations will provide results with distinct survey biases and increase significantly the statistics when combining the samples. I plan to analyze the local environments of the ATLAS CCSN sample, look for environment differences between the CCSN subtypes, and look for correlations between their LC properties and environments.

The techniques presented here can also be applied for the characterization of a large range of transient events other than CCSNe. I plan to propose new observations and to use similar methods to study the *environments of other transient events*, such as tidal-disruption events (TDEs), fast blue optical transients (FBOTs), and SNe Ia. Current (e.g., ZTF and ATLAS) and future (e.g., LSST) surveys will allow for the discovery and characterization of a large amount of these and new transients in the sky. Finally, *future instruments*, such as HARMONI and MICADO at the Extremely Large Telescope (ELT) will represent a revolution in the study of transient host galaxies, as it will allow for a more precise analysis and observations of their environments at higher redshift.

My Ph.D. studies have provided me with the necessary abilities to become an independent researcher. My future projects will expand the results presented in this thesis, as well as opening new paths for future questions. Future surveys and instruments represent exciting new possibilities for the study of SNe and other transient events. I plan to prepare myself for these future possibilities and make significant contributions for the field of transient environments.

References

- [1] David R. Aguilera-Dena et al. “Stripped-envelope stars in different metallicity environments. I. Evolutionary phases, classification, and populations”. In: *A&A* 661, A60 (May 2022), A60. doi: [10.1051/0004-6361/202142895](https://doi.org/10.1051/0004-6361/202142895). arXiv: [2112.06948](https://arxiv.org/abs/2112.06948) [[astro-ph.SR](#)].
- [2] David R. Aguilera-Dena et al. “Stripped-envelope stars in different metallicity environments. II. Type I supernovae and compact remnants”. In: *A&A* 671, A134 (Mar. 2023), A134. doi: [10.1051/0004-6361/202243519](https://doi.org/10.1051/0004-6361/202243519). arXiv: [2204.00025](https://arxiv.org/abs/2204.00025) [[astro-ph.SR](#)].
- [3] D. Alloin et al. “Nitrogen and oxygen abundances in galaxies.” In: *A&A* 78 (Sept. 1979), pp. 200–216.
- [4] J. P. Anderson and P. A. James. “Constraints on core-collapse supernova progenitors from correlations with H α emission”. In: *MNRAS* 390.4 (Nov. 2008), pp. 1527–1538. doi: [10.1111/j.1365-2966.2008.13843.x](https://doi.org/10.1111/j.1365-2966.2008.13843.x). arXiv: [0809.0236](https://arxiv.org/abs/0809.0236) [[astro-ph](#)].
- [5] J. P. Anderson et al. “Observational constraints on the progenitor metallicities of core-collapse supernovae”. In: *MNRAS* 407.4 (Oct. 2010), pp. 2660–2672. doi: [10.1111/j.1365-2966.2010.17118.x](https://doi.org/10.1111/j.1365-2966.2010.17118.x). arXiv: [1006.0968](https://arxiv.org/abs/1006.0968) [[astro-ph.CO](#)].
- [6] J. P. Anderson et al. “Progenitor mass constraints for core-collapse supernovae from correlations with host galaxy star formation”. In: *MNRAS* 424.2 (Aug. 2012), pp. 1372–1391. doi: [10.1111/j.1365-2966.2012.21324.x](https://doi.org/10.1111/j.1365-2966.2012.21324.x). arXiv: [1205.3802](https://arxiv.org/abs/1205.3802) [[astro-ph.CO](#)].
- [7] Joseph P. Anderson et al. “Characterizing the V-band Light-curves of Hydrogen-rich Type II Supernovae”. In: *ApJ* 786.1, 67 (May 2014), p. 67. doi: [10.1088/0004-637X/786/1/67](https://doi.org/10.1088/0004-637X/786/1/67). arXiv: [1403.7091](https://arxiv.org/abs/1403.7091) [[astro-ph.HE](#)].

- [8] Joseph P. Anderson et al. "Statistical Studies of Supernova Environments". In: *PASA* 32, e019 (May 2015), e019. doi: [10.1017/pasa.2015.19](https://doi.org/10.1017/pasa.2015.19). arXiv: [1504.04043](https://arxiv.org/abs/1504.04043) [[astro-ph.HE](#)].
- [9] J. E. Andrews et al. "VizieR Online Data Catalog: UBVRI & ugriz photometry of supernova SN 2017gmr (Andrews+, 2019)". In: *VizieR Online Data Catalog*, J/ApJ/885/43 (Mar. 2021), J/ApJ/885/43.
- [10] Iair Arcavi et al. "Core-collapse Supernovae from the Palomar Transient Factory: Indications for a Different Population in Dwarf Galaxies". In: *ApJ* 721.1 (Sept. 2010), pp. 777–784. doi: [10.1088/0004-637X/721/1/777](https://doi.org/10.1088/0004-637X/721/1/777). arXiv: [1004.0615](https://arxiv.org/abs/1004.0615) [[astro-ph.CO](#)].
- [11] W. David Arnett et al. "Supernova 1987A." In: *ARA&A* 27 (Jan. 1989), pp. 629–700. doi: [10.1146/annurev.aa.27.090189.003213](https://doi.org/10.1146/annurev.aa.27.090189.003213).
- [12] M. Asplund, A. M. Amarsi, and N. Grevesse. "The chemical make-up of the Sun: A 2020 vision". In: *A&A* 653, A141 (Sept. 2021), A141. doi: [10.1051/0004-6361/202140445](https://doi.org/10.1051/0004-6361/202140445). arXiv: [2105.01661](https://arxiv.org/abs/2105.01661) [[astro-ph.SR](#)].
- [13] Astropy Collaboration et al. "Astropy: A community Python package for astronomy". In: *A&A* 558, A33 (Oct. 2013), A33. doi: [10.1051/0004-6361/201322068](https://doi.org/10.1051/0004-6361/201322068). arXiv: [1307.6212](https://arxiv.org/abs/1307.6212) [[astro-ph.IM](#)].
- [14] R. Bacon et al. "MUSE Commissioning". In: *The Messenger* 157 (Sept. 2014), pp. 13–16.
- [15] Carles Badenes et al. "Stellar Multiplicity Meets Stellar Evolution and Metallicity: The APOGEE View". In: *ApJ* 854.2, 147 (Feb. 2018), p. 147. doi: [10.3847/1538-4357/aaa765](https://doi.org/10.3847/1538-4357/aaa765). arXiv: [1711.00660](https://arxiv.org/abs/1711.00660) [[astro-ph.SR](#)].
- [16] J. A. Baldwin, M. M. Phillips, and R. Terlevich. "Classification parameters for the emission-line spectra of extragalactic objects." In: *PASP* 93 (Feb. 1981), pp. 5–19. doi: [10.1086/130766](https://doi.org/10.1086/130766).
- [17] O. S. Bartunov, D. Yu. Tsvetkov, and I. V. Filimonova. "Distribution of Supernovae Relative to Spiral Arms and H II Regions". In: *PASP* 106 (Dec. 1994), p. 1276. doi: [10.1086/133505](https://doi.org/10.1086/133505).

- [18] Tom Ben-Ami et al. “The Type Icn Supernova 2019kbn: Indications for Diversity in Type Icn Supernova Progenitors”. In: 946.1, 30 (Mar. 2023), p. 30. doi: [10.3847/1538-4357/acb432](https://doi.org/10.3847/1538-4357/acb432). arXiv: [2212.03407](https://arxiv.org/abs/2212.03407) [astro-ph.HE].
- [19] Melina C. Bersten, Omar Benvenuto, and Mario Hamuy. “Hydrodynamical Models of Type II Plateau Supernovae”. In: *ApJ* 729.1, 61 (Mar. 2011), p. 61. doi: [10.1088/0004-637X/729/1/61](https://doi.org/10.1088/0004-637X/729/1/61). arXiv: [1101.0467](https://arxiv.org/abs/1101.0467) [astro-ph.SR].
- [20] H. A. Bethe. “Supernova mechanisms”. In: *Reviews of Modern Physics* 62.4 (Oct. 1990), pp. 801–866. doi: [10.1103/RevModPhys.62.801](https://doi.org/10.1103/RevModPhys.62.801).
- [21] H. A. Bethe et al. “Equation of state in the gravitational collapse of stars”. In: *NPHYSA* 324.2-3 (July 1979), pp. 487–533. doi: [10.1016/0375-9474\(79\)90596-7](https://doi.org/10.1016/0375-9474(79)90596-7).
- [22] S. Boissier and N. Prantzos. “Relative frequencies of supernovae types: dependence on host galaxy magnitude, galactocentric radius, and local metallicity”. In: *A&A* 503.1 (Aug. 2009), pp. 137–150. doi: [10.1051/0004-6361/200811234](https://doi.org/10.1051/0004-6361/200811234). arXiv: [0905.3986](https://arxiv.org/abs/0905.3986) [astro-ph.HE].
- [23] Eduardo Bravo, Carles Badenes, and Héctor Martínez-Rodríguez. “SNR-calibrated Type Ia supernova models”. In: *MNRAS* 482.4 (Feb. 2019), pp. 4346–4363. doi: [10.1093/mnras/sty2951](https://doi.org/10.1093/mnras/sty2951). arXiv: [1810.13123](https://arxiv.org/abs/1810.13123) [astro-ph.SR].
- [24] Max M. Briel et al. “Estimating transient rates from cosmological simulations and BPASS”. In: *MNRAS* 514.1 (July 2022), pp. 1315–1334. doi: [10.1093/mnras/stac1100](https://doi.org/10.1093/mnras/stac1100). arXiv: [2111.08124](https://arxiv.org/abs/2111.08124) [astro-ph.CO].
- [25] J. S. Brown et al. “The relative specific Type Ia supernovae rate from three years of ASAS-SN”. In: *MNRAS* 484.3 (Apr. 2019), pp. 3785–3796. doi: [10.1093/mnras/stz258](https://doi.org/10.1093/mnras/stz258). arXiv: [1810.00011](https://arxiv.org/abs/1810.00011) [astro-ph.GA].
- [26] G. Bruzual and S. Charlot. “Stellar population synthesis at the resolution of 2003”. In: 344.4 (Oct. 2003), pp. 1000–1028. doi: [10.1046/j.1365-8711.2003.06897.x](https://doi.org/10.1046/j.1365-8711.2003.06897.x). arXiv: [astro-ph/0309134](https://arxiv.org/abs/astro-ph/0309134) [astro-ph].

- [27] A. Burrows and D. Vartanyan. “Core-collapse supernova explosion theory”. In: *Nature* 589.7840 (Jan. 2021), pp. 29–39. doi: [10.1038/s41586-020-03059-w](https://doi.org/10.1038/s41586-020-03059-w). arXiv: [2009.14157](https://arxiv.org/abs/2009.14157) [astro-ph.SR].
- [28] C. M. Byrne et al. “The dependence of theoretical synthetic spectra on α -enhancement in young, binary stellar populations”. In: *MNRAS* 512.4 (June 2022), pp. 5329–5338. doi: [10.1093/mnras/stac807](https://doi.org/10.1093/mnras/stac807). arXiv: [2203.13275](https://arxiv.org/abs/2203.13275) [astro-ph.SR].
- [29] Zach Cano. “A new method for estimating the bolometric properties of Ibc supernovae”. In: *MNRAS* 434.2 (Sept. 2013), pp. 1098–1116. doi: [10.1093/mnras/stt1048](https://doi.org/10.1093/mnras/stt1048). arXiv: [1306.1488](https://arxiv.org/abs/1306.1488) [astro-ph.SR].
- [30] Jason A. Cardelli, Geoffrey C. Clayton, and John S. Mathis. “The Relationship between Infrared, Optical, and Ultraviolet Extinction”. In: *ApJ* 345 (Oct. 1989), p. 245. doi: [10.1086/167900](https://doi.org/10.1086/167900).
- [31] Jonathan Carrick et al. “Cosmological parameters from the comparison of peculiar velocities with predictions from the 2M++ density field”. In: *MNRAS* 450.1 (June 2015), pp. 317–332. doi: [10.1093/mnras/stv547](https://doi.org/10.1093/mnras/stv547). arXiv: [1504.04627](https://arxiv.org/abs/1504.04627) [astro-ph.CO].
- [32] Gilles Chabrier. “Galactic Stellar and Substellar Initial Mass Function”. In: 115.809 (July 2003), pp. 763–795. doi: [10.1086/376392](https://doi.org/10.1086/376392). arXiv: [astro-ph/0304382](https://arxiv.org/abs/astro-ph/0304382) [astro-ph].
- [33] I. M. Chakravarti, R. G. Laha, and J. Roy. *Handbook of Methods of Applied Statistics, Volume I*. John Wiley and Sons, 1967, pp. 392–394.
- [34] K. C. Chambers et al. “The Pan-STARRS1 Surveys”. In: *arXiv e-prints*, arXiv:1612.05560 (Dec. 2016), arXiv:1612.05560. doi: [10.48550/arXiv.1612.05560](https://doi.org/10.48550/arXiv.1612.05560). arXiv: [1612.05560](https://arxiv.org/abs/1612.05560) [astro-ph.IM].
- [35] Ting-Wan Chen et al. “Superluminous supernova progenitors have a half-solar metallicity threshold”. In: *MNRAS* 470.3 (Sept. 2017), pp. 3566–3573. doi: [10.1093/mnras/stx1428](https://doi.org/10.1093/mnras/stx1428). arXiv: [1605.04925](https://arxiv.org/abs/1605.04925) [astro-ph.GA].
- [36] Ting-Wan Chen et al. “The Host Galaxy of the Super-luminous SN 2010gx and Limits on Explosive ^{56}Ni Production”. In: *ApJL* 763.2, L28 (Feb. 2013), p. L28. doi: [10.1088/2041-8205/763/2/L28](https://doi.org/10.1088/2041-8205/763/2/L28). arXiv: [1210.4027](https://arxiv.org/abs/1210.4027) [astro-ph.CO].

- [37] R. Cid Fernandes et al. “Detection of supernova remnants in NGC 4030”. In: *MNRAS* 502.1 (Mar. 2021), pp. 1386–1400. doi: [10.1093/mnras/stab059](https://doi.org/10.1093/mnras/stab059). arXiv: [2101.12022](https://arxiv.org/abs/2101.12022) [astro-ph.GA].
- [38] Roberto Cid Fernandes et al. “Semi-empirical analysis of Sloan Digital Sky Survey galaxies - I. Spectral synthesis method”. In: *MNRAS* 358.2 (Apr. 2005), pp. 363–378. doi: [10.1111/j.1365-2966.2005.08752.x](https://doi.org/10.1111/j.1365-2966.2005.08752.x). arXiv: [astro-ph/0412481](https://arxiv.org/abs/astro-ph/0412481) [astro-ph].
- [39] Serena A. Cronin et al. “Local Environments of Low-redshift Supernovae”. In: *ApJ* 923.1, 86 (Dec. 2021), p. 86. doi: [10.3847/1538-4357/ac28a2](https://doi.org/10.3847/1538-4357/ac28a2). arXiv: [2109.07453](https://arxiv.org/abs/2109.07453) [astro-ph.GA].
- [40] Paul A. Crowther. “On the association between core-collapse supernovae and H ii regions”. In: *MNRAS* 428.3 (Jan. 2013), pp. 1927–1943. doi: [10.1093/mnras/sts145](https://doi.org/10.1093/mnras/sts145). arXiv: [1210.1126](https://arxiv.org/abs/1210.1126) [astro-ph.SR].
- [41] K. W. Davis et al. “SN 2022ann: a Type Icn supernova from a dwarf galaxy that reveals helium in its circumstellar environment”. In: *MNRAS* 523.2 (Aug. 2023), pp. 2530–2550. doi: [10.1093/mnras/stad1433](https://doi.org/10.1093/mnras/stad1433). arXiv: [2211.05134](https://arxiv.org/abs/2211.05134) [astro-ph.HE].
- [42] A. Domínguez et al. “Dust Extinction from Balmer Decrements of Star-forming Galaxies at $0.75 \leq z \leq 1.5$ with Hubble Space Telescope/Wide-Field-Camera 3 Spectroscopy from the WFC3 Infrared Spectroscopic Parallel Survey”. In: *ApJ* 763.2, 145 (Feb. 2013), p. 145. doi: [10.1088/0004-637X/763/2/145](https://doi.org/10.1088/0004-637X/763/2/145). arXiv: [1206.1867](https://arxiv.org/abs/1206.1867) [astro-ph.CO].
- [43] Michael A. Dopita et al. “Chemical abundances in high-redshift galaxies: a powerful new emission line diagnostic”. In: *APSS* 361, 61 (Feb. 2016), p. 61. doi: [10.1007/s10509-016-2657-8](https://doi.org/10.1007/s10509-016-2657-8). arXiv: [1601.01337](https://arxiv.org/abs/1601.01337) [astro-ph.GA].
- [44] Maria R. Drout et al. “The First Systematic Study of Type Ibc Supernova Multi-band Light Curves”. In: *ApJ* 741.2, 97 (Nov. 2011), p. 97. doi: [10.1088/0004-637X/741/2/97](https://doi.org/10.1088/0004-637X/741/2/97). arXiv: [1011.4959](https://arxiv.org/abs/1011.4959) [astro-ph.CO].
- [45] P. R. Dunstall et al. “The VLT-FLAMES Tarantula Survey. XXII. Multiplicity properties of the B-type stars”. In: *A&A* 580, A93 (Aug. 2015), A93. doi: [10.1051/0004-6361/201526192](https://doi.org/10.1051/0004-6361/201526192). arXiv: [1505.07121](https://arxiv.org/abs/1505.07121) [astro-ph.SR].

- [46] Kevin Ebinger et al. “PUSHing Core-collapse Supernovae to Explosions in Spherical Symmetry. IV. Explodability, Remnant Properties, and Nucleosynthesis Yields of Low-metallicity Stars”. In: *ApJ* 888.2, 91 (Jan. 2020), p. 91. doi: [10.3847/1538-4357/ab5dcb](https://doi.org/10.3847/1538-4357/ab5dcb). arXiv: [1910.08958](https://arxiv.org/abs/1910.08958) [astro-ph.SR].
- [47] J. J. Eldridge and C. A. Tout. “The progenitors of core-collapse supernovae”. In: *MNRAS* 353.1 (Sept. 2004), pp. 87–97. doi: [10.1111/j.1365-2966.2004.08041.x](https://doi.org/10.1111/j.1365-2966.2004.08041.x). arXiv: [astro-ph/0405408](https://arxiv.org/abs/astro-ph/0405408) [astro-ph].
- [48] J. J. Eldridge et al. “Binary Population and Spectral Synthesis Version 2.1: Construction, Observational Verification, and New Results”. In: 34, e058 (Nov. 2017), e058. doi: [10.1017/pasa.2017.51](https://doi.org/10.1017/pasa.2017.51). arXiv: [1710.02154](https://arxiv.org/abs/1710.02154) [astro-ph.SR].
- [49] John J. Eldridge, Robert G. Izzard, and Christopher A. Tout. “The effect of massive binaries on stellar populations and supernova progenitors”. In: *MNRAS* 384.3 (Mar. 2008), pp. 1109–1118. doi: [10.1111/j.1365-2966.2007.12738.x](https://doi.org/10.1111/j.1365-2966.2007.12738.x). arXiv: [0711.3079](https://arxiv.org/abs/0711.3079) [astro-ph].
- [50] John J. Eldridge et al. “The death of massive stars - II. Observational constraints on the progenitors of Type Ibc supernovae”. In: *MNRAS* 436.1 (Nov. 2013), pp. 774–795. doi: [10.1093/mnras/stt1612](https://doi.org/10.1093/mnras/stt1612). arXiv: [1301.1975](https://arxiv.org/abs/1301.1975) [astro-ph.SR].
- [51] N. Elias-Rosa et al. “Dead or Alive? Long-term evolution of SN 2015bh (SNhunt275)”. In: *MNRAS* 463.4 (Dec. 2016), pp. 3894–3920. doi: [10.1093/mnras/stw2253](https://doi.org/10.1093/mnras/stw2253). arXiv: [1606.09024](https://arxiv.org/abs/1606.09024) [astro-ph.SR].
- [52] T. Ertl et al. “A Two-parameter Criterion for Classifying the Explodability of Massive Stars by the Neutrino-driven Mechanism”. In: *ApJ* 818.2, 124 (Feb. 2016), p. 124. doi: [10.3847/0004-637X/818/2/124](https://doi.org/10.3847/0004-637X/818/2/124). arXiv: [1503.07522](https://arxiv.org/abs/1503.07522) [astro-ph.SR].
- [53] Qiliang Fang et al. “Statistical Properties of the Nebular Spectra of 103 Stripped-envelope Core-collapse Supernovae”. In: 928.2, 151 (Apr. 2022), p. 151. doi: [10.3847/1538-4357/ac4f60](https://doi.org/10.3847/1538-4357/ac4f60). arXiv: [2201.11467](https://arxiv.org/abs/2201.11467) [astro-ph.HE].
- [54] A. Fassia et al. “Optical and infrared photometry of the Type IIn SN 1998S: days 11–146”. In: *MNRAS* 318.4 (Nov. 2000), pp. 1093–1104. doi: [10.1046/j.1365-8711.2000.03797.x](https://doi.org/10.1046/j.1365-8711.2000.03797.x). arXiv: [astro-ph/0006080](https://arxiv.org/abs/astro-ph/0006080) [astro-ph].

- [55] Alexei V. Filippenko. “Optical Spectra of Supernovae”. In: *ARA&A* 35 (Jan. 1997), pp. 309–355. doi: [10.1146/annurev.astro.35.1.309](https://doi.org/10.1146/annurev.astro.35.1.309).
- [56] Alexei V. Filippenko, Thomas Matheson, and Aaron J. Barth. “The Peculiar Type II Supernova 1993J in M81: Transition to the Nebular Phase”. In: *AJ* 108 (Dec. 1994), p. 2220. doi: [10.1086/117234](https://doi.org/10.1086/117234).
- [57] Alexei V. Filippenko et al. “The Lick Observatory Supernova Search with the Katzman Automatic Imaging Telescope”. In: *IAU Colloq. 183: Small Telescope Astronomy on Global Scales*. Ed. by Bohdan Paczynski, Wen-Ping Chen, and Claudia Lemme. Vol. 246. Astronomical Society of the Pacific Conference Series. Jan. 2001, p. 121.
- [58] Brenna Flaugher. “The Dark Energy Survey”. In: *International Journal of Modern Physics A* 20.14 (Jan. 2005), pp. 3121–3123. doi: [10.1142/S0217751X05025917](https://doi.org/10.1142/S0217751X05025917).
- [59] H. A. Flewelling et al. “The Pan-STARRS1 Database and Data Products”. In: *ApJs* 251.1, 7 (Nov. 2020), p. 7. doi: [10.3847/1538-4365/abb82d](https://doi.org/10.3847/1538-4365/abb82d). arXiv: [1612.05243](https://arxiv.org/abs/1612.05243) [[astro-ph.IM](#)].
- [60] Gastón Folatelli et al. “The Progenitor of the Type IIb SN 2008ax Revisited”. In: *ApJ* 811.2, 147 (Oct. 2015), p. 147. doi: [10.1088/0004-637X/811/2/147](https://doi.org/10.1088/0004-637X/811/2/147). arXiv: [1509.01588](https://arxiv.org/abs/1509.01588) [[astro-ph.SR](#)].
- [61] Ori D. Fox et al. “A Spitzer survey for dust-obscured supernovae”. In: *MNRAS* 506.3 (Sept. 2021), pp. 4199–4209. doi: [10.1093/mnras/stab1740](https://doi.org/10.1093/mnras/stab1740). arXiv: [2106.09733](https://arxiv.org/abs/2106.09733) [[astro-ph.HE](#)].
- [62] Ori D. Fox et al. “The Candidate Progenitor Companion Star of the Type Ib/c SN 2013ge”. In: *ApJ* 929.1, L15 (Apr. 2022), p. L15. doi: [10.3847/2041-8213/ac5890](https://doi.org/10.3847/2041-8213/ac5890). arXiv: [2203.01357](https://arxiv.org/abs/2203.01357) [[astro-ph.HE](#)].
- [63] Ori D. Fox et al. “Uncovering the Putative B-star Binary Companion of the SN 1993J Progenitor”. In: *ApJ* 790.1, 17 (July 2014), p. 17. doi: [10.1088/0004-637X/790/1/17](https://doi.org/10.1088/0004-637X/790/1/17). arXiv: [1405.4863](https://arxiv.org/abs/1405.4863) [[astro-ph.HE](#)].
- [64] Claes Fransson et al. “Optical and Ultraviolet Spectroscopy of SN 1995N: Evidence for Strong Circumstellar Interaction”. In: *ApJ* 572.1 (June 2002), pp. 350–370. doi: [10.1086/340295](https://doi.org/10.1086/340295). arXiv: [astro-ph/0108149](https://arxiv.org/abs/astro-ph/0108149) [[astro-ph](#)].

- [65] Morgan Fraser. “The disappearance of the progenitor of SN 2012aw in late-time imaging”. In: *MNRAS* 456.1 (Feb. 2016), pp. L16–L19. doi: [10.1093/mnras1/slv168](https://doi.org/10.1093/mnras1/slv168). arXiv: [1507.06579](https://arxiv.org/abs/1507.06579) [astro-ph.SR].
- [66] Morgan Fraser et al. “SN 2021csp – the explosion of a stripped envelope star within a H and He-poor circumstellar medium”. In: *arXiv e-prints*, arXiv:2108.07278 (Aug. 2021), arXiv:2108.07278. arXiv: [2108.07278](https://arxiv.org/abs/2108.07278) [astro-ph.SR].
- [67] W. Freudling et al. “Automated data reduction workflows for astronomy. The ESO Reflex environment”. In: *A&A* 559, A96 (Nov. 2013), A96. doi: [10.1051/0004-6361/201322494](https://doi.org/10.1051/0004-6361/201322494). arXiv: [1311.5411](https://arxiv.org/abs/1311.5411) [astro-ph.IM].
- [68] C. Frohmaier et al. “From core collapse to superluminous: the rates of massive stellar explosions from the Palomar Transient Factory”. In: *MNRAS* 500.4 (Jan. 2021), pp. 5142–5158. doi: [10.1093/mnras/staa3607](https://doi.org/10.1093/mnras/staa3607). arXiv: [2010.15270](https://arxiv.org/abs/2010.15270) [astro-ph.HE].
- [69] A. S. Fruchter et al. “Long γ -ray bursts and core-collapse supernovae have different environments”. In: 441.7092 (May 2006), pp. 463–468. doi: [10.1038/nature04787](https://doi.org/10.1038/nature04787). arXiv: [astro-ph/0603537](https://arxiv.org/abs/astro-ph/0603537) [astro-ph].
- [70] Gaia Collaboration et al. “Gaia Data Release 2. Summary of the contents and survey properties”. In: *A&A* 616, A1 (Aug. 2018), A1. doi: [10.1051/0004-6361/201833051](https://doi.org/10.1051/0004-6361/201833051). arXiv: [1804.09365](https://arxiv.org/abs/1804.09365) [astro-ph.GA].
- [71] A. Gal-Yam and D. C. Leonard. “A massive hypergiant star as the progenitor of the supernova SN 2005gl”. In: *Nature* 458.7240 (Apr. 2009), pp. 865–867. doi: [10.1038/nature07934](https://doi.org/10.1038/nature07934).
- [72] A. Gal-Yam et al. “Introducing a new Supernova classification type: SN Icn”. In: *Transient Name Server AstroNote* 76 (Feb. 2021), pp. 1–76.
- [73] Avishay Gal-Yam. “Observational and Physical Classification of Supernovae”. In: *Handbook of Supernovae*. Ed. by Athem W. Alsabti and Paul Murdin. 2017, p. 195. doi: [10.1007/978-3-319-21846-5_35](https://doi.org/10.1007/978-3-319-21846-5_35).
- [74] L. Galbany et al. “Characterizing the environments of supernovae with MUSE”. In: *MNRAS* 455.4 (Feb. 2016), pp. 4087–4099. doi: [10.1093/mnras/stv2620](https://doi.org/10.1093/mnras/stv2620). arXiv: [1511.01495](https://arxiv.org/abs/1511.01495) [astro-ph.GA].

- [75] L. Galbany et al. “Molecular gas in supernova local environments unveiled by EDGE”. In: *MNRAS* 468.1 (June 2017), pp. 628–644. doi: [10.1093/mnras/stx367](https://doi.org/10.1093/mnras/stx367). arXiv: [1702.02945](https://arxiv.org/abs/1702.02945) [astro-ph.GA].
- [76] L. Galbany et al. “Nearby supernova host galaxies from the CALIFA Survey. I. Sample, data analysis, and correlation to star-forming regions”. In: *A&A* 572, A38 (Dec. 2014), A38. doi: [10.1051/0004-6361/201424717](https://doi.org/10.1051/0004-6361/201424717). arXiv: [1409.1623](https://arxiv.org/abs/1409.1623) [astro-ph.GA].
- [77] L. Galbany et al. “Nearby supernova host galaxies from the CALIFA survey. II. Supernova environmental metallicity”. In: *A&A* 591, A48 (June 2016), A48. doi: [10.1051/0004-6361/201528045](https://doi.org/10.1051/0004-6361/201528045). arXiv: [1603.07808](https://arxiv.org/abs/1603.07808) [astro-ph.GA].
- [78] L. Galbany et al. “PISCO: The PMAS/PPak Integral-field Supernova Hosts Compilation”. In: *ApJ* 855.2, 107 (Mar. 2018), p. 107. doi: [10.3847/1538-4357/aaaf20](https://doi.org/10.3847/1538-4357/aaaf20). arXiv: [1802.01589](https://arxiv.org/abs/1802.01589) [astro-ph.GA].
- [79] Lluís Galbany et al. “UBVR_Iz Light Curves of 51 Type II Supernovae”. In: *AJ* 151.2, 33 (Feb. 2016), p. 33. doi: [10.3847/0004-6256/151/2/33](https://doi.org/10.3847/0004-6256/151/2/33). arXiv: [1511.08402](https://arxiv.org/abs/1511.08402) [astro-ph.SR].
- [80] C. Georgy et al. “The different progenitors of type Ib, Ic SNe, and of GRB”. In: *A&A* 502.2 (Aug. 2009), pp. 611–622. doi: [10.1051/0004-6361/200811339](https://doi.org/10.1051/0004-6361/200811339). arXiv: [0906.2284](https://arxiv.org/abs/0906.2284) [astro-ph.SR].
- [81] Adam Ginsburg et al. “astroquery: An Astronomical Web-querying Package in Python”. In: *AJ* 157.3, 98 (Mar. 2019), p. 98. doi: [10.3847/1538-3881/aafc33](https://doi.org/10.3847/1538-3881/aafc33). arXiv: [1901.04520](https://arxiv.org/abs/1901.04520) [astro-ph.IM].
- [82] Stephanie M. Gogarten et al. “The ACS Nearby Galaxy Survey Treasury. II. Young Stars and their Relation to H α and UV Emission Timescales in the M81 Outer Disk”. In: 691.1 (Jan. 2009), pp. 115–130. doi: [10.1088/0004-637X/691/1/115](https://doi.org/10.1088/0004-637X/691/1/115). arXiv: [0810.0266](https://arxiv.org/abs/0810.0266) [astro-ph].
- [83] J. F. Graham and A. S. Fruchter. “The Metal Aversion of Long-duration Gamma-Ray Bursts”. In: *ApJ* 774.2, 119 (Sept. 2013), p. 119. doi: [10.1088/0004-637X/774/2/119](https://doi.org/10.1088/0004-637X/774/2/119). arXiv: [1211.7068](https://arxiv.org/abs/1211.7068) [astro-ph.HE].

- [84] J. F. Graham and A. S. Fruchter. “The Relative Rate of LGRB Formation as a Function of Metallicity”. In: *ApJ* 834.2, 170 (Jan. 2017), p. 170. doi: [10.3847/1538-4357/834/2/170](https://doi.org/10.3847/1538-4357/834/2/170). arXiv: [1511.01079](https://arxiv.org/abs/1511.01079) [[astro-ph.HE](#)].
- [85] Or Graur and Dan Maoz. “Discovery of 90 Type Ia supernovae among 700 000 Sloan spectra: the Type Ia supernova rate versus galaxy mass and star formation rate at redshift ~ 0.1 ”. In: *MNRAS* 430.3 (Apr. 2013), pp. 1746–1763. doi: [10.1093/mnras/sts718](https://doi.org/10.1093/mnras/sts718). arXiv: [1209.0008](https://arxiv.org/abs/1209.0008) [[astro-ph.CO](#)].
- [86] Or Graur et al. “LOSS Revisited. I. Unraveling Correlations Between Supernova Rates and Galaxy Properties, as Measured in a Reanalysis of the Lick Observatory Supernova Search”. In: *ApJ* 837.2, 120 (Mar. 2017), p. 120. doi: [10.3847/1538-4357/aa5eb8](https://doi.org/10.3847/1538-4357/aa5eb8). arXiv: [1609.02921](https://arxiv.org/abs/1609.02921) [[astro-ph.HE](#)].
- [87] C. P. Gutiérrez et al. “Type II supernovae in low-luminosity host galaxies”. In: *MNRAS* 479.3 (Sept. 2018), pp. 3232–3253. doi: [10.1093/mnras/sty1581](https://doi.org/10.1093/mnras/sty1581). arXiv: [1806.03855](https://arxiv.org/abs/1806.03855) [[astro-ph.HE](#)].
- [88] Claudia P. Gutiérrez et al. “Type II Supernova Spectral Diversity. I. Observations, Sample Characterization, and Spectral Line Evolution”. In: *ApJ* 850.1, 89 (Nov. 2017), p. 89. doi: [10.3847/1538-4357/aa8f52](https://doi.org/10.3847/1538-4357/aa8f52). arXiv: [1709.02487](https://arxiv.org/abs/1709.02487) [[astro-ph.HE](#)].
- [89] S. M. Habergham et al. “Environments of interacting transients: impostors and Type IIIn supernovae”. In: *MNRAS* 441.3 (July 2014), pp. 2230–2252. doi: [10.1093/mnras/stu684](https://doi.org/10.1093/mnras/stu684). arXiv: [1404.2282](https://arxiv.org/abs/1404.2282) [[astro-ph.HE](#)].
- [90] A. A. Hakobyan et al. “The radial distribution of core-collapse supernovae in spiral host galaxies”. In: *A&A* 508.3 (Dec. 2009), pp. 1259–1268. doi: [10.1051/0004-6361/200912795](https://doi.org/10.1051/0004-6361/200912795). arXiv: [0910.1801](https://arxiv.org/abs/0910.1801) [[astro-ph.CO](#)].
- [91] Mario Hamuy et al. “The Absolute Luminosities of the Calan/Tololo Type Ia Supernovae”. In: *AJ* 112 (Dec. 1996), p. 2391. doi: [10.1086/118190](https://doi.org/10.1086/118190). arXiv: [astro-ph/9609059](https://arxiv.org/abs/astro-ph/9609059) [[astro-ph](#)].
- [92] A. Heger et al. “How Massive Single Stars End Their Life”. In: *ApJ* 591.1 (2003), pp. 288–300. doi: [10.1086/375341](https://doi.org/10.1086/375341). arXiv: [astro-ph/0212469](https://arxiv.org/abs/astro-ph/0212469) [[astro-ph](#)].

- [93] T. W. S. Holoién et al. “The ASAS-SN bright supernova catalogue - II. 2015”. In: *MNRAS* 467.1 (May 2017), pp. 1098–1111. doi: [10.1093/mnras/stx057](https://doi.org/10.1093/mnras/stx057). arXiv: [1610.03061](https://arxiv.org/abs/1610.03061) [astro-ph.HE].
- [94] T. W. S. Holoién et al. “The ASAS-SN bright supernova catalogue - III. 2016”. In: *MNRAS* 471.4 (Nov. 2017), pp. 4966–4981. doi: [10.1093/mnras/stx1544](https://doi.org/10.1093/mnras/stx1544). arXiv: [1704.02320](https://arxiv.org/abs/1704.02320) [astro-ph.HE].
- [95] T. W. S. Holoién et al. “The ASAS-SN bright supernova catalogue - IV. 2017”. In: *MNRAS* 484.2 (Apr. 2019), pp. 1899–1911. doi: [10.1093/mnras/stz073](https://doi.org/10.1093/mnras/stz073). arXiv: [1811.08904](https://arxiv.org/abs/1811.08904) [astro-ph.HE].
- [96] T. W. S. Holoién et al. “The ASAS-SN bright supernova catalogue - I. 2013–2014”. In: *MNRAS* 464.3 (Jan. 2017), pp. 2672–2686. doi: [10.1093/mnras/stw2273](https://doi.org/10.1093/mnras/stw2273). arXiv: [1604.00396](https://arxiv.org/abs/1604.00396) [astro-ph.HE].
- [97] G. Hosseinzadeh et al. “ASASSN-16ff/AT 2016cdd”. In: *The Astronomer’s Telegram* 9065 (May 2016), p. 1.
- [98] Griffin Hosseinzadeh et al. “Type Ibn Supernovae May not all Come from Massive Stars”. In: 871.1, L9 (Jan. 2019), p. L9. doi: [10.3847/2041-8213/aafc61](https://doi.org/10.3847/2041-8213/aafc61). arXiv: [1901.03332](https://arxiv.org/abs/1901.03332) [astro-ph.HE].
- [99] F. Hoyle and William A. Fowler. “Nucleosynthesis in Supernovae.” In: 132 (Nov. 1960), p. 565. doi: [10.1086/146963](https://doi.org/10.1086/146963).
- [100] Duligur Ibeling and Alexander Heger. “The Metallicity Dependence of the Minimum Mass for Core-collapse Supernovae”. In: *ApJl* 765.2, L43 (Mar. 2013), p. L43. doi: [10.1088/2041-8205/765/2/L43](https://doi.org/10.1088/2041-8205/765/2/L43). arXiv: [1301.5783](https://arxiv.org/abs/1301.5783) [astro-ph.SR].
- [101] Jr. Iben I. and A. V. Tutukov. “Supernovae of type I as end products of the evolution of binaries with components of moderate initial mass.” In: *ApJs* 54 (Feb. 1984), pp. 335–372. doi: [10.1086/190932](https://doi.org/10.1086/190932).
- [102] P. A. James and J. P. Anderson. “The H α Galaxy Survey . III. Constraints on supernova progenitors from spatial correlations with H α emission”. In: *A&A* 453.1 (July 2006), pp. 57–65. doi: [10.1051/0004-6361:20054509](https://doi.org/10.1051/0004-6361:20054509). arXiv: [astro-ph/0602471](https://arxiv.org/abs/astro-ph/0602471) [astro-ph].

- [103] T. Jayasinghe et al. “A unicorn in monoceros: the $3 M_{\odot}$ dark companion to the bright, nearby red giant V723 Mon is a non-interacting, mass-gap black hole candidate”. In: 504.2 (June 2021), pp. 2577–2602. doi: [10.1093/mnras/stab907](https://doi.org/10.1093/mnras/stab907). arXiv: [2101.02212](https://arxiv.org/abs/2101.02212) [astro-ph.SR].
- [104] S. Jha. “Transient Classification Report for 2017-08-15”. In: *Transient Name Server Classification Report* 2017-870 (Aug. 2017), p. 1.
- [105] Benjamin D. Johnson et al. “Stellar Population Inference with Prospector”. In: 254.2, 22 (June 2021), p. 22. doi: [10.3847/1538-4365/abef67](https://doi.org/10.3847/1538-4365/abef67). arXiv: [2012.01426](https://arxiv.org/abs/2012.01426) [astro-ph.GA].
- [106] James W. Johnson, Christopher S. Kochanek, and K. Z. Stanek. “Binaries drive high Type Ia supernova rates in dwarf galaxies”. In: *arXiv e-prints*, arXiv:2210.01818 (Oct. 2022), arXiv:2210.01818. doi: [10.48550/arXiv.2210.01818](https://doi.org/10.48550/arXiv.2210.01818). arXiv: [2210.01818](https://arxiv.org/abs/2210.01818) [astro-ph.GA].
- [107] Jennifer A. Johnson. “Populating the periodic table: Nucleosynthesis of the elements”. In: *Science* 363.6426 (Feb. 2019), pp. 474–478. doi: [10.1126/science.aau9540](https://doi.org/10.1126/science.aau9540).
- [108] Nicholas Kaiser et al. “Pan-STARRS: A Large Synoptic Survey Telescope Array”. In: *Survey and Other Telescope Technologies and Discoveries*. Ed. by J. Anthony Tyson and Sidney Wolff. Vol. 4836. Society of Photo-Optical Instrumentation Engineers (SPIE) Conference Series. Dec. 2002, pp. 154–164. doi: [10.1117/12.457365](https://doi.org/10.1117/12.457365).
- [109] T. Kangas et al. “Core-collapse supernova progenitor constraints using the spatial distributions of massive stars in local galaxies”. In: *A&A* 597, A92 (Jan. 2017), A92. doi: [10.1051/0004-6361/201628705](https://doi.org/10.1051/0004-6361/201628705). arXiv: [1608.06097](https://arxiv.org/abs/1608.06097) [astro-ph.SR].
- [110] T. Kangas et al. “Spatial distributions of core-collapse supernovae in infrared-bright galaxies”. In: 436.4 (Dec. 2013), pp. 3464–3479. doi: [10.1093/mnras/stt1833](https://doi.org/10.1093/mnras/stt1833). arXiv: [1309.6781](https://arxiv.org/abs/1309.6781) [astro-ph.HE].
- [111] Torgny Karlsson, Volker Bromm, and Joss Bland-Hawthorn. “Pregalactic metal enrichment: The chemical signatures of the first stars”. In: *Reviews of Modern Physics* 85.2 (Apr. 2013), pp. 809–848. doi: [10.1103/RevModPhys.85.809](https://doi.org/10.1103/RevModPhys.85.809). arXiv: [1101.4024](https://arxiv.org/abs/1101.4024) [astro-ph.CO].

- [112] Daniel Kasen and S. E. Woosley. “Type II Supernovae: Model Light Curves and Standard Candle Relationships”. In: *ApJ* 703.2 (Oct. 2009), pp. 2205–2216. doi: [10.1088/0004-637X/703/2/2205](https://doi.org/10.1088/0004-637X/703/2/2205). arXiv: [0910.1590](https://arxiv.org/abs/0910.1590) [[astro-ph.CO](#)].
- [113] Guinevere Kauffmann et al. “The host galaxies of active galactic nuclei”. In: *MNRAS* 346.4 (Dec. 2003), pp. 1055–1077. doi: [10.1111/j.1365-2966.2003.07154.x](https://doi.org/10.1111/j.1365-2966.2003.07154.x). arXiv: [astro-ph/0304239](https://arxiv.org/abs/astro-ph/0304239) [[astro-ph](#)].
- [114] Patrick L. Kelly and Robert P. Kirshner. “Core-collapse Supernovae and Host Galaxy Stellar Populations”. In: *ApJ* 759.2, 107 (Nov. 2012), p. 107. doi: [10.1088/0004-637X/759/2/107](https://doi.org/10.1088/0004-637X/759/2/107). arXiv: [1110.1377](https://arxiv.org/abs/1110.1377) [[astro-ph.CO](#)].
- [115] Patrick L. Kelly, Robert P. Kirshner, and Michael Pahre. “Long γ -Ray Bursts and Type Ic Core-Collapse Supernovae Have Similar Locations in Hosts”. In: 687.2 (Nov. 2008), pp. 1201–1207. doi: [10.1086/591925](https://doi.org/10.1086/591925). arXiv: [0712.0430](https://arxiv.org/abs/0712.0430) [[astro-ph](#)].
- [116] Jr. Kennicutt Robert C. “Star Formation in Galaxies Along the Hubble Sequence”. In: *ARA&A* 36 (Jan. 1998), pp. 189–232. doi: [10.1146/annurev.astro.36.1.189](https://doi.org/10.1146/annurev.astro.36.1.189). arXiv: [astro-ph/9807187](https://arxiv.org/abs/astro-ph/9807187) [[astro-ph](#)].
- [117] Jr. Kennicutt Robert C. “The Global Schmidt Law in Star-forming Galaxies”. In: *ApJ* 498.2 (May 1998), pp. 541–552. doi: [10.1086/305588](https://doi.org/10.1086/305588). arXiv: [astro-ph/9712213](https://arxiv.org/abs/astro-ph/9712213) [[astro-ph](#)].
- [118] L. J. Kewley et al. “Theoretical Modeling of Starburst Galaxies”. In: *ApJ* 556.1 (July 2001), pp. 121–140. doi: [10.1086/321545](https://doi.org/10.1086/321545). arXiv: [astro-ph/0106324](https://arxiv.org/abs/astro-ph/0106324) [[astro-ph](#)].
- [119] Lisa J. Kewley and Sara L. Ellison. “Metallicity Calibrations and the Mass-Metallicity Relation for Star-forming Galaxies”. In: *ApJ* 681.2 (July 2008), pp. 1183–1204. doi: [10.1086/587500](https://doi.org/10.1086/587500). arXiv: [0801.1849](https://arxiv.org/abs/0801.1849) [[astro-ph](#)].
- [120] Lisa J. Kewley et al. “Metallicity Gradients and Gas Flows in Galaxy Pairs”. In: *ApJ* 721.1 (Sept. 2010), pp. L48–L52. doi: [10.1088/2041-8205/721/1/L48](https://doi.org/10.1088/2041-8205/721/1/L48). arXiv: [1008.2204](https://arxiv.org/abs/1008.2204) [[astro-ph.CO](#)].
- [121] Lisa J. Kewley et al. “SDSS 0809+1729: Connections Between Extremely Metal-Poor Galaxies and Gamma-Ray Burst Hosts”. In: *AJ* 133.3 (Mar. 2007), pp. 882–888. doi: [10.1086/509135](https://doi.org/10.1086/509135). arXiv: [astro-ph/0609246](https://arxiv.org/abs/astro-ph/0609246) [[astro-ph](#)].

- [122] Charles D. Kilpatrick et al. “A cool and inflated progenitor candidate for the Type Ib supernova 2019yvr at 2.6 yr before explosion”. In: *MNRAS* 504.2 (June 2021), pp. 2073–2093. doi: [10.1093/mnras/stab838](https://doi.org/10.1093/mnras/stab838). arXiv: [2101.03206](https://arxiv.org/abs/2101.03206) [[astro-ph.HE](#)].
- [123] Charles D. Kilpatrick et al. “The Gravity Collective: A Search for the Electromagnetic Counterpart to the Neutron Star-Black Hole Merger GW190814”. In: 923.2, 258 (Dec. 2021), p. 258. doi: [10.3847/1538-4357/ac23c6](https://doi.org/10.3847/1538-4357/ac23c6). arXiv: [2106.06897](https://arxiv.org/abs/2106.06897) [[astro-ph.HE](#)].
- [124] Hyun-Jeong Kim, Sung-Chul Yoon, and Bon-Chul Koo. “Observational Properties of Type Ib/c Supernova Progenitors in Binary Systems”. In: *ApJ* 809.2, 131 (Aug. 2015), p. 131. doi: [10.1088/0004-637X/809/2/131](https://doi.org/10.1088/0004-637X/809/2/131). arXiv: [1506.06354](https://arxiv.org/abs/1506.06354) [[astro-ph.SR](#)].
- [125] Matthew D. Kistler et al. “The Impact of Metallicity on the Rate of Type Ia Supernovae”. In: *ApJ* 770.2, 88 (June 2013), p. 88. doi: [10.1088/0004-637X/770/2/88](https://doi.org/10.1088/0004-637X/770/2/88). arXiv: [1106.3115](https://arxiv.org/abs/1106.3115) [[astro-ph.CO](#)].
- [126] Jakub Klencki et al. “Massive donors in interacting binaries: effect of metallicity”. In: *A&A* 638, A55 (June 2020), A55. doi: [10.1051/0004-6361/202037694](https://doi.org/10.1051/0004-6361/202037694). arXiv: [2004.00628](https://arxiv.org/abs/2004.00628) [[astro-ph.SR](#)].
- [127] Chiaki Kobayashi and Naohito Nakasato. “Chemodynamical Simulations of the Milky Way Galaxy”. In: *ApJ* 729.1, 16 (Mar. 2011), p. 16. doi: [10.1088/0004-637X/729/1/16](https://doi.org/10.1088/0004-637X/729/1/16). arXiv: [1012.5144](https://arxiv.org/abs/1012.5144) [[astro-ph.GA](#)].
- [128] C. S. Kochanek. “On the red supergiant problem”. In: 493.4 (Apr. 2020), pp. 4945–4949. doi: [10.1093/mnras/staa605](https://doi.org/10.1093/mnras/staa605). arXiv: [2001.07216](https://arxiv.org/abs/2001.07216) [[astro-ph.SR](#)].
- [129] C. S. Kochanek et al. “The All-Sky Automated Survey for Supernovae (ASAS-SN) Light Curve Server v1.0”. In: *PASP* 129.980 (Oct. 2017), p. 104502. doi: [10.1088/1538-3873/aa80d9](https://doi.org/10.1088/1538-3873/aa80d9). arXiv: [1706.07060](https://arxiv.org/abs/1706.07060) [[astro-ph.SR](#)].
- [130] Christopher S. Kochanek et al. “A Survey About Nothing: Monitoring a Million Supergiants for Failed Supernovae”. In: *ApJ* 684.2 (Sept. 2008), pp. 1336–1342. doi: [10.1086/590053](https://doi.org/10.1086/590053). arXiv: [0802.0456](https://arxiv.org/abs/0802.0456) [[astro-ph](#)].

- [131] M. Kopsacheili, A. Zezas, and I. Leonidaki. “A diagnostic tool for the identification of supernova remnants”. In: *MNRAS* 491.1 (Jan. 2020), pp. 889–902. doi: [10.1093/mnras/stz2594](https://doi.org/10.1093/mnras/stz2594). arXiv: [1909.05879](https://arxiv.org/abs/1909.05879) [[astro-ph.GA](#)].
- [132] T. Kozasa et al. “Dust in Supernovae: Formation and Evolution”. In: *Cosmic Dust - Near and Far*. Ed. by T. Henning, E. Grün, and J. Steinacker. Vol. 414. Astronomical Society of the Pacific Conference Series. Dec. 2009, p. 43. doi: [10.48550/arXiv.0903.0217](https://doi.org/10.48550/arXiv.0903.0217). arXiv: [0903.0217](https://arxiv.org/abs/0903.0217) [[astro-ph.GA](#)].
- [133] Pavel Kroupa, Christopher A. Tout, and Gerard Gilmore. “The Distribution of Low-Mass Stars in the Galactic Disc”. In: *MNRAS* 262 (June 1993), pp. 545–587. doi: [10.1093/mnras/262.3.545](https://doi.org/10.1093/mnras/262.3.545).
- [134] T. Krühler et al. “Hot gas around SN 1998bw: Inferring the progenitor from its environment”. In: *A&A* 602, A85 (June 2017), A85. doi: [10.1051/0004-6361/201630268](https://doi.org/10.1051/0004-6361/201630268). arXiv: [1702.05430](https://arxiv.org/abs/1702.05430) [[astro-ph.GA](#)].
- [135] H. Kuncarayakti et al. “Constraints on core-collapse supernova progenitors from explosion site integral field spectroscopy”. In: *A&A* 613, A35 (May 2018), A35. doi: [10.1051/0004-6361/201731923](https://doi.org/10.1051/0004-6361/201731923). arXiv: [1711.05765](https://arxiv.org/abs/1711.05765) [[astro-ph.SR](#)].
- [136] Hanindyo Kuncarayakti et al. “Integral Field Spectroscopy of Supernova Explosion Sites: Constraining the Mass and Metallicity of the Progenitors. I. Type Ib and Ic Supernovae”. In: *AJ* 146.2, 30 (Aug. 2013), p. 30. doi: [10.1088/0004-6256/146/2/30](https://doi.org/10.1088/0004-6256/146/2/30). arXiv: [1305.1105](https://arxiv.org/abs/1305.1105) [[astro-ph.CO](#)].
- [137] Hanindyo Kuncarayakti et al. “Integral Field Spectroscopy of Supernova Explosion Sites: Constraining the Mass and Metallicity of the Progenitors. II. Type II-P and II-L Supernovae”. In: *AJ* 146.2, 31 (Aug. 2013), p. 31. doi: [10.1088/0004-6256/146/2/31](https://doi.org/10.1088/0004-6256/146/2/31). arXiv: [1306.2106](https://arxiv.org/abs/1306.2106) [[astro-ph.CO](#)].
- [138] N. Langer. “Mass-dependent mass loss rates of Wolf-Rayet stars.” In: *A&A* 220 (Aug. 1989), pp. 135–143.
- [139] E. Laplace et al. “Different to the core: The pre-supernova structures of massive single and binary-stripped stars”. In: *A&A* 656, A58 (Dec. 2021), A58. doi: [10.1051/0004-6361/202140506](https://doi.org/10.1051/0004-6361/202140506). arXiv: [2102.05036](https://arxiv.org/abs/2102.05036) [[astro-ph.SR](#)].

- [140] E. Laplace et al. "The expansion of stripped-envelope stars: Consequences for supernovae and gravitational-wave progenitors". In: *A&A* 637, A6 (May 2020), A6. doi: [10.1051/0004-6361/201937300](https://doi.org/10.1051/0004-6361/201937300). arXiv: [2003.01120](https://arxiv.org/abs/2003.01120) [[astro-ph.SR](#)].
- [141] Oliver Le Fèvre et al. "Commissioning and performances of the VLT-VIMOS instrument". In: *Instrument Design and Performance for Optical/Infrared Ground-based Telescopes*. Ed. by Masanori Iye and Alan F. M. Moorwood. Vol. 4841. Society of Photo-Optical Instrumentation Engineers (SPIE) Conference Series. Mar. 2003, pp. 1670–1681. doi: [10.1117/12.460959](https://doi.org/10.1117/12.460959).
- [142] Claus Leitherer et al. "Starburst99: Synthesis Models for Galaxies with Active Star Formation". In: *ApJs* 123.1 (July 1999), pp. 3–40. doi: [10.1086/313233](https://doi.org/10.1086/313233). arXiv: [astro-ph/9902334](https://arxiv.org/abs/astro-ph/9902334) [[astro-ph](#)].
- [143] G. Leloudas et al. "Spectroscopy of superluminous supernova host galaxies. A preference of hydrogen-poor events for extreme emission line galaxies". In: *MNRAS* 449.1 (May 2015), pp. 917–932. doi: [10.1093/mnras/stv320](https://doi.org/10.1093/mnras/stv320). arXiv: [1409.8331](https://arxiv.org/abs/1409.8331) [[astro-ph.GA](#)].
- [144] G. Leloudas et al. "The properties of SN Ib/c locations". In: *A&A* 530, A95 (June 2011), A95. doi: [10.1051/0004-6361/201116692](https://doi.org/10.1051/0004-6361/201116692). arXiv: [1102.2249](https://arxiv.org/abs/1102.2249) [[astro-ph.SR](#)].
- [145] Jiadong Li et al. "Stellar initial mass function varies with metallicity and time". In: *Nature* 613.7944 (Jan. 2023), pp. 460–462. doi: [10.1038/s41586-022-05488-1](https://doi.org/10.1038/s41586-022-05488-1). arXiv: [2301.07029](https://arxiv.org/abs/2301.07029) [[astro-ph.GA](#)].
- [146] W. D. Li et al. "The Lick Observatory Supernova Search". In: *Cosmic Explosions: Tenth AstroPhysics Conference*. Ed. by Stephen S. Holt and William W. Zhang. Vol. 522. American Institute of Physics Conference Series. June 2000, pp. 103–106. doi: [10.1063/1.1291702](https://doi.org/10.1063/1.1291702). arXiv: [astro-ph/9912336](https://arxiv.org/abs/astro-ph/9912336) [[astro-ph](#)].
- [147] Weidong Li et al. "Nearby supernova rates from the Lick Observatory Supernova Search - II. The observed luminosity functions and fractions of supernovae in a complete sample". In: *MNRAS* 412.3 (Apr. 2011), pp. 1441–1472. doi: [10.1111/j.1365-2966.2011.18160.x](https://doi.org/10.1111/j.1365-2966.2011.18160.x). arXiv: [1006.4612](https://arxiv.org/abs/1006.4612) [[astro-ph.SR](#)].

- [148] Weidong Li et al. “Nearby supernova rates from the Lick Observatory Supernova Search - III. The rate-size relation, and the rates as a function of galaxy Hubble type and colour”. In: *MNRAS* 412.3 (Apr. 2011), pp. 1473–1507. doi: [10.1111/j.1365-2966.2011.18162.x](https://doi.org/10.1111/j.1365-2966.2011.18162.x). arXiv: [1006.4613](https://arxiv.org/abs/1006.4613) [astro-ph.SR].
- [149] C. H. Lineweaver. “The CMB dipole: the most recent measurement and some history.” In: *Microwave Background Anisotropies*. Vol. 16. Jan. 1997, pp. 69–75. arXiv: [astro-ph/9609034](https://arxiv.org/abs/astro-ph/9609034) [astro-ph].
- [150] Carlos López-Cobá et al. “The AMUSING++ Nearby Galaxy Compilation. I. Full Sample Characterization and Galactic-scale Outflow Selection”. In: 159.4, 167 (Apr. 2020), p. 167. doi: [10.3847/1538-3881/ab7848](https://doi.org/10.3847/1538-3881/ab7848). arXiv: [2002.09328](https://arxiv.org/abs/2002.09328) [astro-ph.GA].
- [151] A. Z. Lugo-Aranda et al. “PYHIIEXTRACTOR: a tool to detect and extract physical properties of H II regions from integral field spectroscopic data”. In: *RAS Techniques and Instruments* 1.1 (Apr. 2022), pp. 3–28. doi: [10.1093/rasti/rzac001](https://doi.org/10.1093/rasti/rzac001). arXiv: [2204.04252](https://arxiv.org/abs/2204.04252) [astro-ph.GA].
- [152] R. Lunnan et al. “PS1-10bzj: A Fast, Hydrogen-poor Superluminous Supernova in a Metal-poor Host Galaxy”. In: *ApJ* 771.2, 97 (July 2013), p. 97. doi: [10.1088/0004-637X/771/2/97](https://doi.org/10.1088/0004-637X/771/2/97). arXiv: [1303.1531](https://arxiv.org/abs/1303.1531) [astro-ph.HE].
- [153] J. D. Lyman et al. “Bolometric light curves and explosion parameters of 38 stripped-envelope core-collapse supernovae”. In: *MNRAS* 457.1 (Mar. 2016), pp. 328–350. doi: [10.1093/mnras/stv2983](https://doi.org/10.1093/mnras/stv2983). arXiv: [1406.3667](https://arxiv.org/abs/1406.3667) [astro-ph.SR].
- [154] J. D. Lyman et al. “Investigating the diversity of supernovae type Iax: a MUSE and NOT spectroscopic study of their environments”. In: 473.1 (Jan. 2018), pp. 1359–1387. doi: [10.1093/mnras/stx2414](https://doi.org/10.1093/mnras/stx2414). arXiv: [1707.04270](https://arxiv.org/abs/1707.04270) [astro-ph.HE].
- [155] D. Makarov et al. “HyperLEDA. III. The catalogue of extragalactic distances”. In: *A&A* 570, A13 (Oct. 2014), A13. doi: [10.1051/0004-6361/201423496](https://doi.org/10.1051/0004-6361/201423496).
- [156] F. Mannucci, R. Salvaterra, and M. A. Campisi. “The metallicity of the long GRB hosts and the fundamental metallicity relation of low-mass galaxies”. In: *MNRAS* 414.2 (June 2011), pp. 1263–1268. doi: [10.1111/j.1365-2966.2011.18459.x](https://doi.org/10.1111/j.1365-2966.2011.18459.x). arXiv: [1011.4506](https://arxiv.org/abs/1011.4506) [astro-ph.CO].

- [157] R. A. Marino et al. “The O3N2 and N2 abundance indicators revisited: improved calibrations based on CALIFA and T_e -based literature data”. In: *A&A* 559, A114 (Nov. 2013), A114. doi: [10.1051/0004-6361/201321956](https://doi.org/10.1051/0004-6361/201321956). arXiv: [1307.5316](https://arxiv.org/abs/1307.5316) [[astro-ph.CO](#)].
- [158] Marie Martig and Frédéric Bournaud. “Formation of Late-type Spiral Galaxies: Gas Return from Stellar Populations Regulates Disk Destruction and Bulge Growth”. In: *ApJ* 714.2 (May 2010), pp. L275–L279. doi: [10.1088/2041-8205/714/2/L275](https://doi.org/10.1088/2041-8205/714/2/L275). arXiv: [0911.0891](https://arxiv.org/abs/0911.0891) [[astro-ph.CO](#)].
- [159] L. Martinez et al. “Type II supernovae from the Carnegie Supernova Project-I. III. Understanding SN II diversity through correlations between physical and observed properties”. In: *A&A* 660, A42 (Apr. 2022), A42. doi: [10.1051/0004-6361/202142555](https://doi.org/10.1051/0004-6361/202142555). arXiv: [2202.11220](https://arxiv.org/abs/2202.11220) [[astro-ph.SR](#)].
- [160] Abílio Mateus et al. “Semi-empirical analysis of Sloan Digital Sky Survey galaxies - II. The bimodality of the galaxy population revisited”. In: *MNRAS* 370.2 (Aug. 2006), pp. 721–737. doi: [10.1111/j.1365-2966.2006.10565.x](https://doi.org/10.1111/j.1365-2966.2006.10565.x). arXiv: [astro-ph/0511578](https://arxiv.org/abs/astro-ph/0511578) [[astro-ph](#)].
- [161] F. Matteucci and L. Greggio. “Relative roles of type I and II supernovae in the chemical enrichment of the interstellar gas”. In: *A&A* 154.1-2 (Jan. 1986), pp. 279–287.
- [162] Seppo Mattila et al. “The Disappearance of the Red Supergiant Progenitor of Supernova 2008bk”. In: *arXiv e-prints*, arXiv:1011.5494 (Nov. 2010), arXiv:1011.5494. doi: [10.48550/arXiv.1011.5494](https://doi.org/10.48550/arXiv.1011.5494). arXiv: [1011.5494](https://arxiv.org/abs/1011.5494) [[astro-ph.SR](#)].
- [163] Jon Mauerhan and Nathan Smith. “Supernova 1998S at 14 years postmortem: continuing circumstellar interaction and dust formation”. In: *MNRAS* 424.4 (Aug. 2012), pp. 2659–2666. doi: [10.1111/j.1365-2966.2012.21325.x](https://doi.org/10.1111/j.1365-2966.2012.21325.x). arXiv: [1204.1610](https://arxiv.org/abs/1204.1610) [[astro-ph.SR](#)].
- [164] Jon C. Mauerhan et al. “The unprecedented 2012 outburst of SN 2009ip: a luminous blue variable star becomes a true supernova”. In: *MNRAS* 430.3 (Apr. 2013), pp. 1801–1810. doi: [10.1093/mnras/stt009](https://doi.org/10.1093/mnras/stt009). arXiv: [1209.6320](https://arxiv.org/abs/1209.6320) [[astro-ph.SR](#)].

- [165] J. R. Maund et al. “The Yellow Supergiant Progenitor of the Type II Supernova 2011dh in M51”. In: *ApJ* 739.2, L37 (Oct. 2011), p. L37. doi: [10.1088/2041-8205/739/2/L37](https://doi.org/10.1088/2041-8205/739/2/L37). arXiv: [1106.2565](https://arxiv.org/abs/1106.2565) [astro-ph.SR].
- [166] Justyn R. Maund. “The very young resolved stellar populations around stripped-envelope supernovae”. In: 476.2 (May 2018), pp. 2629–2663. doi: [10.1093/mnras/sty093](https://doi.org/10.1093/mnras/sty093). arXiv: [1712.07714](https://arxiv.org/abs/1712.07714) [astro-ph.SR].
- [167] Justyn R. Maund, Emma Reilly, and Seppo Mattila. “A late-time view of the progenitors of five Type IIP supernovae”. In: *MNRAS* 438.2 (Feb. 2014), pp. 938–958. doi: [10.1093/mnras/stt2131](https://doi.org/10.1093/mnras/stt2131). arXiv: [1302.7152](https://arxiv.org/abs/1302.7152) [astro-ph.SR].
- [168] Justyn R. Maund and Stephen J. Smartt. “The Disappearance of the Progenitors of Supernovae 1993J and 2003gd”. In: *Science* 324.5926 (Apr. 2009), p. 486. doi: [10.1126/science.1170198](https://doi.org/10.1126/science.1170198). arXiv: [0903.3772](https://arxiv.org/abs/0903.3772) [astro-ph.SR].
- [169] Justyn R. Maund et al. “Whatever happened to the progenitors of supernovae 2008cn, 2009kr and 2009md?” In: *MNRAS* 447.4 (Mar. 2015), pp. 3207–3217. doi: [10.1093/mnras/stu2658](https://doi.org/10.1093/mnras/stu2658).
- [170] Ness Mayker Chen et al. “Comparing the Locations of Supernovae to CO (2-1) Emission in Their Host Galaxies”. In: *ApJ* 944.1, 110 (Feb. 2023), p. 110. doi: [10.3847/1538-4357/acab00](https://doi.org/10.3847/1538-4357/acab00). arXiv: [2212.09766](https://arxiv.org/abs/2212.09766) [astro-ph.GA].
- [171] J. Maza and S. van den Bergh. “Statistics of extragalactic supernovae.” In: *ApJ* 204 (Mar. 1976), pp. 519–529. doi: [10.1086/154198](https://doi.org/10.1086/154198).
- [172] P. A. Mazzali et al. “The Type Ic Hypernova SN 2002ap”. In: *ApJ* 572.1 (June 2002), pp. L61–L65. doi: [10.1086/341504](https://doi.org/10.1086/341504).
- [173] R. J. McMillan and R. Ciardullo. “Constraining the Ages of Supernova Progenitors. I. Supernovae and Spiral Arms”. In: *ApJ* 473 (Dec. 1996), p. 707. doi: [10.1086/178183](https://doi.org/10.1086/178183).
- [174] G. Meynet et al. “Grids of massive stars with high mass loss rates. V. From 12 to 120 M_{sun} at $Z=0.001$, 0.004, 0.008, 0.020 and 0.040”. In: 103 (Jan. 1994), pp. 97–105.

- [175] N. Meza et al. “VizieR Online Data Catalog: Supernova ASASSN-14jb light curves and spectra (Meza+, 2019)”. In: *VizieR Online Data Catalog*, J/A+A/629/A57 (Aug. 2019), J/A+A/629/A57.
- [176] Nicolás Meza et al. “The extraplanar type II supernova ASASSN-14jb in the nearby edge-on galaxy ESO 467-G051”. In: *A&A* 629, A57 (Sept. 2019), A57. doi: [10.1051/0004-6361/201834972](https://doi.org/10.1051/0004-6361/201834972). arXiv: [1811.11771](https://arxiv.org/abs/1811.11771) [[astro-ph.HE](#)].
- [177] Anthony Mezzacappa. “ASCERTAINING THE CORE COLLAPSE SUPERNOVA MECHANISM: The State of the Art and the Road Ahead”. In: *Annual Review of Nuclear and Particle Science* 55.1 (Dec. 2005), pp. 467–515. doi: [10.1146/annurev.nuc1.55.090704.151608](https://doi.org/10.1146/annurev.nuc1.55.090704.151608).
- [178] R. Minkowski. “Spectra of Supernovae”. In: *PASP* 53.314 (Aug. 1941), p. 224. doi: [10.1086/125315](https://doi.org/10.1086/125315).
- [179] S. Miyaji et al. “Supernova triggered by electron captures.” In: *PASJ* 32 (Jan. 1980), pp. 303–329.
- [180] M. Modjaz et al. “Measured Metallicities at the Sites of Nearby Broad-Lined Type Ic Supernovae and Implications for the Supernovae Gamma-Ray Burst Connection”. In: *AJ* 135.4 (Apr. 2008), pp. 1136–1150. doi: [10.1088/0004-6256/135/4/1136](https://doi.org/10.1088/0004-6256/135/4/1136). arXiv: [astro-ph/0701246](https://arxiv.org/abs/astro-ph/0701246) [[astro-ph](#)].
- [181] M. Modjaz et al. “Progenitor Diagnostics for Stripped Core-collapse Supernovae: Measured Metallicities at Explosion Sites”. In: *ApJL* 731.1, L4 (Apr. 2011), p. L4. doi: [10.1088/2041-8205/731/1/L4](https://doi.org/10.1088/2041-8205/731/1/L4). arXiv: [1007.0661](https://arxiv.org/abs/1007.0661) [[astro-ph.CO](#)].
- [182] M. R. Mokiem et al. “The empirical metallicity dependence of the mass-loss rate of O- and early B-type stars”. In: 473.2 (Oct. 2007), pp. 603–614. doi: [10.1051/0004-6361:20077545](https://doi.org/10.1051/0004-6361:20077545). arXiv: [0708.2042](https://arxiv.org/abs/0708.2042) [[astro-ph](#)].
- [183] Takashi J. Moriya et al. “Environmental dependence of Type IIn supernova properties”. In: 677, A20 (Sept. 2023), A20. doi: [10.1051/0004-6361/202346703](https://doi.org/10.1051/0004-6361/202346703). arXiv: [2306.09647](https://arxiv.org/abs/2306.09647) [[astro-ph.HE](#)].

- [184] T. Nagao et al. “Photometry and spectroscopy of the Type Icn supernova 2021ckj. The diverse properties of the ejecta and circumstellar matter of Type Icn supernovae”. In: *AAP* 673, A27 (May 2023), A27. doi: [10.1051/0004-6361/202346084](https://doi.org/10.1051/0004-6361/202346084). arXiv: [2303.07721](https://arxiv.org/abs/2303.07721) [[astro-ph.HE](#)].
- [185] K. D. Neumann et al. “The ASAS-SN bright supernova catalogue - V. 2018-2020”. In: 520.3 (Apr. 2023), pp. 4356–4369. doi: [10.1093/mnras/stad355](https://doi.org/10.1093/mnras/stad355). arXiv: [2210.06492](https://arxiv.org/abs/2210.06492) [[astro-ph.HE](#)].
- [186] K. D. Neumann et al. “The ASAS-SN bright supernova catalogue - V. 2018-2020”. In: 520.3 (Apr. 2023), pp. 4356–4369. doi: [10.1093/mnras/stad355](https://doi.org/10.1093/mnras/stad355). arXiv: [2210.06492](https://arxiv.org/abs/2210.06492) [[astro-ph.HE](#)].
- [187] M. Nicholl et al. “AT 2022aedm and a New Class of Luminous, Fast-cooling Transients in Elliptical Galaxies”. In: 954.1, L28 (Sept. 2023), p. L28. doi: [10.3847/2041-8213/acf0ba](https://doi.org/10.3847/2041-8213/acf0ba). arXiv: [2307.02556](https://arxiv.org/abs/2307.02556) [[astro-ph.HE](#)].
- [188] M. Nicholl et al. “SN 2015BN: A Detailed Multi-wavelength View of a Nearby Superluminous Supernova”. In: *ApJ* 826.1, 39 (July 2016), p. 39. doi: [10.3847/0004-637X/826/1/39](https://doi.org/10.3847/0004-637X/826/1/39). arXiv: [1603.04748](https://arxiv.org/abs/1603.04748) [[astro-ph.SR](#)].
- [189] Matt Nicholl et al. “One Thousand Days of SN2015bn: HST Imaging Shows a Light Curve Flattening Consistent with Magnetar Predictions”. In: *ApJl* 866.2, L24 (Oct. 2018), p. L24. doi: [10.3847/2041-8213/aee70d](https://doi.org/10.3847/2041-8213/aee70d). arXiv: [1809.02755](https://arxiv.org/abs/1809.02755) [[astro-ph.HE](#)].
- [190] K. Nomoto. “Accreting white dwarf models for type I supernovae. I - Presupernova evolution and triggering mechanisms”. In: *ApJ* 253 (Feb. 1982), pp. 798–810. doi: [10.1086/159682](https://doi.org/10.1086/159682).
- [191] Ken’ichi Nomoto et al. “The Crab Nebula’s progenitor”. In: *Nature* 299.5886 (Oct. 1982), pp. 803–805. doi: [10.1038/299803a0](https://doi.org/10.1038/299803a0).
- [192] A. Nyholm et al. “Type IIn supernova light-curve properties measured from an untargeted survey sample”. In: *A&A* 637, A73 (May 2020), A73. doi: [10.1051/0004-6361/201936097](https://doi.org/10.1051/0004-6361/201936097). arXiv: [1906.05812](https://arxiv.org/abs/1906.05812) [[astro-ph.SR](#)].

- [193] Evan O'Connor and Christian D. Ott. "Black Hole Formation in Failing Core-Collapse Supernovae". In: *ApJ* 730.2, 70 (Apr. 2011), p. 70. doi: [10.1088/0004-637X/730/2/70](https://doi.org/10.1088/0004-637X/730/2/70). arXiv: [1010.5550](https://arxiv.org/abs/1010.5550) [[astro-ph.HE](#)].
- [194] E. O. Ofek et al. "SN 2006gy: An Extremely Luminous Supernova in the Galaxy NGC 1260". In: *ApJL* 659.1 (Apr. 2007), pp. L13–L16. doi: [10.1086/516749](https://doi.org/10.1086/516749). arXiv: [astro-ph/0612408](https://arxiv.org/abs/astro-ph/0612408) [[astro-ph](#)].
- [195] A. Pastorello et al. "A giant outburst two years before the core-collapse of a massive star". In: *Nature* 447.7146 (June 2007), pp. 829–832. doi: [10.1038/nature05825](https://doi.org/10.1038/nature05825). arXiv: [astro-ph/0703663](https://arxiv.org/abs/astro-ph/0703663) [[astro-ph](#)].
- [196] A. Pastorello et al. "Interacting Supernovae and Supernova Impostors: SN 2009ip, is this the End?" In: *ApJ* 767.1, 1 (Apr. 2013), p. 1. doi: [10.1088/0004-637X/767/1/1](https://doi.org/10.1088/0004-637X/767/1/1). arXiv: [1210.3568](https://arxiv.org/abs/1210.3568) [[astro-ph.SR](#)].
- [197] A. Pastorello et al. "Massive stars exploding in a He-rich circumstellar medium - I. Type Ibn (SN 2006jc-like) events". In: *MNRAS* 389.1 (Sept. 2008), pp. 113–130. doi: [10.1111/j.1365-2966.2008.13602.x](https://doi.org/10.1111/j.1365-2966.2008.13602.x). arXiv: [0801.2277](https://arxiv.org/abs/0801.2277) [[astro-ph](#)].
- [198] Ferdinando Patat et al. "The Metamorphosis of SN 1998bw". In: *ApJ* 555.2 (July 2001), pp. 900–917. doi: [10.1086/321526](https://doi.org/10.1086/321526). arXiv: [astro-ph/0103111](https://arxiv.org/abs/astro-ph/0103111) [[astro-ph](#)].
- [199] Ondřej Pejcha and Todd A. Thompson. "The Landscape of the Neutrino Mechanism of Core-collapse Supernovae: Neutron Star and Black Hole Mass Functions, Explosion Energies, and Nickel Yields". In: *ApJ* 801.2, 90 (Mar. 2015), p. 90. doi: [10.1088/0004-637X/801/2/90](https://doi.org/10.1088/0004-637X/801/2/90). arXiv: [1409.0540](https://arxiv.org/abs/1409.0540) [[astro-ph.HE](#)].
- [200] D. A. Perley et al. "Host-galaxy Properties of 32 Low-redshift Superluminous Supernovae from the Palomar Transient Factory". In: *ApJ* 830.1, 13 (Oct. 2016), p. 13. doi: [10.3847/0004-637X/830/1/13](https://doi.org/10.3847/0004-637X/830/1/13). arXiv: [1604.08207](https://arxiv.org/abs/1604.08207) [[astro-ph.HE](#)].
- [201] Daniel A. Perley et al. "The Type Icn SN 2021csp: Implications for the Origins of the Fastest Supernovae and the Fates of Wolf-Rayet Stars". In: *ApJ* 927.2, 180 (Mar. 2022), p. 180. doi: [10.3847/1538-4357/ac478e](https://doi.org/10.3847/1538-4357/ac478e). arXiv: [2111.12110](https://arxiv.org/abs/2111.12110) [[astro-ph.HE](#)].

- [202] S. Perlmutter et al. “Measurements of Ω and Λ from 42 High-Redshift Supernovae”. In: *ApJ* 517.2 (June 1999), pp. 565–586. doi: [10.1086/307221](https://doi.org/10.1086/307221). arXiv: [astro-ph/9812133](https://arxiv.org/abs/astro-ph/9812133) [astro-ph].
- [203] T. Pessi et al. “A characterization of ASAS-SN core-collapse supernova environments with VLT+MUSE. I. Sample selection, analysis of local environments, and correlations with light curve properties”. In: 677, A28 (Sept. 2023), A28. doi: [10.1051/0004-6361/202346512](https://doi.org/10.1051/0004-6361/202346512). arXiv: [2306.11961](https://arxiv.org/abs/2306.11961) [astro-ph.SR].
- [204] Thallis Pessi, Jose L. Prieto, and Luc Dessart. “Very late-time spectroscopy of SN 2009ip: Constraints on the ongoing H α emission”. In: 677, L1 (Sept. 2023), p. L1. doi: [10.1051/0004-6361/202347319](https://doi.org/10.1051/0004-6361/202347319). arXiv: [2308.07370](https://arxiv.org/abs/2308.07370) [astro-ph.SR].
- [205] Thallis Pessi et al. “A Metallicity Dependence on the Occurrence of Core-collapse Supernovae”. In: 955.2, L29 (Oct. 2023), p. L29. doi: [10.3847/2041-8213/acf7c6](https://doi.org/10.3847/2041-8213/acf7c6). arXiv: [2306.11962](https://arxiv.org/abs/2306.11962) [astro-ph.SR].
- [206] Thallis Pessi et al. “Unveiling the Nature of SN 2011fh: A Young and Massive Star Gives Rise to a Luminous SN 2009ip-like Event”. In: 928.2, 138 (Apr. 2022), p. 138. doi: [10.3847/1538-4357/ac562d](https://doi.org/10.3847/1538-4357/ac562d). arXiv: [2110.09546](https://arxiv.org/abs/2110.09546) [astro-ph.HE].
- [207] Max Pettini and Bernard E. J. Pagel. “[OIII]/[NII] as an abundance indicator at high redshift”. In: *MNRAS* 348.3 (Mar. 2004), pp. L59–L63. doi: [10.1111/j.1365-2966.2004.07591.x](https://doi.org/10.1111/j.1365-2966.2004.07591.x). arXiv: [astro-ph/0401128](https://arxiv.org/abs/astro-ph/0401128) [astro-ph].
- [208] M. M. Phillips. “The Absolute Magnitudes of Type IA Supernovae”. In: *ApJL* 413 (Aug. 1993), p. L105. doi: [10.1086/186970](https://doi.org/10.1086/186970).
- [209] M. M. Phillips. “Type Ia Supernovae as Distance Indicators”. In: *1604-2004: Supernovae as Cosmological Lighthouses*. Ed. by M. Turatto et al. Vol. 342. Astronomical Society of the Pacific Conference Series. Dec. 2005, p. 211.
- [210] Anthony L. Piro. “Taking the “Un” out of “Unnovae””. In: *ApJl* 768.1, L14 (May 2013), p. L14. doi: [10.1088/2041-8205/768/1/L14](https://doi.org/10.1088/2041-8205/768/1/L14). arXiv: [1304.1539](https://arxiv.org/abs/1304.1539) [astro-ph.HE].
- [211] N. Prantzos and S. Boissier. “On the relative frequencies of core-collapse supernovae sub-types: The role of progenitor metallicity”. In: *A&A* 406 (July 2003), pp. 259–264. doi: [10.1051/0004-6361:20030717](https://doi.org/10.1051/0004-6361:20030717). arXiv: [astro-ph/0305376](https://arxiv.org/abs/astro-ph/0305376) [astro-ph].

- [212] S. J. Prentice et al. “The bolometric light curves and physical parameters of stripped-envelope supernovae”. In: *MNRAS* 458.3 (May 2016), pp. 2973–3002. doi: [10.1093/mnras/stw299](https://doi.org/10.1093/mnras/stw299). arXiv: [1602.01736](https://arxiv.org/abs/1602.01736) [[astro-ph.HE](#)].
- [213] José L. Prieto, Krzysztof Z. Stanek, and John F. Beacom. “Characterizing Supernova Progenitors via the Metallicities of their Host Galaxies, from Poor Dwarfs to Rich Spirals”. In: *ApJ* 673.2 (Feb. 2008), pp. 999–1008. doi: [10.1086/524654](https://doi.org/10.1086/524654). arXiv: [0707.0690](https://arxiv.org/abs/0707.0690) [[astro-ph](#)].
- [214] Y. L. Qiu et al. “Supernova 1999dn: Another Well Observed Type Ib SN”. In: *American Astronomical Society Meeting Abstracts*. Vol. 195. American Astronomical Society Meeting Abstracts. Dec. 1999, 38.10, p. 38.10.
- [215] R. M. Quimby et al. “Hydrogen-poor superluminous stellar explosions”. In: *Nature* 474.7352 (June 2011), pp. 487–489. doi: [10.1038/nature10095](https://doi.org/10.1038/nature10095). arXiv: [0910.0059](https://arxiv.org/abs/0910.0059) [[astro-ph.CO](#)].
- [216] D. Raimann et al. “Gas properties of Hii and starburst galaxies: relation with the stellar population”. In: *MNRAS* 316.3 (Aug. 2000), pp. 559–568. doi: [10.1046/j.1365-8711.2000.03526.x](https://doi.org/10.1046/j.1365-8711.2000.03526.x). arXiv: [astro-ph/0004160](https://arxiv.org/abs/astro-ph/0004160) [[astro-ph](#)].
- [217] C. L. Ransome et al. “An H α survey of the host environments of 77 type IIIn supernovae within $z \leq 0.02$ ”. In: *MNRAS* 513.3 (July 2022), pp. 3564–3576. doi: [10.1093/mnras/stac1093](https://doi.org/10.1093/mnras/stac1093). arXiv: [2204.09706](https://arxiv.org/abs/2204.09706) [[astro-ph.HE](#)].
- [218] Cody Raskin et al. “Using Spatial Distributions to Constrain Progenitors of Supernovae and Gamma-Ray Bursts”. In: 689.1 (Dec. 2008), pp. 358–370. doi: [10.1086/592495](https://doi.org/10.1086/592495). arXiv: [0808.3766](https://arxiv.org/abs/0808.3766) [[astro-ph](#)].
- [219] Adam G. Riess et al. “Observational Evidence from Supernovae for an Accelerating Universe and a Cosmological Constant”. In: *AJ* 116.3 (Sept. 1998), pp. 1009–1038. doi: [10.1086/300499](https://doi.org/10.1086/300499). arXiv: [astro-ph/9805201](https://arxiv.org/abs/astro-ph/9805201) [[astro-ph](#)].
- [220] Ashley J. Ruiter. “Type Ia supernova sub-classes and progenitor origin”. In: *White Dwarfs as Probes of Fundamental Physics: Tracers of Planetary, Stellar and Galactic Evolution*. Ed. by Martin A. Barstow et al. Vol. 357. Jan. 2020, pp. 1–15. doi: [10.1017/S1743921320000587](https://doi.org/10.1017/S1743921320000587). arXiv: [2001.02947](https://arxiv.org/abs/2001.02947) [[astro-ph.SR](#)].

- [221] Stuart Ryder et al. “SN 1978K: an Extraordinary Supernova in the Nearby Galaxy NGC 1313”. In: *ApJ* 416 (Oct. 1993), p. 167. doi: [10.1086/173223](https://doi.org/10.1086/173223).
- [222] H. Sana et al. “The VLT-FLAMES Tarantula Survey. VIII. Multiplicity properties of the O-type star population”. In: *A&A* 550, A107 (Feb. 2013), A107. doi: [10.1051/0004-6361/201219621](https://doi.org/10.1051/0004-6361/201219621). arXiv: [1209.4638](https://arxiv.org/abs/1209.4638) [[astro-ph.SR](#)].
- [223] S. F. Sánchez et al. “A characteristic oxygen abundance gradient in galaxy disks unveiled with CALIFA”. In: *A&A* 563, A49 (Mar. 2014), A49. doi: [10.1051/0004-6361/201322343](https://doi.org/10.1051/0004-6361/201322343). arXiv: [1311.7052](https://arxiv.org/abs/1311.7052) [[astro-ph.CO](#)].
- [224] P. Sánchez-Blázquez et al. “Medium-resolution Isaac Newton Telescope library of empirical spectra”. In: 371.2 (Sept. 2006), pp. 703–718. doi: [10.1111/j.1365-2966.2006.10699.x](https://doi.org/10.1111/j.1365-2966.2006.10699.x). arXiv: [astro-ph/0607009](https://arxiv.org/abs/astro-ph/0607009) [[astro-ph](#)].
- [225] N. E. Sanders et al. “A Spectroscopic Study of Type Ibc Supernova Host Galaxies from Untargeted Surveys”. In: *ApJ* 758.2, 132 (Oct. 2012), p. 132. doi: [10.1088/0004-637X/758/2/132](https://doi.org/10.1088/0004-637X/758/2/132). arXiv: [1206.2643](https://arxiv.org/abs/1206.2643) [[astro-ph.HE](#)].
- [226] Cecilia Scannapieco et al. “Effects of supernova feedback on the formation of galaxy discs”. In: *MNRAS* 389.3 (Sept. 2008), pp. 1137–1149. doi: [10.1111/j.1365-2966.2008.13678.x](https://doi.org/10.1111/j.1365-2966.2008.13678.x). arXiv: [0804.3795](https://arxiv.org/abs/0804.3795) [[astro-ph](#)].
- [227] P. Schady et al. “The 50-100 pc scale parent stellar populations of Type II supernovae and limitations of single star evolution models”. In: 490.4 (Dec. 2019), pp. 4515–4535. doi: [10.1093/mnras/stz2843](https://doi.org/10.1093/mnras/stz2843). arXiv: [1907.12260](https://arxiv.org/abs/1907.12260) [[astro-ph.SR](#)].
- [228] Edward F. Schlafly and Douglas P. Finkbeiner. “Measuring Reddening with Sloan Digital Sky Survey Stellar Spectra and Recalibrating SFD”. In: *ApJ* 737.2, 103 (Aug. 2011), p. 103. doi: [10.1088/0004-637X/737/2/103](https://doi.org/10.1088/0004-637X/737/2/103). arXiv: [1012.4804](https://arxiv.org/abs/1012.4804) [[astro-ph.GA](#)].
- [229] Eric M. Schlegel. “A new subclass of type II supernovae ?” In: *MNRAS* 244 (May 1990), pp. 269–271.
- [230] Steve Schulze et al. “1100 days in the life of the supernova 2018ibb. The best pair-instability supernova candidate, to date”. In: 683, A223 (Mar. 2024), A223. doi: [10.1051/0004-6361/202346855](https://doi.org/10.1051/0004-6361/202346855). arXiv: [2305.05796](https://arxiv.org/abs/2305.05796) [[astro-ph.HE](#)].

- [231] Steve Schulze et al. “The Palomar Transient Factory Core-collapse Supernova Host-galaxy Sample. I. Host-galaxy Distribution Functions and Environment Dependence of Core-collapse Supernovae”. In: *ApJs* 255.2, 29 (Aug. 2021), p. 29. doi: [10.3847/1538-4365/abff5e](https://doi.org/10.3847/1538-4365/abff5e). arXiv: [2008.05988](https://arxiv.org/abs/2008.05988) [[astro-ph.GA](#)].
- [232] B. J. Shappee et al. “The Man behind the Curtain: X-Rays Drive the UV through NIR Variability in the 2013 Active Galactic Nucleus Outburst in NGC 2617”. In: *ApJ* 788.1, 48 (June 2014), p. 48. doi: [10.1088/0004-637X/788/1/48](https://doi.org/10.1088/0004-637X/788/1/48). arXiv: [1310.2241](https://arxiv.org/abs/1310.2241) [[astro-ph.HE](#)].
- [233] T. Shenar et al. “Why binary interaction does not necessarily dominate the formation of Wolf-Rayet stars at low metallicity”. In: *A&A* 634, A79 (Feb. 2020), A79. doi: [10.1051/0004-6361/201936948](https://doi.org/10.1051/0004-6361/201936948). arXiv: [2001.04476](https://arxiv.org/abs/2001.04476) [[astro-ph.SR](#)].
- [234] Isaac Shivvers et al. “The nearby Type Ibn supernova 2015G: signatures of asymmetry and progenitor constraints”. In: 471.4 (Nov. 2017), pp. 4381–4397. doi: [10.1093/mnras/stx1885](https://doi.org/10.1093/mnras/stx1885). arXiv: [1704.04316](https://arxiv.org/abs/1704.04316) [[astro-ph.HE](#)].
- [235] S. J. Smartt. “Observational Constraints on the Progenitors of Core-Collapse Supernovae: The Case for Missing High-Mass Stars”. In: *PASA* 32, e016 (Apr. 2015), e016. doi: [10.1017/pasa.2015.17](https://doi.org/10.1017/pasa.2015.17). arXiv: [1504.02635](https://arxiv.org/abs/1504.02635) [[astro-ph.SR](#)].
- [236] S. J. Smartt et al. “The death of massive stars - I. Observational constraints on the progenitors of Type II-P supernovae”. In: 395.3 (May 2009), pp. 1409–1437. doi: [10.1111/j.1365-2966.2009.14506.x](https://doi.org/10.1111/j.1365-2966.2009.14506.x). arXiv: [0809.0403](https://arxiv.org/abs/0809.0403) [[astro-ph](#)].
- [237] Stephen J. Smartt. “Progenitors of Core-Collapse Supernovae”. In: 47.1 (Sept. 2009), pp. 63–106. doi: [10.1146/annurev-astro-082708-101737](https://doi.org/10.1146/annurev-astro-082708-101737). arXiv: [0908.0700](https://arxiv.org/abs/0908.0700) [[astro-ph.SR](#)].
- [238] Nathan Smith. “Mass Loss: Its Effect on the Evolution and Fate of High-Mass Stars”. In: *ARA&A* 52 (Aug. 2014), pp. 487–528. doi: [10.1146/annurev-astro-081913-040025](https://doi.org/10.1146/annurev-astro-081913-040025). arXiv: [1402.1237](https://arxiv.org/abs/1402.1237) [[astro-ph.SR](#)].
- [239] Nathan Smith. “The isolation of luminous blue variables resembles aging B-type supergiants, not the most massive unevolved stars”. In: *MNRAS* 489.3 (Nov. 2019), pp. 4378–4388. doi: [10.1093/mnras/stz2277](https://doi.org/10.1093/mnras/stz2277). arXiv: [1908.06104](https://arxiv.org/abs/1908.06104) [[astro-ph.SR](#)].

- [240] Nathan Smith, Kenneth H. Hinkle, and Nils Ryde. “Red Supergiants as Potential Type II In Supernova Progenitors: Spatially Resolved 4.6 μm CO Emission Around VY CMa and Betelgeuse”. In: *AJ* 137.3 (Mar. 2009), pp. 3558–3573. doi: [10.1088/0004-6256/137/3/3558](https://doi.org/10.1088/0004-6256/137/3/3558). arXiv: [0811.3037](https://arxiv.org/abs/0811.3037) [astro-ph].
- [241] Jesper Sollerman, Robert J. Cumming, and Peter Lundqvist. “A Very Low Mass of ^{56}Ni in the Ejecta of SN 1994W”. In: *ApJ* 493.2 (Jan. 1998), pp. 933–939. doi: [10.1086/305163](https://doi.org/10.1086/305163). arXiv: [astro-ph/9709061](https://arxiv.org/abs/astro-ph/9709061) [astro-ph].
- [242] Elena Sorokina et al. “Type I Superluminous Supernovae as Explosions inside Non-hydrogen Circumstellar Envelopes”. In: 829.1, 17 (Sept. 2016), p. 17. doi: [10.3847/0004-637X/829/1/17](https://doi.org/10.3847/0004-637X/829/1/17). arXiv: [1510.00834](https://arxiv.org/abs/1510.00834) [astro-ph.HE].
- [243] K. Z. Stanek et al. ““Anomalous” Optical Gamma-Ray Burst Afterglows Are Common: Two $z \sim 4$ Bursts, GRB 060206 and GRB 060210”. In: *ApJ* 654.1 (Jan. 2007), pp. L21–L24. doi: [10.1086/510884](https://doi.org/10.1086/510884). arXiv: [astro-ph/0602495](https://arxiv.org/abs/astro-ph/0602495) [astro-ph].
- [244] K. Z. Stanek et al. “Protecting Life in the Milky Way: Metals Keep the GRBs Away”. In: *AcA* 56 (Dec. 2006), pp. 333–345. doi: [10.48550/arXiv.astro-ph/0604113](https://doi.org/10.48550/arXiv.astro-ph/0604113). arXiv: [astro-ph/0604113](https://arxiv.org/abs/astro-ph/0604113) [astro-ph].
- [245] E. R. Stanway and J. J. Eldridge. “Re-evaluating old stellar populations”. In: *MNRAS* 479.1 (Sept. 2018), pp. 75–93. doi: [10.1093/mnras/sty1353](https://doi.org/10.1093/mnras/sty1353). arXiv: [1805.08784](https://arxiv.org/abs/1805.08784) [astro-ph.GA].
- [246] R. Stoll et al. “SN 2010jl in UGC 5189: Yet Another Luminous Type II In Supernova in a Metal-poor Galaxy”. In: *ApJ* 730.1, 34 (Mar. 2011), p. 34. doi: [10.1088/0004-637X/730/1/34](https://doi.org/10.1088/0004-637X/730/1/34). arXiv: [1012.3461](https://arxiv.org/abs/1012.3461) [astro-ph.CO].
- [247] Thaisa Storchi-Bergmann, Daniela Calzetti, and Anne L. Kinney. “Ultraviolet to Near-Infrared Spectral Distributions of Star-forming Galaxies: Metallicity and Age Effects”. In: *ApJ* 429 (July 1994), p. 572. doi: [10.1086/174345](https://doi.org/10.1086/174345).
- [248] Tuguldur Sukhbold et al. “Core-collapse Supernovae from 9 to 120 Solar Masses Based on Neutrino-powered Explosions”. In: *ApJ* 821.1, 38 (Apr. 2016), p. 38. doi: [10.3847/0004-637X/821/1/38](https://doi.org/10.3847/0004-637X/821/1/38). arXiv: [1510.04643](https://arxiv.org/abs/1510.04643) [astro-ph.HE].

- [249] M. Sullivan et al. “Rates and Properties of Type Ia Supernovae as a Function of Mass and Star Formation in Their Host Galaxies”. In: *ApJ* 648.2 (Sept. 2006), pp. 868–883. doi: [10.1086/506137](https://doi.org/10.1086/506137). arXiv: [astro-ph/0605455](https://arxiv.org/abs/astro-ph/0605455) [[astro-ph](#)].
- [250] Ning-Chen Sun, Justyn R. Maund, and Paul A. Crowther. “A UV census of the environments of stripped-envelope supernovae”. In: 521.2 (May 2023), pp. 2860–2873. doi: [10.1093/mnras/stad690](https://doi.org/10.1093/mnras/stad690). arXiv: [2209.05283](https://arxiv.org/abs/2209.05283) [[astro-ph.SR](#)].
- [251] Ning-Chen Sun et al. “An environmental analysis of the Type Ib SN 2019yvr and the possible presence of an inflated binary companion”. In: *MNRAS* 510.3 (Mar. 2022), pp. 3701–3715. doi: [10.1093/mnras/stab3768](https://doi.org/10.1093/mnras/stab3768). arXiv: [2111.06471](https://arxiv.org/abs/2111.06471) [[astro-ph.SR](#)].
- [252] Ning-Chen Sun et al. “Origins of Type Ibn SNe 2006jc/2015G in interacting binaries and implications for pre-SN eruptions”. In: 491.4 (Feb. 2020), pp. 6000–6019. doi: [10.1093/mnras/stz3431](https://doi.org/10.1093/mnras/stz3431). arXiv: [1909.07999](https://arxiv.org/abs/1909.07999) [[astro-ph.SR](#)].
- [253] Ning-Chen Sun et al. “Towards a better understanding of supernova environments: a study of SNe 2004dg and 2012P in NGC 5806 with HST and MUSE”. In: 504.2 (June 2021), pp. 2253–2272. doi: [10.1093/mnras/stab994](https://doi.org/10.1093/mnras/stab994). arXiv: [2011.13667](https://arxiv.org/abs/2011.13667) [[astro-ph.SR](#)].
- [254] F. Taddia et al. “Carnegie Supernova Project: Observations of Type IIn supernovae”. In: *A&A* 555, A10 (July 2013), A10. doi: [10.1051/0004-6361/201321180](https://doi.org/10.1051/0004-6361/201321180). arXiv: [1304.3038](https://arxiv.org/abs/1304.3038) [[astro-ph.CO](#)].
- [255] F. Taddia et al. “Early-time light curves of Type Ib/c supernovae from the SDSS-II Supernova Survey”. In: *A&A* 574, A60 (Feb. 2015), A60. doi: [10.1051/0004-6361/201423915](https://doi.org/10.1051/0004-6361/201423915). arXiv: [1408.4084](https://arxiv.org/abs/1408.4084) [[astro-ph.HE](#)].
- [256] F. Taddia et al. “Metallicity at the explosion sites of interacting transients”. In: *A&A* 580, A131 (Aug. 2015), A131. doi: [10.1051/0004-6361/201525989](https://doi.org/10.1051/0004-6361/201525989). arXiv: [1505.04719](https://arxiv.org/abs/1505.04719) [[astro-ph.HE](#)].
- [257] F. Taddia et al. “The Carnegie Supernova Project I. Analysis of stripped-envelope supernova light curves”. In: *A&A* 609, A136 (Feb. 2018), A136. doi: [10.1051/0004-6361/201730844](https://doi.org/10.1051/0004-6361/201730844). arXiv: [1707.07614](https://arxiv.org/abs/1707.07614) [[astro-ph.HE](#)].

- [258] K. Taggart and D. A. Perley. “Core-collapse, superluminous, and gamma-ray burst supernova host galaxy populations at low redshift: the importance of dwarf and star-bursting galaxies”. In: *MNRAS* 503.3 (May 2021), pp. 3931–3952. doi: [10.1093/mnras/stab174](https://doi.org/10.1093/mnras/stab174). arXiv: [1911.09112](https://arxiv.org/abs/1911.09112) [[astro-ph.HE](#)].
- [259] S. Taibi et al. “Stellar metallicity gradients of Local Group dwarf galaxies”. In: *A&A* 665, A92 (Sept. 2022), A92. doi: [10.1051/0004-6361/202243508](https://doi.org/10.1051/0004-6361/202243508). arXiv: [2206.08988](https://arxiv.org/abs/2206.08988) [[astro-ph.GA](#)].
- [260] The Dark Energy Survey Collaboration. “The Dark Energy Survey”. In: *arXiv e-prints*, astro-ph/0510346 (Oct. 2005), astro-ph/0510346. arXiv: [astro-ph/0510346](https://arxiv.org/abs/astro-ph/0510346) [[astro-ph](#)].
- [261] C. C. Thone et al. “A young stellar environment for the superluminous supernova PTF12dam.” In: *MNRAS* 451 (July 2015), pp. L65–L69. doi: [10.1093/mnrasl/slv051](https://doi.org/10.1093/mnrasl/slv051). arXiv: [1411.1104](https://arxiv.org/abs/1411.1104) [[astro-ph.GA](#)].
- [262] L. Toribio San Cipriano et al. “Carbon and oxygen in H II regions of the Magellanic Clouds: abundance discrepancy and chemical evolution”. In: *MNRAS* 467.3 (May 2017), pp. 3759–3774. doi: [10.1093/mnras/stx328](https://doi.org/10.1093/mnras/stx328). arXiv: [1702.01120](https://arxiv.org/abs/1702.01120) [[astro-ph.GA](#)].
- [263] P. Tremblin et al. “Age, size, and position of H ii regions in the Galaxy. Expansion of ionized gas in turbulent molecular clouds”. In: *A&A* 568, A4 (Aug. 2014), A4. doi: [10.1051/0004-6361/201423959](https://doi.org/10.1051/0004-6361/201423959). arXiv: [1406.1801](https://arxiv.org/abs/1406.1801) [[astro-ph.SR](#)].
- [264] D. Yu. Tsvetkov, N. N. Pavlyuk, and O. S. Bartunov. “The SAI Catalog of Supernovae and Radial Distributions of Supernovae of Various Types in Galaxies”. In: *Astronomy Letters* 30.11 (Nov. 2004), pp. 729–736. doi: [10.1134/1.1819491](https://doi.org/10.1134/1.1819491).
- [265] M. Turatto et al. “The type II supernova 1988Z in MCG +03-28-022 : increasing evidence of interaction of supernova ejecta with a circumstellar wind.” In: *MNRAS* 262 (May 1993), pp. 128–140. doi: [10.1093/mnras/262.1.128](https://doi.org/10.1093/mnras/262.1.128).
- [266] S. Valenti et al. “The diversity of Type II supernova versus the similarity in their progenitors”. In: *MNRAS* 459.4 (July 2016), pp. 3939–3962. doi: [10.1093/mnras/stw870](https://doi.org/10.1093/mnras/stw870). arXiv: [1603.08953](https://arxiv.org/abs/1603.08953) [[astro-ph.SR](#)].

- [267] Sidney van den Bergh. "Distribution of Supernovae in Spiral Galaxies". In: *AJ* 113 (Jan. 1997), p. 197. doi: [10.1086/118244](https://doi.org/10.1086/118244). arXiv: [astro-ph/9611025](https://arxiv.org/abs/astro-ph/9611025) [[astro-ph](#)].
- [268] Schuyler D. van Dyk. "Association of Supernovae with Recent Star Formation Regions in Late Type Galaxies". In: *AJ* 103 (June 1992), p. 1788. doi: [10.1086/116195](https://doi.org/10.1086/116195).
- [269] Schuyler D. Van Dyk et al. "Supernova 2008bk and Its Red Supergiant Progenitor". In: *AJ* 143.1, 19 (Jan. 2012), p. 19. doi: [10.1088/0004-6256/143/1/19](https://doi.org/10.1088/0004-6256/143/1/19). arXiv: [1011.5873](https://arxiv.org/abs/1011.5873) [[astro-ph.SR](#)].
- [270] Schuyler D. Van Dyk et al. "The Type IIb Supernova 2013df and its Cool Supergiant Progenitor". In: *AJ* 147.2, 37 (Feb. 2014), p. 37. doi: [10.1088/0004-6256/147/2/37](https://doi.org/10.1088/0004-6256/147/2/37). arXiv: [1312.3984](https://arxiv.org/abs/1312.3984) [[astro-ph.SR](#)].
- [271] Liese van Zee, John J. Salzer, and Martha P. Haynes. "Abundances in Spiral Galaxies: Evidence for Primary Nitrogen Production". In: *ApJl* 497.1 (Apr. 1998), pp. L1–L4. doi: [10.1086/311263](https://doi.org/10.1086/311263). arXiv: [astro-ph/9802147](https://arxiv.org/abs/astro-ph/9802147) [[astro-ph](#)].
- [272] David Vartanyan et al. "Binary-stripped Stars as Core-collapse Supernovae Progenitors". In: *ApJl* 916.1, L5 (July 2021), p. L5. doi: [10.3847/2041-8213/ac0b42](https://doi.org/10.3847/2041-8213/ac0b42). arXiv: [2104.03317](https://arxiv.org/abs/2104.03317) [[astro-ph.SR](#)].
- [273] Pauli Virtanen et al. "SciPy 1.0: Fundamental Algorithms for Scientific Computing in Python". In: *Nature Methods* 17 (2020), pp. 261–272. doi: [10.1038/s41592-019-0686-2](https://doi.org/10.1038/s41592-019-0686-2).
- [274] Lifan Wang, Peter Höflich, and J. Craig Wheeler. "Supernovae and Their Host Galaxies". In: *ApJl* 483.1 (July 1997), pp. L29–L32. doi: [10.1086/310737](https://doi.org/10.1086/310737).
- [275] R. F. Webbink. "The evolution of low-mass close binary systems. I. The evolutionary fate of contact binaries." In: *ApJ* 209 (Nov. 1976), pp. 829–845. doi: [10.1086/154781](https://doi.org/10.1086/154781).
- [276] P. M. Weilbacher et al. "The MUSE Data Reduction Pipeline: Status after Preliminary Acceptance Europe". In: *Astronomical Data Analysis Software and Systems XXIII*. Ed. by N. Manset and P. Forshay. Vol. 485. Astronomical Society of the Pacific Conference Series. May 2014, p. 451. arXiv: [1507.00034](https://arxiv.org/abs/1507.00034) [[astro-ph.IM](#)].

- [277] John Whelan and Jr. Iben Icko. “Binaries and Supernovae of Type I”. In: *ApJ* 186 (Dec. 1973), pp. 1007–1014. doi: [10.1086/152565](https://doi.org/10.1086/152565).
- [278] S. E. Woosley. “Bright Supernovae from Magnetar Birth”. In: 719.2 (Aug. 2010), pp. L204–L207. doi: [10.1088/2041-8205/719/2/L204](https://doi.org/10.1088/2041-8205/719/2/L204). arXiv: [0911.0698](https://arxiv.org/abs/0911.0698) [[astro-ph.HE](#)].
- [279] S. E. Woosley and J. S. Bloom. “The Supernova Gamma-Ray Burst Connection”. In: *ARA&A* 44.1 (Sept. 2006), pp. 507–556. doi: [10.1146/annurev.astro.43.072103.150558](https://doi.org/10.1146/annurev.astro.43.072103.150558). arXiv: [astro-ph/0609142](https://arxiv.org/abs/astro-ph/0609142) [[astro-ph](#)].
- [280] S. E. Woosley, Norbert Langer, and Thomas A. Weaver. “The Evolution of Massive Stars Including Mass Loss: Presupernova Models and Explosion”. In: *ApJ* 411 (July 1993), p. 823. doi: [10.1086/172886](https://doi.org/10.1086/172886).
- [281] S. E. Woosley and Thomas A. Weaver. “The Evolution and Explosion of Massive Stars. II. Explosive Hydrodynamics and Nucleosynthesis”. In: *ApJs* 101 (Nov. 1995), p. 181. doi: [10.1086/192237](https://doi.org/10.1086/192237).
- [282] S. E. Woosley and Thomas A. Weaver. “The physics of supernova explosions.” In: *ARA&A* 24 (Jan. 1986), pp. 205–253. doi: [10.1146/annurev.aa.24.090186.001225](https://doi.org/10.1146/annurev.aa.24.090186.001225).
- [283] Lin Xiao, Elizabeth R. Stanway, and J. J. Eldridge. “Emission-line diagnostics of nearby H II regions including interacting binary populations”. In: *MNRAS* 477.1 (June 2018), pp. 904–934. doi: [10.1093/mnras/sty646](https://doi.org/10.1093/mnras/sty646). arXiv: [1801.07068](https://arxiv.org/abs/1801.07068) [[astro-ph.GA](#)].
- [284] Lin Xiao et al. “Core-collapse supernovae ages and metallicities from emission-line diagnostics of nearby stellar populations”. In: *MNRAS* 482.1 (Jan. 2019), pp. 384–401. doi: [10.1093/mnras/sty2557](https://doi.org/10.1093/mnras/sty2557). arXiv: [1805.01213](https://arxiv.org/abs/1805.01213) [[astro-ph.GA](#)].
- [285] Lin Yan et al. “Detection of Broad H α Emission Lines in the Late-time Spectra of a Hydrogen-poor Superluminous Supernova”. In: 814.2, 108 (Dec. 2015), p. 108. doi: [10.1088/0004-637X/814/2/108](https://doi.org/10.1088/0004-637X/814/2/108). arXiv: [1508.04420](https://arxiv.org/abs/1508.04420) [[astro-ph.GA](#)].

- [286] S. C. Yoon, S. E. Woosley, and N. Langer. “Type Ib/c Supernovae in Binary Systems. I. Evolution and Properties of the Progenitor Stars”. In: *ApJ* 725.1 (Dec. 2010), pp. 940–954. doi: [10.1088/0004-637X/725/1/940](https://doi.org/10.1088/0004-637X/725/1/940). arXiv: [1004.0843](https://arxiv.org/abs/1004.0843) [[astro-ph.SR](#)].
- [287] Sung-Chul Yoon. “Towards a better understanding of the evolution of Wolf-Rayet stars and Type Ib/Ic supernova progenitors”. In: *MNRAS* 470.4 (Oct. 2017), pp. 3970–3980. doi: [10.1093/mnras/stx1496](https://doi.org/10.1093/mnras/stx1496). arXiv: [1706.04716](https://arxiv.org/abs/1706.04716) [[astro-ph.SR](#)].
- [288] Donald G. York et al. “The Sloan Digital Sky Survey: Technical Summary”. In: *AJ* 120.3 (Sept. 2000), pp. 1579–1587. doi: [10.1086/301513](https://doi.org/10.1086/301513). arXiv: [astro-ph/0006396](https://arxiv.org/abs/astro-ph/0006396) [[astro-ph](#)].
- [289] E. Zapartas et al. “Delay-time distribution of core-collapse supernovae with late events resulting from binary interaction”. In: *A&A* 601, A29 (May 2017), A29. doi: [10.1051/0004-6361/201629685](https://doi.org/10.1051/0004-6361/201629685). arXiv: [1701.07032](https://arxiv.org/abs/1701.07032) [[astro-ph.HE](#)].
- [290] E. Zapartas et al. “Revisiting the explodability of single massive star progenitors of stripped-envelope supernovae”. In: *A&A* 656, L19 (Dec. 2021), p. L19. doi: [10.1051/0004-6361/202141506](https://doi.org/10.1051/0004-6361/202141506). arXiv: [2106.05228](https://arxiv.org/abs/2106.05228) [[astro-ph.HE](#)].